A STUDY OF AN IMPROVED INSTALLATION METHOD FOR REINFORCED CONCRETE PIPES UNDER HIGH EMBANKMENTS

by

S.A. Costin, B.E.

A thesis presented to the Faculty of Engineering of the University of Adelaide in fulfillment of the requirements for the Degree of Master of Engineering Science.

awarded 28-7-1986.

Department of Civil Engineering,
University of Adelaide

April 1986

TABLE OF CONTENTS

LIST OF FIGURES

LIST OF PLATES

ABSTRACT

The cover height and bedding condition for reinforced concrete pipe were evaluated by both experimental and analytical methods in order to establish a means of bedding such pipes under greater heights of fill than would be permitted under existing codes.

The investigation described herein consisted of two parts. After surveying all available literature on the soil-structure interaction problem, a linear elastic finite element model of a pipe bedded on a proposed improved bedding under a high embankment was formulated. The model used values of elastic modulus obtained from a three-edge bearing test for the pipe, and from plate load tests for the bedding materials and simulated embankment.

Two 750 mm diameter concrete pipes with double concentric reinforcing grids were instrumented with strain gauges and displacement transducers to measure their responses under load. One of these pipes was subjected to a three-edge bearing test to measure its stiffness and cracking strength. The other pipe was installed on the proposed improved bedding inside the test bin and surrounded by a sand fill. The effect of an embankment above a nominal cover height was simulated by applying a surcharge to the surface of the sand with an inflated air bag.

The responses of the bedded pipe were recorded and later compared with the results of the finite element analysis. The comparison revealed that the moduli of the crushed rock materials measured in the plate load tests were low by more than a degree of magnitude indicating that measurement of modulus using the plate load test is unsuitable for compacted crushed rock materials.

Revised values of modulus were used in the finite element model in an attempt to reproduce the experimental deflection profile of the pipe.

In addition, using the strain gauge readings taken at the pipe's haunches, the thrusts at these locations were calculated. The sum of these thrusts was shown to be consistent with that predicted by the revised finite element model.

From the cracking behaviour of the pipe, a value of bedding factor was calculated in accordance with the classical Spangler approach and this value was shown to be consistent with a value of bedding factor calculated from the Mountainhouse Creek tests in the U.S.A..

The proposed bedding was shown to be capable of supporting up to twice the height of embankment fill permitted by the Class B beddings as laid down in Australian Standard AS 1342-1973.

DECLARATION

This thesis contains no material which has been accepted for the award of any other degree or diploma in any University, and to the best of my knowledge and belief, contains no material previously published or written by another person, except where due reference is made in the text of the thesis. I consent to the thesis being made available for photocopying and loan if accepted for the award of the degree.

S.A. Costin

ACKNOWLEDGEMENTS

The investigation on which this thesis is based was undertaken under the supervision of Dr. J.N. Kay, senior lecturer in the Department of Civil Engineering at the University of Adelaide. The author acknowledges his encouragement and guidance received during the course of this work. Acknowledgement is also made to Mr. R.C.L. Flint for help with computing aspects of the project and for the use of many of his own programmes, and to the Concrete Pipe Association of Australia who financed the study as part of a programme aimed at increasing the knowledge of the performance of concrete pipes.

INTRODUCTION

The aim of this study was to investigate by measurement and by theoretical analysis the height of fill supported by a specific installation arrangement and to hopefully develop a method for predicting such a fill height.

Observations of pipe behaviour over the years have suggested that a pipe buried beneath an embankment can carry more height of fill if restrained from deflecting horizontally at the haunches. The Mountainhouse Creek tests in California used several different types of bedding under fill heights of up to 41 m. Of the various types tested, those on which the pipes showed the best performance were those used in Zones 7 and 8. In both of these zones the pipes were laid in trenches in the foundation material beneath the embankment such that only 40% of their external diameter was projecting above the foundation, and the trenches were backfilled with fine crushed rock. In Zone 7 the pipe was laid on a bedding shaped to fit it, whereas the Zone 8 pipe was laid on a flat layer of fine aggregate. Under the load of the embankment very little difference was observed between the performances of the two zones indicating that the additional work involved in shaping the foundation material to fit the curve of the pipe was not worthwhile.

Bacher (49) used the results of the Mountainhouse Creek tests together with those of earlier tests to propose a design method for concrete pipes buried under embankments on partial trench beddings. The method takes account of the observation that the ratio of lateral to vertical pressure is higher for pipes which are thinner in comparison to their diameter, than those which are thick.

It was felt that since American concrete pipes are generally thicker than pipes of a similar strength and diameter used in Australia, it was desirable to test an Australian pipe on a bedding similar to that used in

Zone 8 at Mountainhouse Creek. Such a bedding has recently been included in the draft Australian Standard "86013 - Loads on Buried Concrete Pipes".

The University of Adelaide had earlier constructed a test rig in which pipes and arches could be buried in soil and then subjected to vertical loads simulating the effect of an embankment, it was decided to use this test rig to load a 750 mm diameter pipe bedded as described above.

In addition a finite element model was used initially in a effort to predict results but it was subsequently "fitted" to results to provide a means for approximately determining the actual modulus values. Values measured by means of plate load tests on a trial bedding and on materials compacted in the laboratory were found to give finite element analysis results that varied considerably from those obtained experimentally and it was felt that considerably more attention to modulus characterization would be needed before confident extrapolation from the test conditions could be effected.

Nevertheless, the test yielded sufficient information to allow determination of the required strength class of a pipe laid under the conditions specified.

SECTION 1: LITERATURE SURVEY

1.1. Current Design Practice

Virtually all currently used design procedures for buried reinforced concrete pipes can be attributed to work carried out by Marston and Spangler at Iowa Engineering Experiment Station in the USA during the period 1910-1950, (1).

They divided buried conduits into two main groups, those installed in a trench, and those installed under an embankment. Embankment installations were then further subdivided into positive projecting, negative projecting and induced trench installations.

The Marston theory of load calculation gives the vertical load on a circular pipe as being the product of the unit weight of the fill material, the square of a horizontal dimension (either trench width at the top of the pipe, for trench or negative projection installations, or pipe external diameter for positive projection embankment installations) and a load coefficient determined by the conditions of installation.

The load coefficient is determined by the geometry of the soil pipe system and the properties of the fill. Normally it is expressed as a function of the ratio of fill height to the horizontal dimensions mentioned in the previous paragraph, the coefficient of internal friction of the soil, the projection ratio and the settlement ratio. Since the soil and the pipe will compress by different amounts under the weight of the soil above, the relative deformation is assumed to cause sliding between the soil prism above the pipe and the adjacent soil. This causes shear forces to develop along these assumed sliding surfaces. The resulting vertical load is the sum of the weight of the soil prism above the pipe and the shear forces along these surfaces. This means that for a trench installation the vertical load on the pipe will be less than the

weight of the prism, and for an embankment installation it will be greater.

Because of lateral support at the sides of the pipe and the way in which the vertical load is distributed over the top and bottom surfaces, the pipe in a real installation, will support more load than it will in a load test under line loads top and bottom. The ratio between the supporting strength in the field and under the test load is called the bedding factor. The vertical load calculated is divided by the appropriate bedding factor and the quotient is the design load. This is the load associated with the three-edge bearing test. As long as shear failure at the invert does not control, the supporting strength under both test and field conditions is based on limiting crack widths which in turn are related to limiting steel stresses and hence bending moments. For testing conditions the load limit has traditionally been defined by the presence of a 0.15 mm crack (see Australian Standard AS 1342 - 1973), a completely arbitrary choice.

Under field conditions a wider crack can, however, be permitted, the width limit depending on the degree of aggressiveness of the particular environment.

Flexural cracking is of no significance structurally since the tensile strength of the concrete in reinforced concrete is assumed to be zero. The limit on field cracking must be based on the corrosive effect of the cracking on the reinforcement. Knowledge in this area is still very limited but two points rate a mention:

(1) Smaller cracks in the field heal autogenously under the influence of moisture and the lime in the cement.

(2) The trend in the United States is for authorities to accept quite wide flexural field cracks as structurally insignificant. (Up to 2.5 mm under non-corrosive conditions is accepted by the

California Department of Transportation.)

1.2. Drawbacks of Current Methods

While the Marston-Spangler theory gives quite a reasonable approximation to the vertical load on a buried pipe, it does not provide for appropriate values of bedding factor for modern construction practice. Effectively it does not take proper account of the lateral resistance of the soil to the pipe's horizontal diameter increase. The bedding factors calculated by Spangler are based on the assumption that the soil pressure acting on the sides of the pipe is active rather than passive. This assumption is obviously conservative since for active conditions to exist, the sides of the pipe would need to deflect inwards. This is never likely to occur in a real installation, so the lateral pressure would be expected to be at least the "at rest" pressure.

In order to sort out more thoroughly the way in which the various components of a soil-pipe system work, i.e. pipe, backfill, sidefill, foundation, it is useful to treat them all as being elastic continua joined together and with compatible displacements and forces along their edges. In order to do this it is necessary to have a constitutive model of the stress strain behaviour of the pipe, the bedding, and the surrounding soil. This is discussed in the following section.

1.3. Stress-Strain Relationships for Soil

1.3.1. Linear Elastic Model

The simplest assumption to make when representing the stress-strain behaviour of soil is that of linear elasticity. If the further assumption is made of material isotropy then only two parameters (modulus and Poisson's ratio) are needed to describe the stress-strain behaviour of a soil. The modulus is generally determined from the conventional

triaxial compression test and Poisson's ratio is usually estimated for the soil type. A constant value for both parameters is assumed throughout the entire loading history.

Whilst this model has been usefully applied to find the stress distributions within homogeneous soil masses (2), when applied to soil-pipe interactions it can only be regarded as a first approximation.

An extension to the concept of linear elasticity is piecewise linearity, where the tangent modulus $\Delta\sigma/\Delta\epsilon$ of a nonlinear stress-strain relationship is taken to apply over a range of stress around the point at which the tangent modulus is evaluated. The stress-strain relationship is then taken as linear over this range, this is particularly useful in finite element models.

1.3.2. Constrained Modulus Formulation

This model was firstly proposed by Janbu (3), the constrained modulus M_s being determined by a uniaxial strain test on a laterally confined soil sample. The value M_s is dependant on the amount of pressure applied, and so this model is nonlinear.

$$\frac{M_s}{p_a} = m\left(\frac{\sigma_1}{p_a}\right)^{1-n} \qquad (1)$$

where:

σ_1 = major principal stress

p_a = atmospheric pressure (introduced to make equation dimensionless)

m = modulus number

n = stress exponent

Both m and n must be determined experimentally, although correlations have been noted with soil type and porosity by Janbu (3) and with dry density by Osterberg (4).

Since elasticitv, E is used in finite element analvsis this can be related to the constrained modulus M_s using a relationship derived from the theorv of linear elasticitv:

$$E = \frac{(1-2\nu)(1+\nu)}{1-\nu} M_s \qquad (2)$$

where ν = Poisson's ratio

Combining Eqs. 1 and 2:

$$\frac{E}{p_a} = \frac{(1-2\nu)(1+\nu)}{1-\nu} \; m \left(\frac{\sigma_1}{p_a}\right)^{1-n} \qquad (3)$$

According to Krizek and Atmatzidis, (11) Equation 1. has been used successfullv to calculate one-dimensional settlements due to consolidation but because of the difficulties associated with estimating Poisson's ratio for a soil, and the assumption of linear elasticitv in Equation 2., Equation 3. is less reliable.

Espinosa, Krizek and Corotis (5) made a large number of consolidation tests on various soils and made a regression analvsis of the results against several consolidation equations. The best fit was obtained using the modified Janbu Equation:

$$\frac{M_s}{p_a} = c \left(\frac{\sigma_1+p_a}{p_a}\right)^d \qquad (4)$$

where the coefficients c and d were determined in terms of the drv densitv, natural water content, liquid limit, plastic limit and percentage of clav.

Krizek, Corotis and Wenzel (15) used the following formulation to characterize various soils in two instrumented full scale installations:

$$\frac{E}{p_a} = \alpha+\beta\left(\frac{\sigma_1}{p_a}\right)^{\eta} \qquad (5)$$

where: E = elasticity calculated from measuring M_s and by using Equation 2.

σ_1 = major principal stress

α_1, β and η = empirical coefficients which depend on dry density and soil type.

1.3.3. Hyperbolic Model

Kondner and his co-workers (6), (7), (8), (9), have shown that the nonlinear stress-strain curves of both sand and clay may be approximated reasonably well by hyperbolic equations of the form:

$$\sigma_1-\sigma_3 = \frac{\epsilon}{a+b\epsilon} \qquad (6)$$

where σ_1 and σ_3 = major and minor principal stresses

ϵ = axial strain

a and b = empirical coefficients

a is related to the initial tangent modulus by:

$$E_i = \frac{1}{a} \qquad (7)$$

b is related to the ultimate stress difference by:

$$b = \frac{1}{(\sigma_1-\sigma_3)_{ult}} \qquad (8)$$

Compressive strength $(\sigma_1-\sigma_3)_f$ is related to the ultimate stress difference and to b by:

$$(\sigma_1-\sigma_3)_f = R(\sigma_1-\sigma_3)_{ult} = \frac{R}{b} \qquad (9)$$

where R is stated to be between 0.75 and 1.00 by Duncan and Chang (10), other authors give values of R within this range.

By substituting values for a and b into Equation 6. we may write:

$$\sigma_1-\sigma_3 = \frac{\epsilon}{\left[\frac{1}{E_i} + \frac{\epsilon R}{(\sigma_1-\sigma_3)_f}\right]} \qquad (10)$$

Experimental work by Janbu (3), shows that the initial tangent modulus E_i is related to the minor principal stress σ_3 by:

$$E_i = K\, p_a \left(\frac{\sigma_3}{p_a}\right)^n \qquad (11)$$

where p_a = atmospheric pressure (introduced to make equation dimensionless)

K = a modulus number

n = the exponent determining the rate of variation of E_i with σ_3

The compressive strength $(\sigma_1-\sigma_3)_f$ can be expressed in terms of the cohesion, c and the angle of internal friction, φ by the Mohr-Coulomb failure criterion:

$$(\sigma_1-\sigma_3)_f = \frac{2c\cos\varphi + 2\sigma_3 \sin\varphi}{1 - \sin\varphi} \qquad (12)$$

Substituting Equations 7. to 12. into Equation 6. allows the tangent modulus E to be expressed as:

$$\frac{E}{p_a} = \left[1 - \frac{R(1-\sin\varphi)(\sigma_1-\sigma_3)}{2c\cos\varphi + 2\sigma_3 \sin\varphi}\right]^2 K\left(\frac{\sigma_3}{p_a}\right)^n \qquad (13)$$

According to Krizek and Atmatzidis (11), Equation 13. is useful for incremental stress analysis and has been used in the analysis of several practical problems.

1.3.4. Hypoelastic Soil Model

This model was originally introduced by Truesdell (35) and was later modified by Corotis, Farzin and Krizek (36) to describe the nonlinear stress-strain behaviour of both cohesive and cohesionless soils. The relationships as used by the latter are as follows:

$$E = E_o \left(\frac{\gamma}{\gamma_o}\right)^n \left(\frac{\sigma_1}{p_a}\right)^{\alpha K+\beta} \tag{14}$$

and

$$\nu = \nu_o + (b-\nu_o)\left[1- \left(\frac{\sigma_1}{p_a}\right)^{-a|\alpha K+\beta|}\right] \tag{15}$$

where: γ = dry density

γ_o = reference dry density

E_o = initial modulus at reference dry density

ν_o = initial value of Poisson's ratio at the reference dry density.

p_a = atmospheric pressure (used to keep equation dimensionless)

σ_1 = major principal stress

$K = \Delta\sigma_3/\Delta\sigma_1$

and α, β, a, b, and n are empirical coefficients. Although this formulation describes reasonably well the behaviour of soils, its usefulness is limited by the number of tests needed to characterize the soil.

1.3.5. Comparison of Soil Stress-Strain Models

Krizek and Corotis (12) compared the results of two field tests with the results of finite element analyses using different soil models.

They concluded that the integrated response characteristics (such as diameter changes) were not extremely sensitive to the specific nature of the input formulation for soil properties. On the other hand they found that the determination of response characteristics at discrete points (such as interface stresses, stresses at a point in the surrounding soil, or strain at a specific point in the pipe wall) were considerably more sensitive to the choice of soil properties. Krizek and Atmatzidis (11) concluded that while the order of magnitude exerts some effect on the response of the soil-pipe system the specific nature of the formulation (whether it be linear or nonlinear) did not have an appreciable influence. This was attributed to the fact that the reinforced concrete pipe was relatively stiff compared to the surrounding soil, regardless of the modulus values selected to characterize the soil. They went on to state that the use of sophisticated testing procedures such as true triaxial or plane strain, and the development of complicated constitutive models, such as hypoelastic or plastic models was not required since other simpler formulations will accomplish virtually the same objective with much less cost and effort. Krizek and Atmatzidis went on to suggest that for many purposes an adequate approximation to the response of a soil-pipe system could be obtained through the use of linear elasticity and a constant modulus.

For a greater degree of refinement they suggested a power law model such as that of Janbu but warned that such an approach necessitated a more expensive incremental or piecewise linear solution procedure for the finite element analysis.

This conclusion was reiterated by Krizek and McQuade (13) who found that

field measurements of pipe stresses and deflections indicated that a linear elastic soil model gave an equally acceptable fit to results as did complex nonlinear models.

1.4. Deformation Behaviour of Concrete Pipe

1.4.1. Concrete Stress-Strain Behaviour

For concrete under uniaxial compression, the relationship between stress and strain is almost linear for small stresses. However once the stress rises above 40% of the compressive strength, the strain will begin to rise more quickly due to the formation of microcracks at the interfaces between the mortar and coarse aggregate particles.

Eventually, increasing strain may cause a decrease in stress before the concrete fails in compression. Various expressions have been put forward to describe the shape for the stress-strain curve. Hognestad (16) proposed the following for the ascending part of the stress-strain curve.

$$\sigma = \sigma_{uc}\left[\, 2\,\frac{\epsilon}{\epsilon_o'} - \left(\frac{\epsilon}{\epsilon_o'}\right)^2 \right] \qquad (16)$$

where σ_{uc} = compressive strength of the concrete

ϵ_o' = strain at $\sigma = \sigma_{uc}$

Desavi and Krishnan (17) used the following to describe both the ascending and descending arms of the curve:

$$\sigma = \frac{E_i\,\epsilon}{1 + \left(\dfrac{\epsilon}{\epsilon_o'}\right)^2} \qquad (17)$$

where $E_i = \Delta\sigma/\Delta\epsilon$ at $\sigma = 0$

1.4.2. Steel Stress-Strain Behaviour

The behaviour of steel under stress is simpler than that of concrete, especially that of hard-drawn wire which is generally used in pipes in Australia today. The strain rises very close to linearly with stress until the stress gets to above 400 MPa, then increases progressively more quickly until the tensile strength of over 500 MPa is reached. Normally the range of stress in a pipe under field conditions will be within the linear range.

1.4.3. Models of Reinforced Concrete Pipe

The simplest model of an R.C. pipe is that of a circular ring of homogeneous linear elastic material. This was used by Kay and Hain (18) and (19) with an average value of E of 20000 MPa and ν of 0.2 . For use in a finite element analysis they divided the ring into 24 segments of 15 degrees each.

Katona (20) described the concrete pipe model used in the programme CANDE, (Culvert Analysis and Design). This finite element model considered both tensile and compressive behaviour of the concrete and used a trilinear stress-strain relationship to represent elastic, initial yielding and crushing behaviour. Steel behaviour was represented as linear elastic up to yielding and then plastic beyond that. Each element of the pipe then contains both tensile and compressive (if used) steel, as well as cracked and uncracked concrete.

Wenzel and Parmelee (21) described the model used in NUPIPE, another finite element programme. Here the thickness of the wall was subdivided into six concentric rings of elements, the second and fifth being steel and the others concrete. The stress-strain behaviour of the steel was taken to be linear while the nonlinear stress-strain formulation of Hognestad was used for the concrete. Tensile cracking of the concrete

and yielding of the steel were taken into account as well as bond slip between steel and concrete. The elements only subtended 3 degrees of arc so that there were 960 elements in the ring.

Krizek, Corotis and Wenzel (15) used a simplified version of the above but with 320 elements in the ring. The nonlinear stress-strain formulation of Hognestad was used for the concrete and the steel was taken to be linear elastic.

1.5. Elastic Continuum Approach

Although neither concrete nor most soils are in reality linear elastic materials, this assumption is useful in order to give an insight into soil-pipe interaction. Both analytical solutions using an assumption of linear elasticity, and finite element method solutions using either linear or nonlinear elastic behaviour have been carried out. Krizek et al (22) list the following advantages for the elastic continuum approach:

(1) The effect of soil-pipe interaction is automatically taken into account.

(2) Relatively basic material parameters are used.

(3) Pipes of intermediate stiffness can be considered.

One analytical approach is that of Burns and Richard (23) in which a pipe of linear elastic material is deeply buried in a weightless, isotropic, homogeneous linear elastic soil. The stresses and deformations of the culvert were determined for uniformly distributed loads applied at the soil surface. Höeg (24) carried out both experimental and analytical work on soil pressures on buried pipes taking into account the nonlinear behaviour of the Ottawa sand in which the pipe was buried. His finding was that while his experiments did not entirely validate his analytical work, they did at least show that the analysis included the significant

variables and correctly evaluated the relative importance of them. He concluded with a recommendation that the more refined numerical techniques taking into account soil inhomogeneities, anisotropy and local plastic yielding be developed. He also suggested that finite element methods would be suited to this task.

Kay and Krizek (25) reduced the Burns and Richard equations to a simplified form by assuming that the pipe is incompressible in the circumferential direction and is only subject to flexure.

Kay and Abel (30) used a finite element method to derive correction factors to the Burns and Richard analytical solution. These correction factors encompassed the effect of the proximity of the soil surface to the pipe, the effect of pipe compressibility, and the effect of the pipe sitting on a soil layer with different stiffness to the soil above.

Krizek, Corotis and Wenzel (15) used the finite element method to analyse both trench and embankment concrete pipe installations. Here a nonlinear stress-strain relationship was used for the soil whilst a more complex model taking into account reinforcement and cracking was used for the pipe. Account was taken in the analysis of the incremental effect of the fill being added. The results agreed reasonably well with measurements taken on the full sized field installations at East Liberty, Ohio.

Krizek and McQuade (13) used the same model to analyse various bedding configurations of the Mountainhouse Creek tests. The predicted diameter changes were in general agreement with those observed in the tests especially those for Zones 8, 9 and 12. The predicted interface stresses, however were quite different to those observed in the tests, but the authors noted that diameter changes are probably a more meaningful evaluation of the applicability of the model.

Kay and Hain (18) and (19) used the finite element method with

assumptions of linear elastic behaviour of pipe and soil to investigate soil-pipe interactions under embankment conditions. When applied to the results for Zone 9 of the Mountainhouse Creek test (31), (33), the model overestimated the height at which a 0.25 mm crack would occur by 20%.

Selig et al (26) developed a finite element model, simulating the nonlinear behaviour of both soil and concrete. This programme, SPIDA (Soil-Pipe Interaction Design and Analysis) can be used on either trench or embankment installations, sequential backfilling being taken into account. The programme was stated to give reasonable results in practice although the correspondence between the deflection results for Mountainhouse Creek and those predicted by the programme was poor.

Other finite element models have been put forward for use in design. CANDE (27), (28), was developed under the sponsorship of the US Federal Highway Administration, while another NUPIPE (29) was sponsored by the American Concrete Pipe Association. The model used in NUPIPE gave a reasonable prediction of the diameter changes in the East Liberty tests under trench and embankment conditions, and of the Mountainhouse Creek tests under embankment conditions. However due to the extreme complexity of this model, the programme required a large capacity computer and with the computers available at that time took a long time (20 - 30 minutes) to run.

1.6. Slippage at the Soil-Pipe Interface

The theoretical solution of Burns and Richard (23) for a pipe buried in an isotropic elastic soil subject to an even pressure used both a frictionless interface between pipe and soil, and a no-slip condition at the interface.

Kay and Krizek (25) showed that the maximum shear stress under this ideal

condition will occur 45 degrees above and below a horizontal line through the pipe centre. For $\nu = 0.4$, the shear stress was shown to range from 29% of the overpressure for rigid pipes to 36% for flexible pipes. They inferred from this that slippage under most circumstances was unlikely, but recommend nevertheless that the calculations be carried out using both slip and no-slip cases. Kay and Abel (30) continued this dual approach to the calculation of the system response. A correction factor was introduced for tangential compression for both cases, however further correction factors for the effect of surface proximity and layered soil were derived from a finite element model and treated only the no-slip case.

The finite element model used in NUPIPE did not allow for slippage, however that used in CANDE did, as well as separation and rebonding of the soil-pipe interfaces. Since NUPIPE was intended solely for use with concrete pipes whereas CANDE was also intended for flexible pipes, it appears that the possibility of slippage was included for the benefit of flexible pipes since the shear stress on the interface is higher on these than for rigid concrete pipes.

1.7. Summary

The Marston-Spangler theory of earth loads on buried pipes has been in use for several decades but is conservative in many cases, particularly for embankment conditions. Several attempts have been made to create accurate models of the soil-pipe system based on the concept of an elastic continuum. These include both analytical and numerical models. The numerical models using finite element computer programmes have used various constitutive laws to describe the stress-strain behaviour of the soils surrounding the pipe whilst both linear and nonlinear laws have been used to model the behaviour of the pipe itself.

Several of the papers surveyed made comparisons between the responses of the pipes in the model, and field measurements taken during the East Liberty and Mountainhouse Creek tests. Generally the comparisons of integrated responses (such as diameter changes) were reasonably good while comparisons of the responses at a point, such as soil-pipe interface pressure were less favourable.

The literature appears to favour the approach that effort is better spent on determining a reasonable value for soil modulus than on developing a complex nonlinear model for the soil. There is strong indication that a linear elastic modulus will give results that, for practical purposes, are as good as those obtained from the other models. At the same time they will use far less computer time during the finite element analysis. The results of this study add considerable weight to this view.

SECTION 2: FINITE ELEMENT ANALYSIS

Since time available on the test installation was limited and the running of many tests would have been expensive, the investigation of the proposed bedding method was firstly tackled by means of the finite element method. This method of calculation requires that the various material zones of the pipe and its surroundings be divided into elements each of which has allocated to it appropriate values of elastic modulus and Poisson's ratio.

2.1. Elastic Modulus Values for the Bedding Materials

Previous attempts at using the Finite Element Method to analyse the elastic response of the soil-pipe system have suffered from a lack of information about the modulus of the soil and bedding materials around the pipe.

Since no information existed to indicate the state of compaction of the bedding materials around the underside of the pipe, or of the elastic modulus of these materials in this situation it was necessary to undertake a preliminary test on a short length of the bedded pipe.

To achieve this end, a trial bedding arrangement was set up in the grounds of the Humes pipe factory at Pooraka, South Australia. Because it was difficult to sample compacted crushed rock and then test its modulus in the laboratory it was decided to attempt in-situ plate load tests through the wall of the pipe on the bedding materials. Wrench, (46) describes a method of using plate load tests along these lines to measure the elastic modulus of gravels.

A 1500 mm diameter test pipe was manufactured with six holes provided at specified locations on its lower surface, see Fig. 1. Teflon bushes were epoxied into these holes and a 75 mm diameter loading plate mounted on a shaft was attached to each of the six bushes.

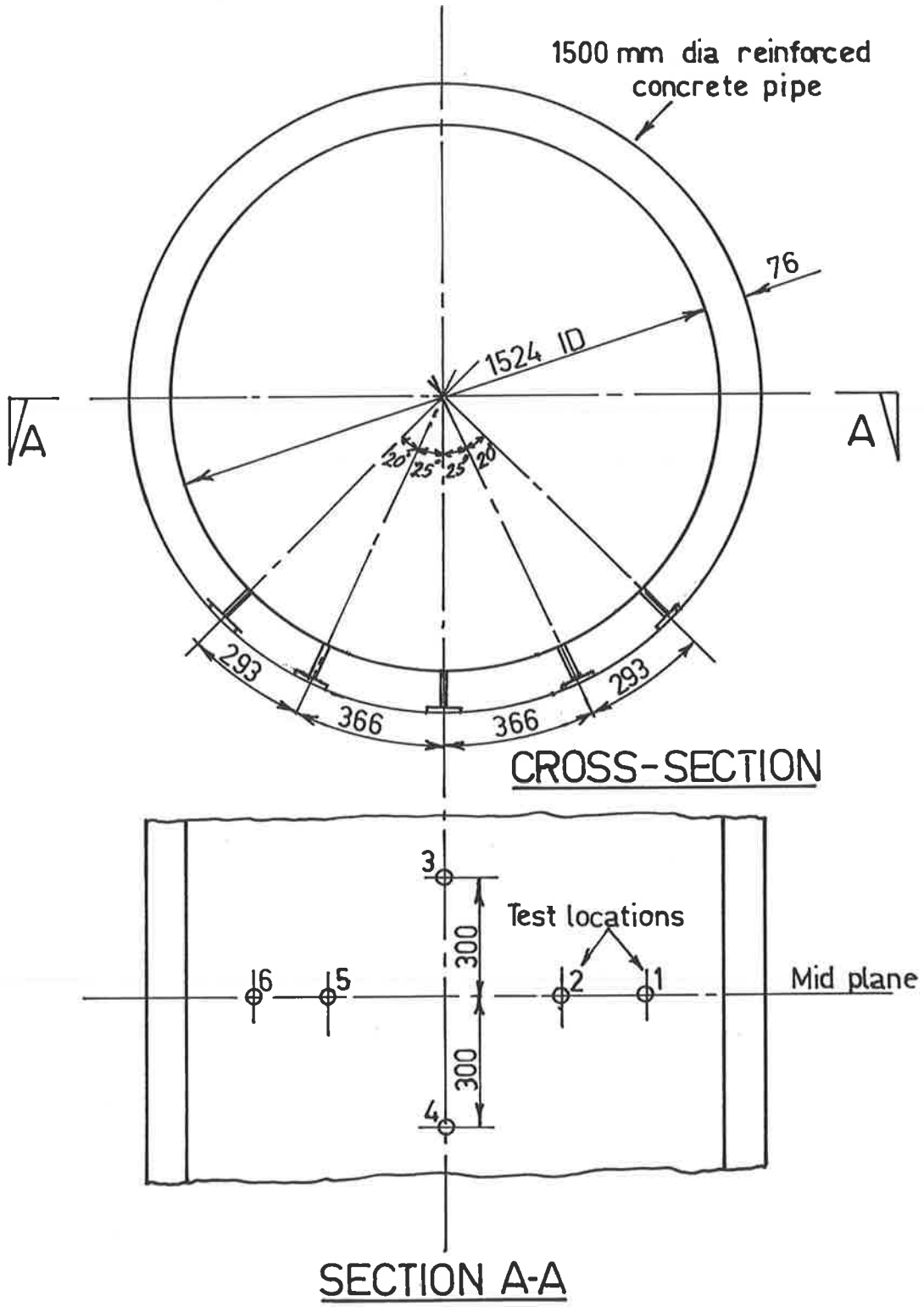

FIG.1 PIPE FOR TRIAL BEDDING

The pipe was placed on a compacted layer of packing sand in a shallow trench as shown in Fig. 2 and then 20 mm fine crushed rock was spread out in 100 mm layers on alternate sides of the pipe and as far under the pipe as possible. Grading analyses for these materials are shown in Figs. 3 and 4. As each layer was placed it was compacted with fourteen passes of a Mikasa MTR-80H tamper, as this type of machine walks forward at each stroke and there was not enough room in the narrow space at the side of the pipe to turn around at the end of each pass, seven of these passes were made by dragging the machine backwards. Compaction reduced the 100 mm layer to about 75 mm during the first couple of passes. Enough water was sprayed on to the material to suppress dust but no attempt was made to adhere to the optimum moisture content. The top two layers of the sidefill were given 20 passes this being intended to give all the lower layers some additional compaction at the same time.

When the sidefill was in place 4.5 tonnes of steel were placed on the crown of the pipe to act as a counterweight during the plate load tests.

A special frame was made up to transfer reaction from the load plate to the inside surface of the pipe, see Fig. 5. This frame was attached by means of M6 Hilti anchors inserted into holes drilled into the concrete. A hydraulic jack attached to the frame was used to apply a controlled rate of displacement to the load plate via the shaft. The applied load was measured by a load cell while the displacement was measured by a linear variable differential transformer (LVDT). Readings from both these instruments were displayed digitally on a readout unit and then recorded manually. Later this data was transferred to files on the Civil Engineering Department's PDP-11/34 computer so that graphs could be made on a plotter. Moduli were calculated using the approximation that the bedding behaved as a semi-infinite isotropic elastic body with the load

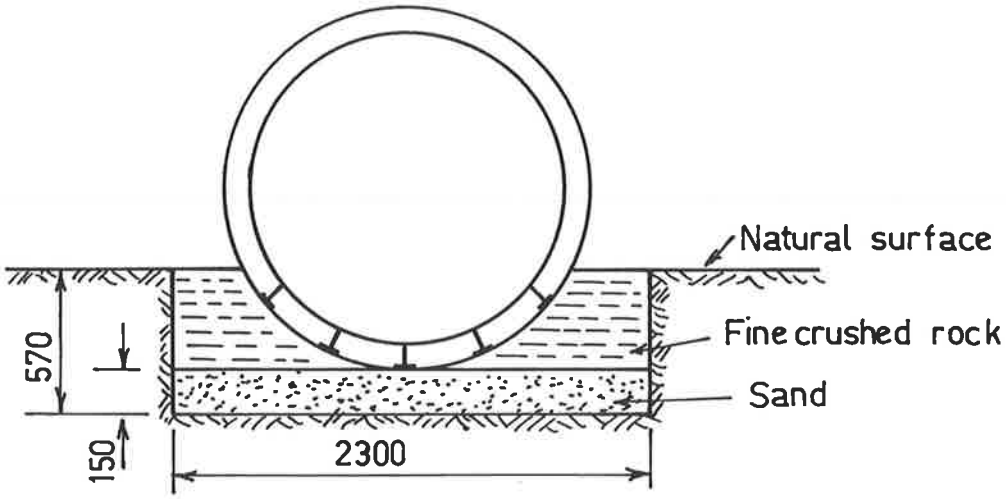

CROSS-SECTION

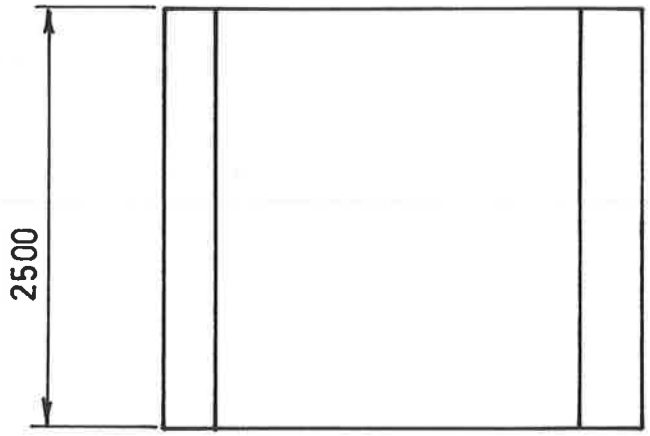

PLAN

FIG. 2 PIPE LAID ON TRIAL BEDDING

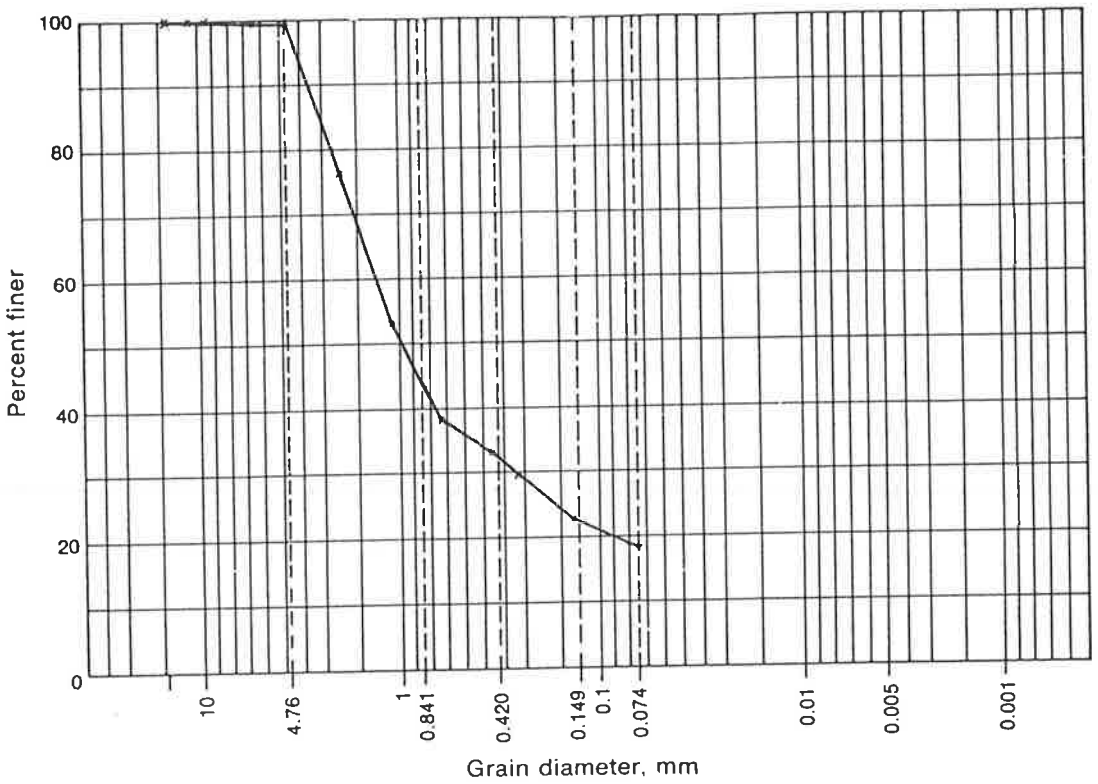

FIG. 3 GRADING ANALYSIS OF PACKING SAND

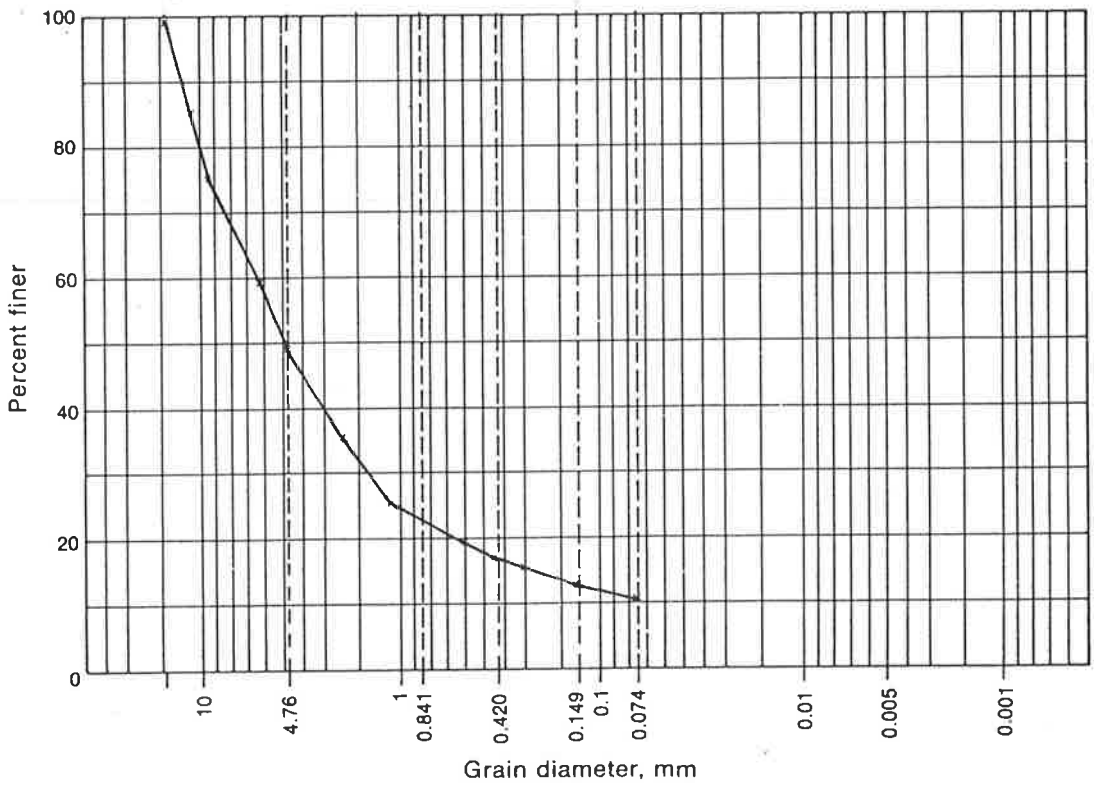

FIG. 4 GRADING ANALYSIS OF 20mm F.C.R

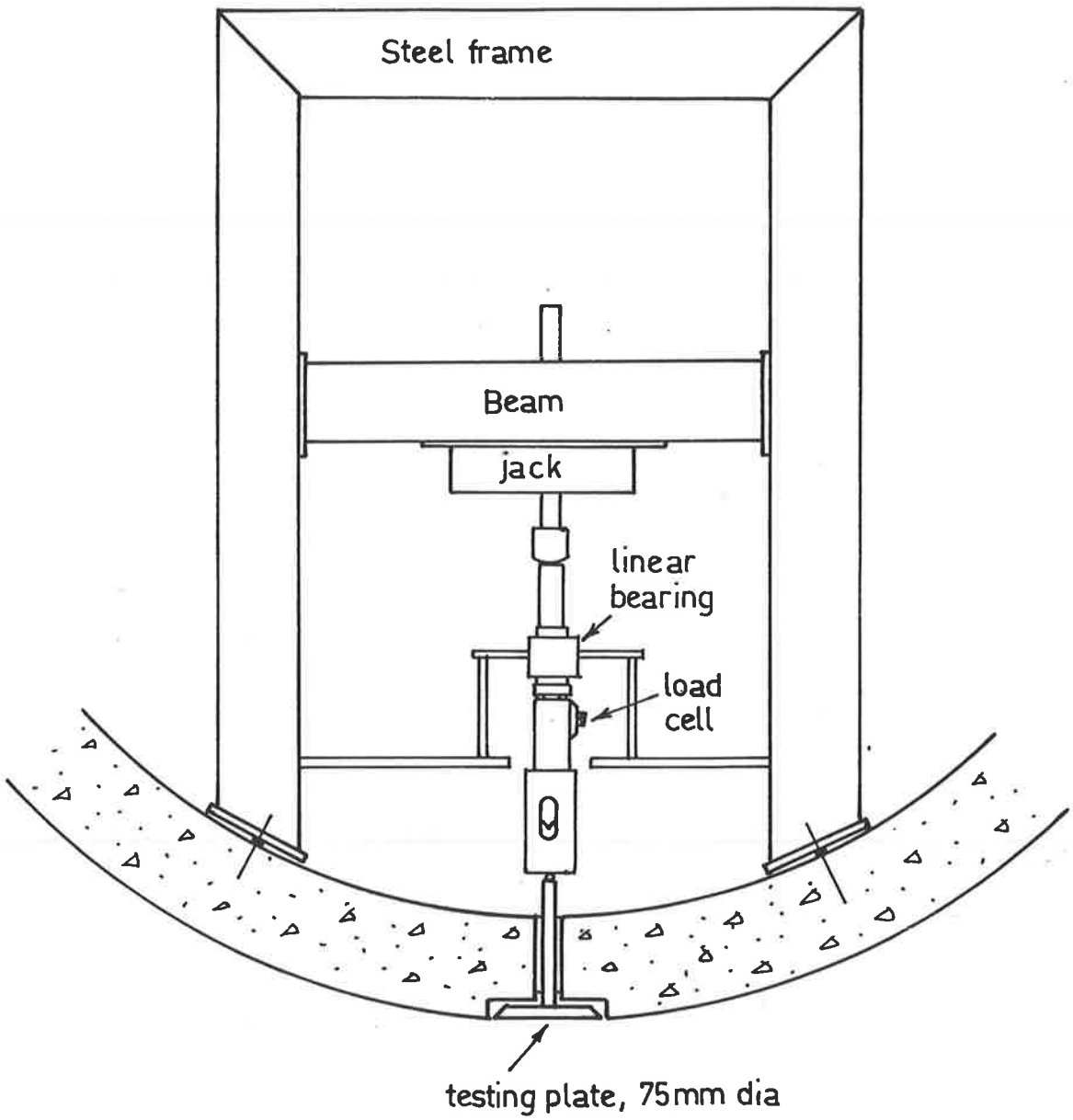

FIG. 5 PLATE LOAD TEST APPARATUS

plate imposing a deflection over a circular region of its surface. The errors introduced by the finite thickness of the tested zone and by the fact that the surface of the material around the test plate was not free, but in contact with the external surface of the pipe, were not expected to substantially affect the estimate of modulus obtained from this test. Poisson's ratio was taken as 0.3 for all the parts of the bedding. Since the bedding material was compacted against the plate by the vibration of the tamper it was expected that there would not be any surface irregularities to influence the initial modulus and that the test plate would "see" the compacted material in the same way as would a similar area of the external pipe surface as it underwent displacement. The results of these six plate load tests are shown in Figs. 25 to 30.

The deflection of a rigid loaded circular plate on a semi-infinite elastic body is given by:

$$\delta = \frac{0.88\ (1-\nu^2)\ q\ B}{E} \qquad (18)$$

where:

δ = deflection of plate

ν = Poisson's ratio of body

q = average load intensity

B = diameter of plate

E = elasticity of body

Rearranging:

$$E = \frac{0.88\ (1-\nu^2)}{\delta}\ \frac{4\ P}{\pi\ B} = \frac{P}{\delta}\ \frac{3.52\ (1-\nu^2)}{\pi\ B} \qquad (19)$$

Using the initial slope to obtain initial modulus:

$$E_i = \frac{\Delta P}{\Delta d}\ \frac{3.52\ (1-\nu^2)}{\pi\ B} \qquad (20)$$

Applying this to the six graphs and assuming $\nu = 0.3$ the results shown in Table 1. were obtained.

TABLE 1.

Location No.	Initial Tangent Modulus (MPa)	Secant Modulus (MPa) 0 to 580 kPa
1	32.9	2.6
2	8.2	2.0
3	29.5	13.8
4	82.7	70.7
5	6.1	1.8
6	40.5	4.3

2.2. Investigation of Relationship Between Modulus of Fine Crushed Rock and its Relative Density

The aim of this part of the study was to supplement the elastic moduli of the bedding materials obtained directly through the wall of the pipe with additional values which could be estimated from the measured field density of the compacted material.

In order to do this, measurements of the modulus of the fine crushed rock used for the sidefill were made in the laboratory, at various states of compaction, using the plate load test, see Fig. 6. A steel tub of 390 mm internal diameter and 312 mm depth was filled with fine crushed rock at variou densities (see Appendix A). A surcharge of 6.9 kPa was applied over an annular area extending from a 100 mm diameter circle at the centre of the tub to the inner edge of the tub. The 100 mm diameter hole at the centre of the surcharge plate enclosed a 99 mm diameter loading plate. The tub was then placed under a 50 tonne Avery testing machine capable of imposing a controllable rate of displacement. The 99 mm diameter disk was slowly pushed into the fine crushed rock by the testing machine while loads and deflections were measured by a load cell and an LVDT, the readings being recorded on a UCAM-5A data logger. The results are shown in Figs. 31 to 34. The range of load used to calculate the secant modulus of the compacted fine crushed rock, 0 to 580 kPa is approximately

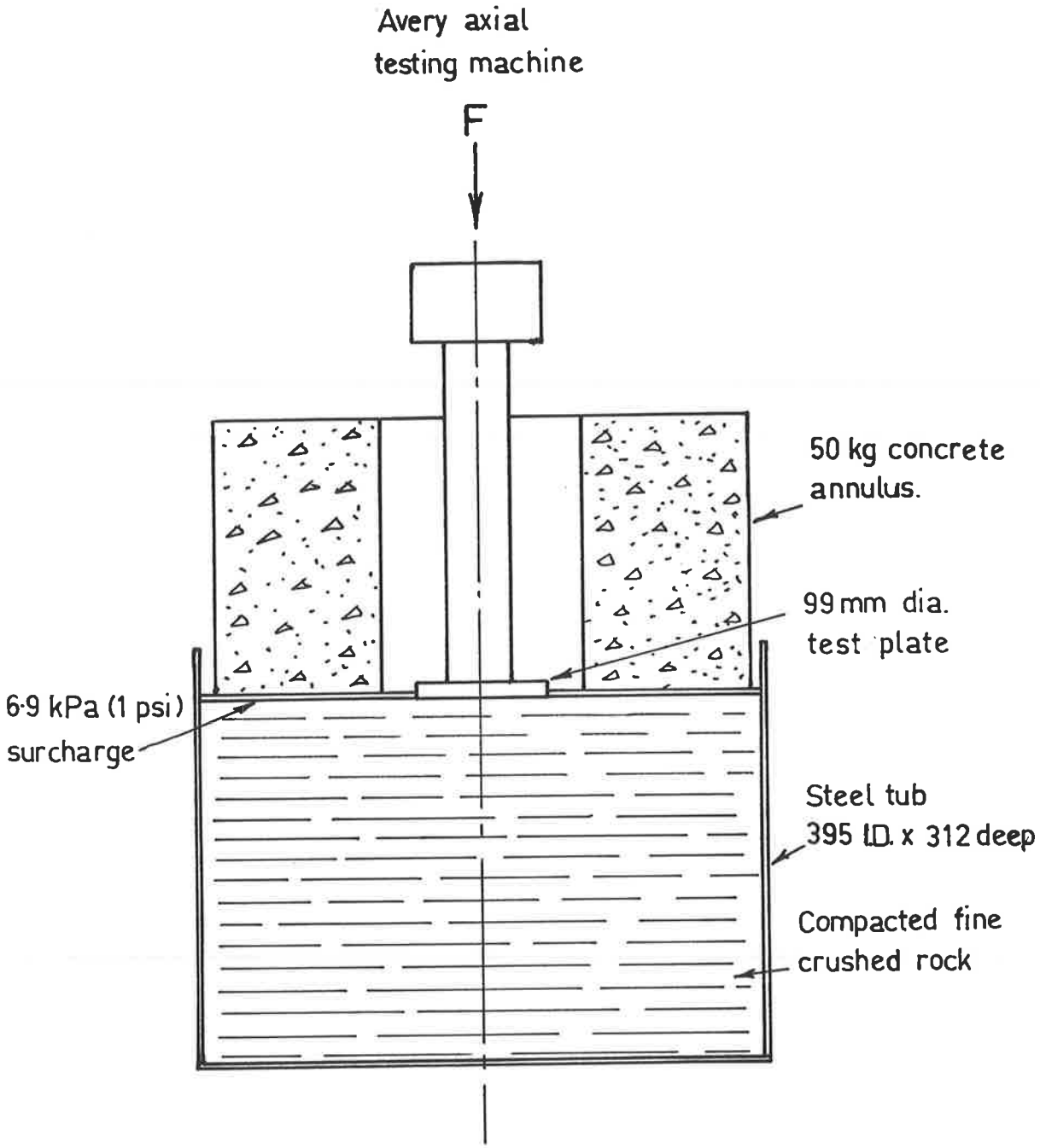

FIG. 6 LABORATORY PLATE LOAD TEST APPARATUS

the range of stress imposed by the construction of an embankment 30 m high.

The calculation of modulus was made using the case of a rigid circular loaded plate on an elastic layer of finite thickness as given by Davis and Poulos (34), p.178. Once again Poisson's ratio was assumed to be 0.3 and modulus values shown in Table 2. were calculated:

TABLE 2

Relative Density %	Initial Tangent Modulus (MPa)	Secant Modulus (MPa) 0 to 580 kPa	Reload Modulus (MPa)
51.8	14.6	1.8	-
70.9	13.7	7.4	-
81.6	29.4	19.1	174
100.0	42.2	42.4	-

2.3. Relative Density of Sidefill

After removing the pipe from the trial bedding the exposed surface of the bedding material was photographed, see Plates 1 to 4. Using the sand replacement method (sand-cone pouring apparatus) as described in Australian Standard AS 1289.E3.1 - 1977, density measurements were made throughout the fine crushed rock zone of the bedding. Measurements of the maximum and minimum dry densities of this material had earlier been made according to the method described in AS 1289.E5.1 - 1977.

Relative densities were calculated by the formula:

$$D_r = \frac{\gamma_{d\ max}}{\gamma_d} \times \frac{\gamma_d - \gamma_{d\ min}}{\gamma_{d\ max} - \gamma_{d\ min}} \times 100\ \% \qquad (21)$$

where:

$\gamma_{d\ max}$ = dry unit weight of soil in densest condition

$\gamma_{d\ min}$ = dry unit weight of soil in loosest condition

γ_d = in-place dry unit weight

Locations of the test holes and resulting relative densities are shown in

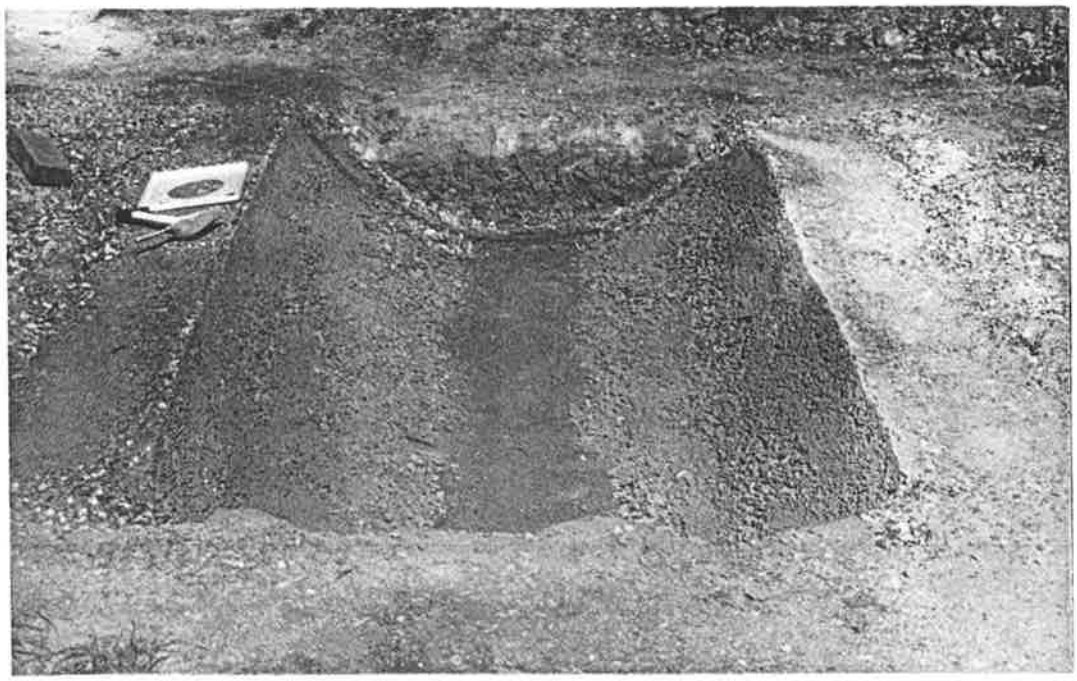

Plate 1

End view of trial bedding after removal of pipe, note exposed strip of fine aggregate base not covered by sidefill.

Plate 2

Note loose and irregular edge to fine crushed rock sidefill, imprint of plate load test visible in centre of base.

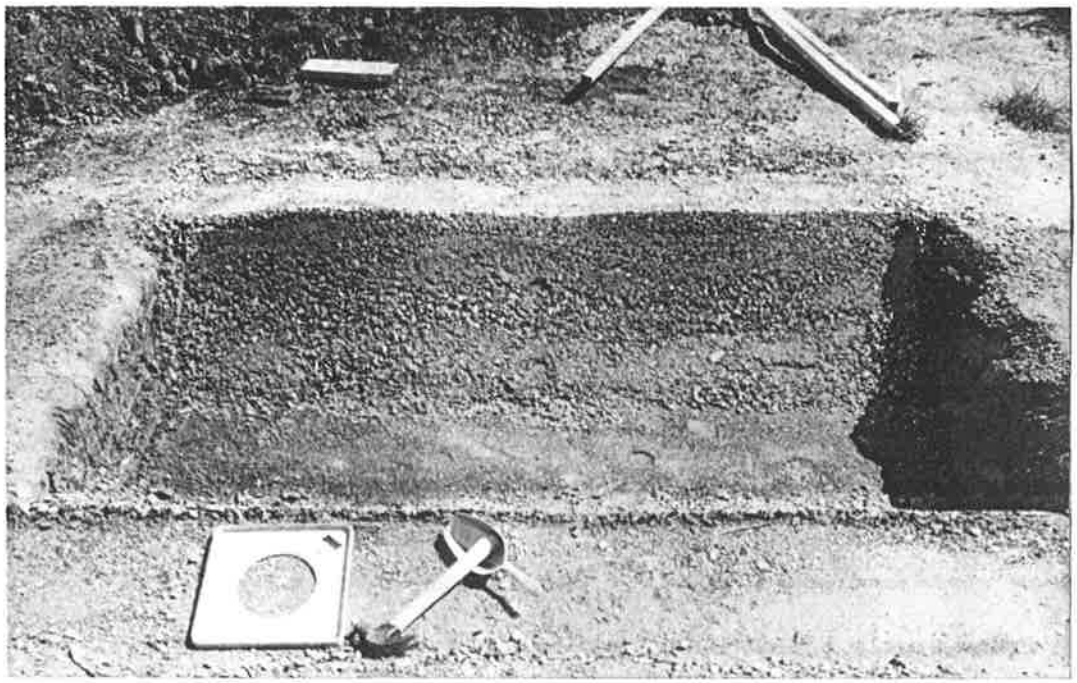

Plate 3

Side view of exposed bedding.

Plate 4

Closeup of exposed face of fine crushed rock sidefill, note gradation from loose at bottom to compact at top.

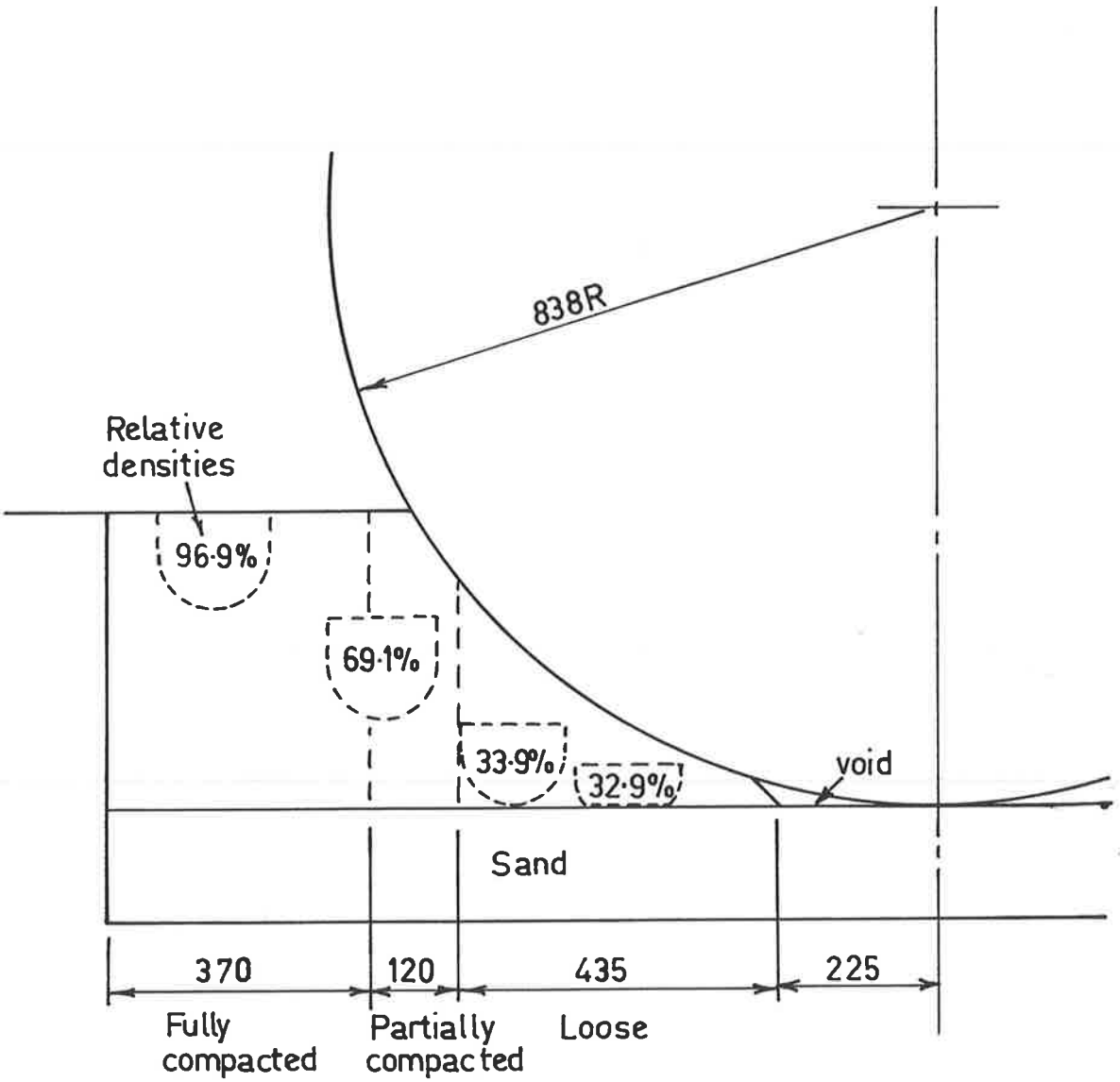

FIG.7 DENSITY HOLE LOCATIONS AND MEASURED DENSITIES

it was chosen for the job. ELASPIPE uses line "pipe" elements which incorporate circumferential compressive and bending stiffness but not wall thickness. The stiffness aspect of wall thickness can be considered by changing the element stiffness parameters. However, this does not provide for the geometric aspect of wall thickness and the average of the internal and external pipe diameters is used to represent the pipe as a line in the finite element grid. This leads to small geometrical inaccuracies in the representation of boundaries between different material zones adjacent to the surface of the pipe.

The boundary of the model representing the pipe in the field was made at 7 pipe radii from the pipe centre in the form of a square. This is in accordance with the recommendation of Kay and Abel (30) that the boundaries will not affect the pipe response if placed at this distance. Plane strain conditions were assumed for both pipe and surroundings in order to represent the condition of a long pipe. The pipe was also assumed to be bonded to the soil and bedding adjacent since according to Krizek et al, (22) p. 48, slippage was unlikely to occur. The slip elements available on ELASPIPE were thus not used. Using the values of modulus previously found the region around the pipe was divided into zones of varying stiffness and these zones were further subdivided into elements.

The finite element grid for the embankment situation is shown in Fig. 8. Advantage was taken of the vertical axis of symmetry of the problem, by only modelling one half of the pipe and its environment. All the nodes along the axis of symmetry were only subject to vertical displacement and the pipe nodes on the axis were fixed against rotation. A check of the model was made by giving all the elements identical elastic properties and comparing the results of a trial run with the analytical solution of Burns and Richard, (23) for an elastic pipe in an isotropic elastic

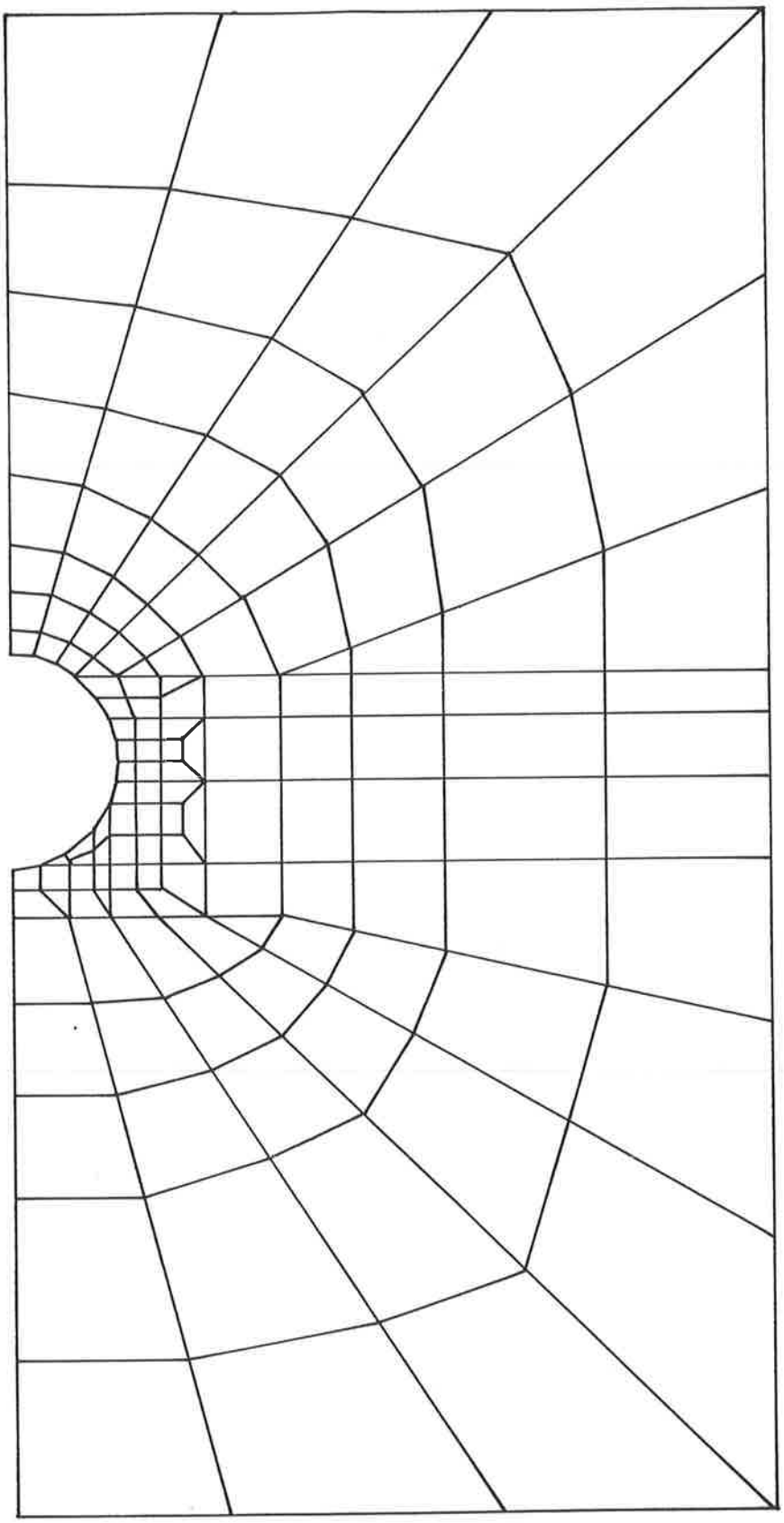

FIG. 8 FINITE ELEMENT GRID FOR PIPE BURIED UNDER EMBANKMENT

medium. Values of deflections and moments agreed within about 1% indicating that the programme and the finite element model were functioning correctly.

Since the pipe in the test bin would be in close proximity to the steel walls another model was considered that more specifically represented this situation. The grid used for this model is shown in Fig. 9, while the modulus values initially attributed to the various zones is shown in Fig. 10. In order to check this model against the Burns and Richard solution (23), the rigid boundary close to the invert of the pipe representing the floor of the test bin was replaced with a series of long elements placing the boundary once more at seven pipe radii from the pipe centre. When all the soil zone properties were made identical a trial run for this configuration again gave results in agreement with the Burns and Richard solution.

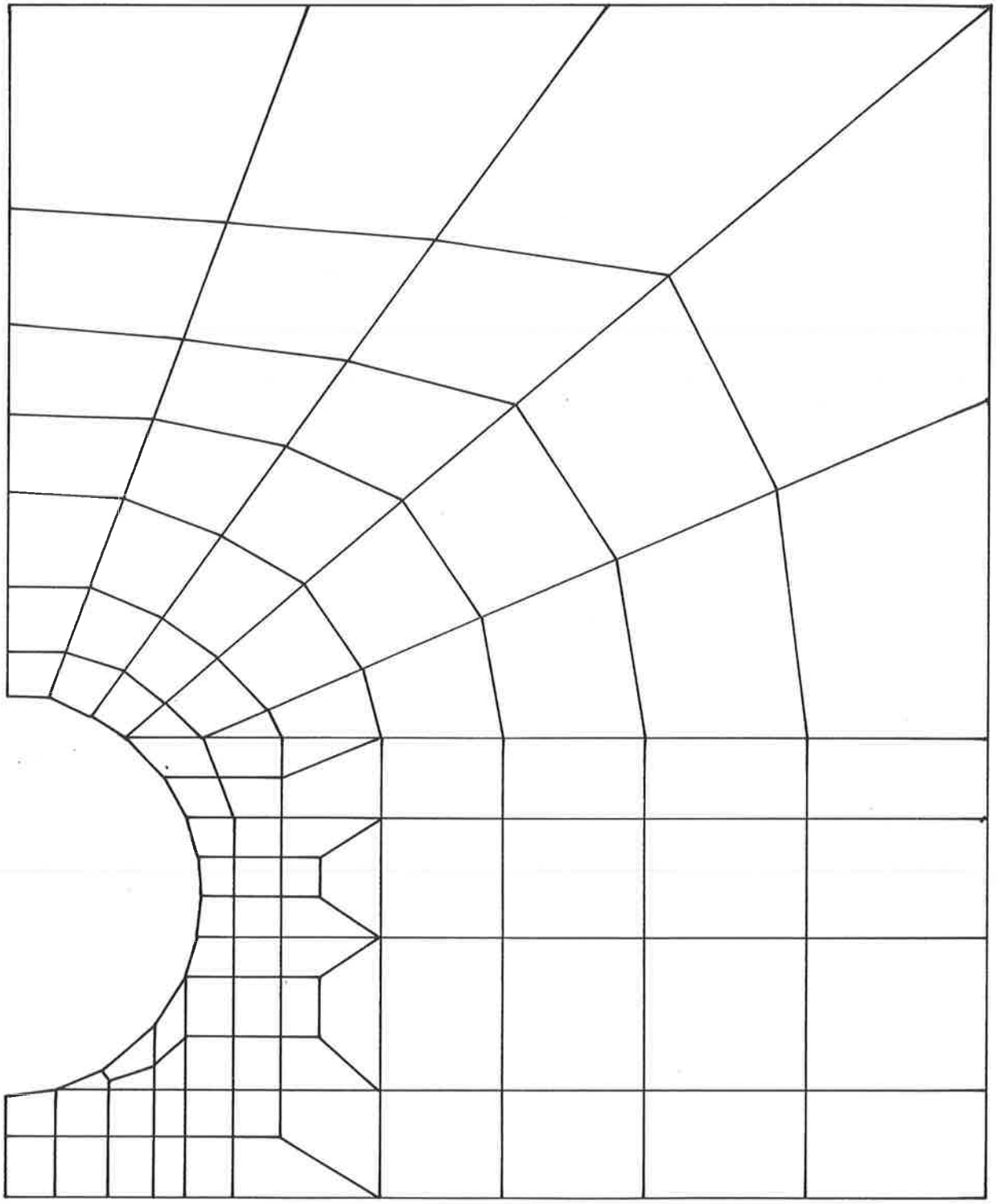

FIG. 9 FINITE ELEMENT GRID FOR PIPE IN TEST INSTALLATION

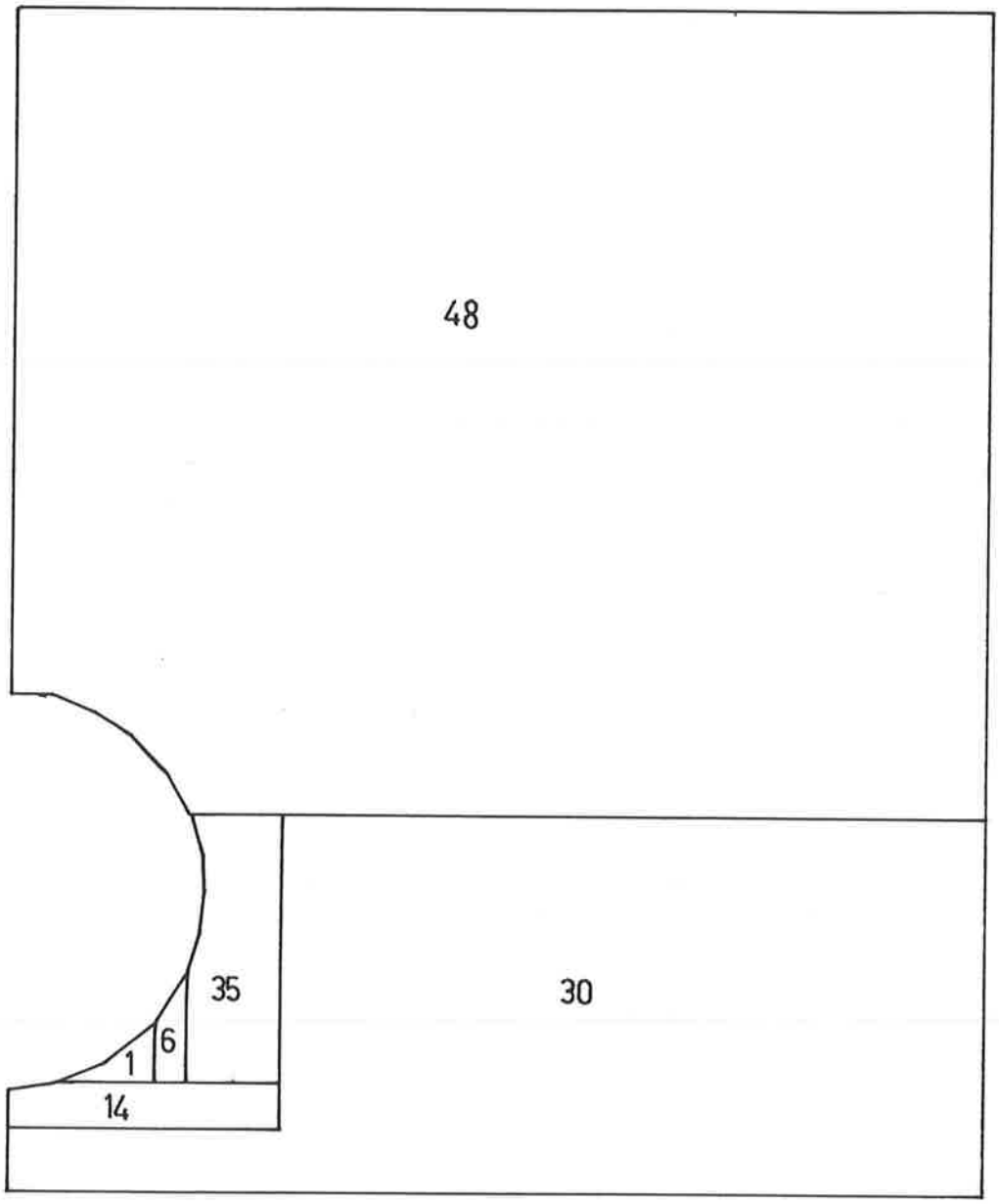

Modulus values marked within zones (MPa).
Poisson's ratio 0·3 for all zones.

FIG.10 MODULUS VALUES USED IN INITIAL FINITE ELEMENT MODEL

SECTION 3: EXPERIMENTAL INVESTIGATION

The experimental investigation consisted of two parts, a three-edge bearing test on a pipe, and a test of a bedded pipe subject to surcharge. The three-edge bearing test was intended to measure the strength of the pipe and enable its stiffness to be calculated. The second part of the investigation was intended to validate the finite element analysis.

3.1. Selection of Pipe for Test

An initial finite element analysis using the bedding moduli as measured indicated that a 750 mm diameter pipe designed to meet the load requirements for Class X as specified in Australian Standard AS 1342 - 1973, would produce a failure of the pipe within the range of load available at the test bin. Normal commercial pipes of this size and class only contain one circular reinforcing grid of hard-drawn deformed wire. Since it was desired to calculate moments and thrusts in the pipe wall at the quadrant points it was necessary to have measurements of strain at two points across the thickness of the wall at each of these locations. The derivation of the equations used in the calculation of the moments and thrusts is shown in Appendix C.

Resistance strain gauges attached to concrete generally fail when the concrete cracks in tension, because of this it was decided to use two concentric reinforcing grids with strain gauges on each grid at the quadrant points. Plain hard-drawn wire had to be used since the deformed wire used to reinforce this size of pipe is of an almost triangular cross-section and so even with the deformations removed, attachment of strain gauges was still virtually impossible.

A specially designed pipe was produced by the centrifugal spinning method, in two different lengths. A 1.22 m length was made for a three-edge bearing test while a 2.03 m length was made for installation in the

test bin. Both pipes were manufactured in accordance with the following dimensions:

Inner diameter = 762 mm

Wall thickness = 51 mm

Cover to inner circumferential wires = 10 mm

Cover to outer circumferential wires = 5 mm

Inner Grid - 6.23 dia wires @ 61 mm cts, Area = 0.497 mm^2/mm

Outer Grid - 6.23 dia wires @ 76 mm cts, Area = 0.400 mm^2/mm

At each quadrant point around the middle of the pipes polystyrene blocks were cast into the concrete to leave holes in which the strain gauges were later to be attached to the reinforcement. The holes measured 110 mm circumferentially by 60 mm in the direction of the pipes' axes and passed right through the thickness of the wall at each location exposing one wire from each grid. Kyowa KFW-5-C1 waterproof strain gauges were cemented to the wires and the holes filled with a fine concrete mix.

It was necessary to adopt this procedure rather than attach the gauges prior to casting because the gauges and leads would have been unlikely to survive either the centrifugal or roller suspension casting processes currently in use in Australia.

An additional strain gauge was cemented to a block of steel sitting inside the pipe to act as a dummy gauge. The lead length for this gauge was identical to that of the other gauges so that the effect of temperature on the strain readings would be minimised.

3.2. Data Collection System

The strain gauges were each connected to a separate channel on a Kyowa UCAM-5AT data logger as shown schematically in Fig. 11. The LVDT's were connected to the UCAM via a universal scanning box, a regulated voltage

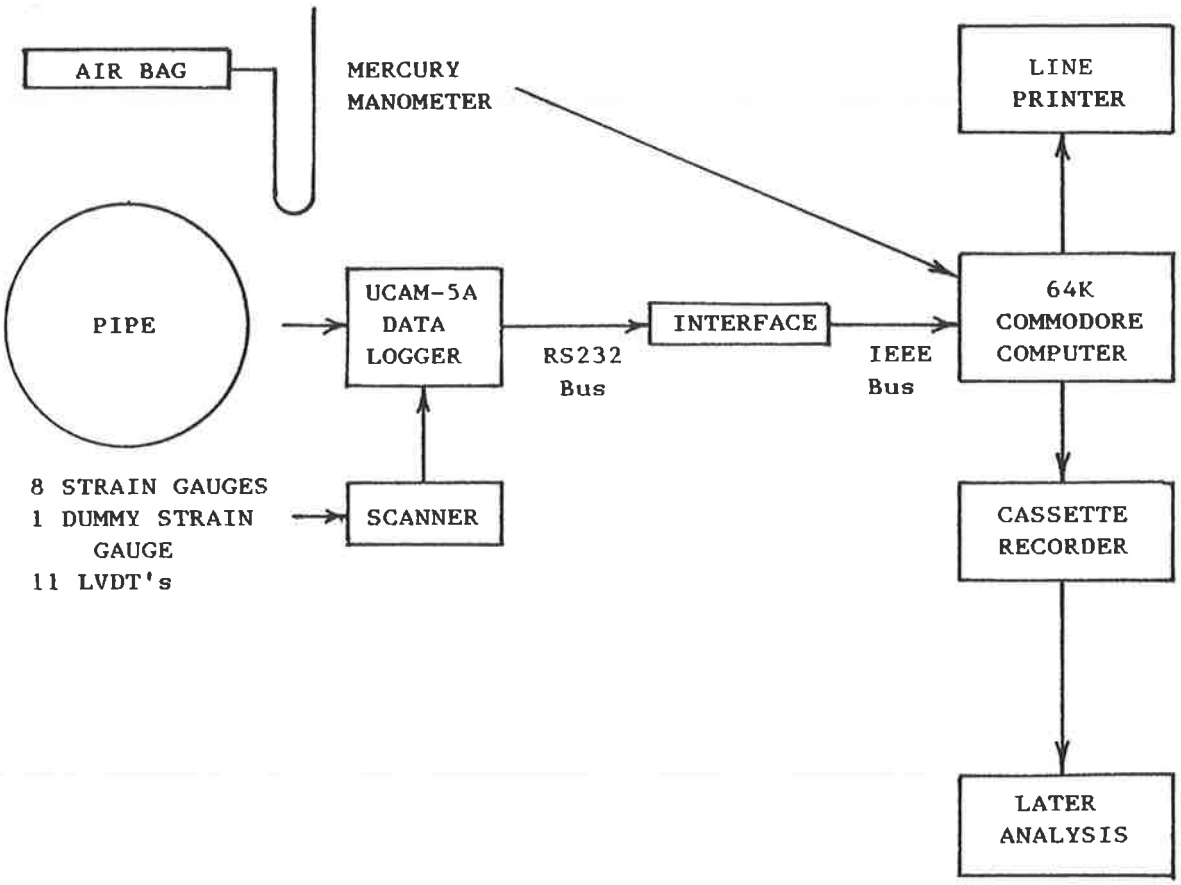

FIG. 11 - SCHEMATIC DIAGRAM OF DATA COLLECTION SYSTEM

being supplied to the LVDT's by a 15 Volt power supply. The UCAM was in turn connected via an IEEE/RS232 interface to a Commodore CBM computer. The computer was programmed so that when the carriage return key was pressed an instruction was sent to the UCAM to take readings of all the channels connected to both itself and the scanning box, and to transmit these back to the computer. The computer then sent these readings to a thermal printer for a hard record and to a data cassette recorder. The information recorded on the cassette was transferred to the Civil Engineering Department's PDP-11/34 computer for further processing and for graph plotting.

This system was used for both the three-edge bearing test and for the test on the bedded pipe at the Mile End test bin, the only difference being that for the three-edge bearing test a load cell was connected to the UCAM whereas for the bedded pipe test the air bag surcharge pressure was read visually from a mercury manometer and manually entered on the keyboard of the computer.

3.3. Three-Edge Bearing Test

The reasons for running this test were as follows:

(a) To establish the the cracking strength of the pipe, that is the load at which the largest crack reaches a width of 0.15 mm in accordance with AS 1342 - 1973.

(b) To determine the load-deflection characteristics of the pipe and so to calculate an appropriate value of the flexural modulus of the cracked pipe wall.

(c) To compare the moments and thrusts at the quadrant points of the pipe as calculated from the steel strains with those predicted by elastic theory.

3.3.1. Equipment

The 1.22 m length of pipe with strain gauges attached as described in 3.1 was set up on two rubber covered timber supports as shown in Fig. 12. Since for this test it was only necessary to measure diameter changes in the horizontal and vertical directions three LVDT's were required. These were mounted on a steel plate connected to the invert of the pipe so that they radiated out from the approximate centre of the pipe towards the crown and the two haunches. Connecting rods transmitted the radial movements of steel balls glued to the inside of the pipe at these three points to the LVDT's.

This arrangement of LVDT's was such that the change in horizontal diameter of the pipe could be found by adding the displacements of the two horizontally mounted LVDT's while the vertical diameter change was simply the displacement of the vertically mounted LVDT.

The vertical load was applied to the pipe by means of a manually operated mechanical jack, a spherical bearing was used to ensure that the load was concentrically applied and the load was spread evenly along the pipe by a universal beam section with timber and rubber packing as specified in Australian Standard AS 1342 - 1973.

A resistance load cell with two outputs was used to measure the load increase.

3.3.2. Procedure and Results

Load was applied in increments of about 1 kN. This was controlled by the jack operator who could read the load displayed on a BLH strain bridge connected to the second output on the load cell. Pressure was maintained on the jack handle to avoid load decrease at each increment.

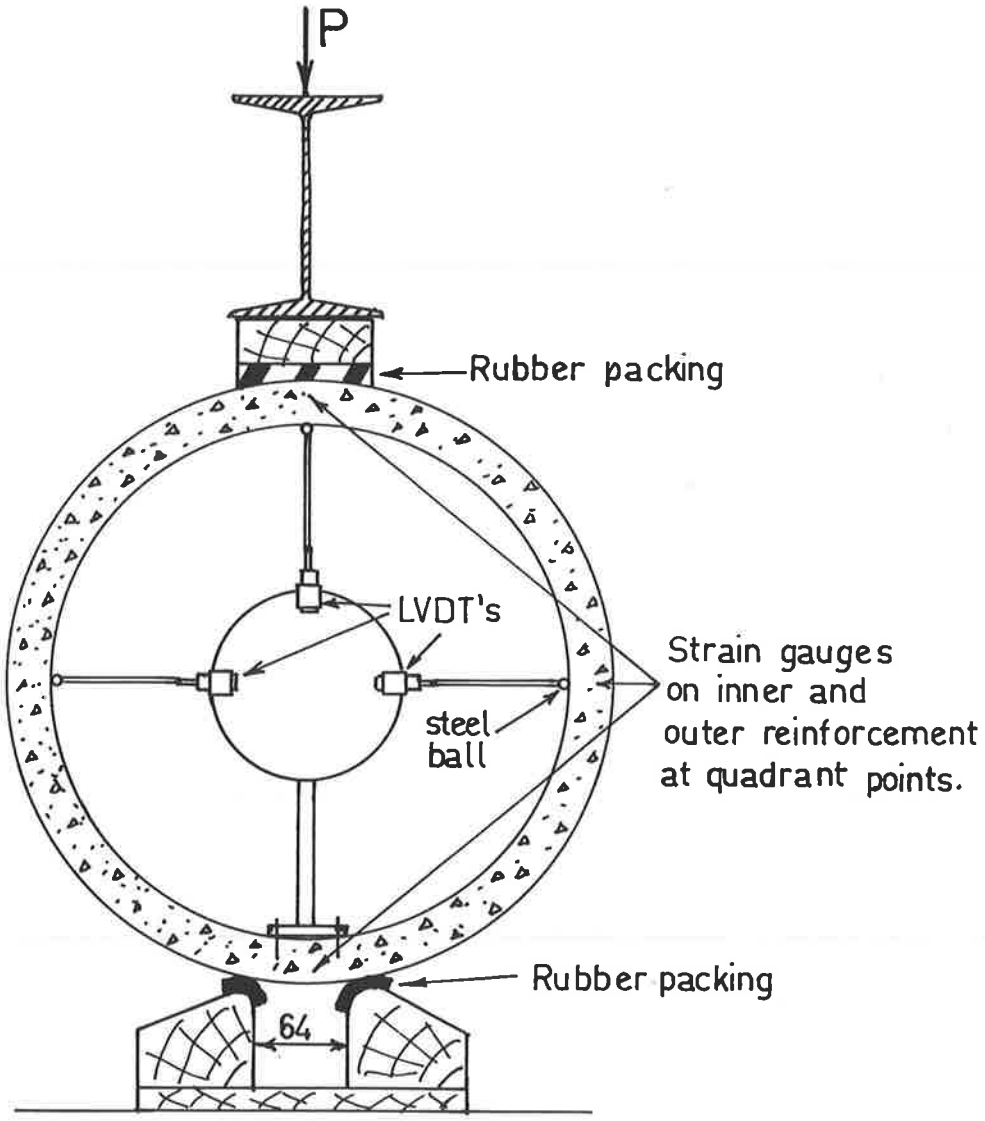

FIG.12 THREE-EDGE BEARING TEST

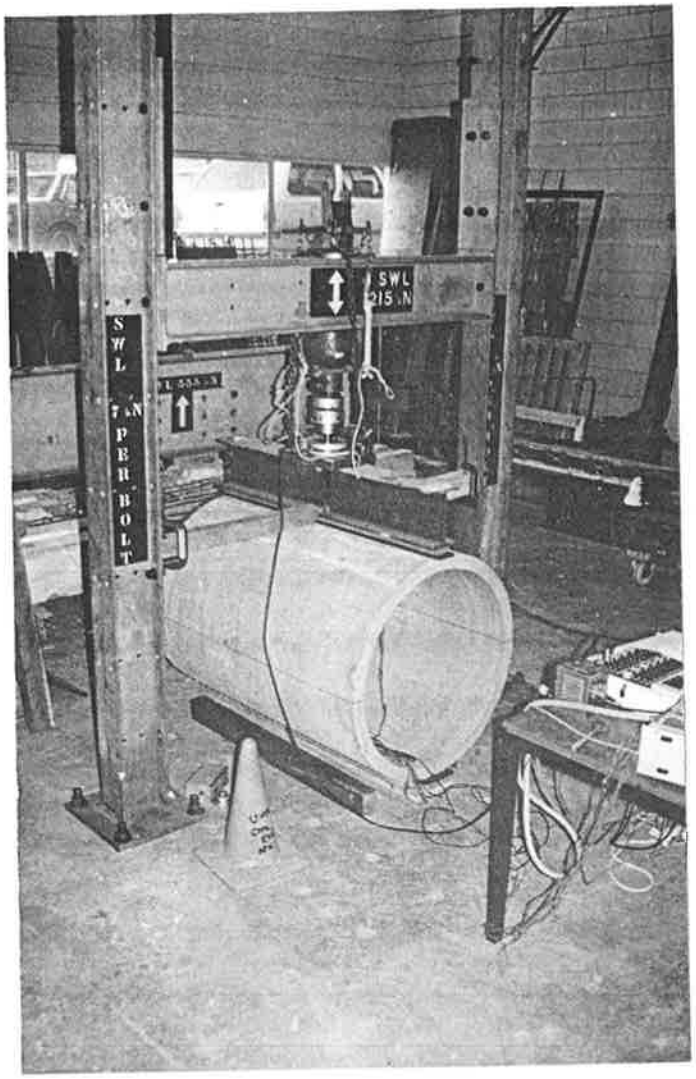

Plate 5

Three-edge bearing test set-up.

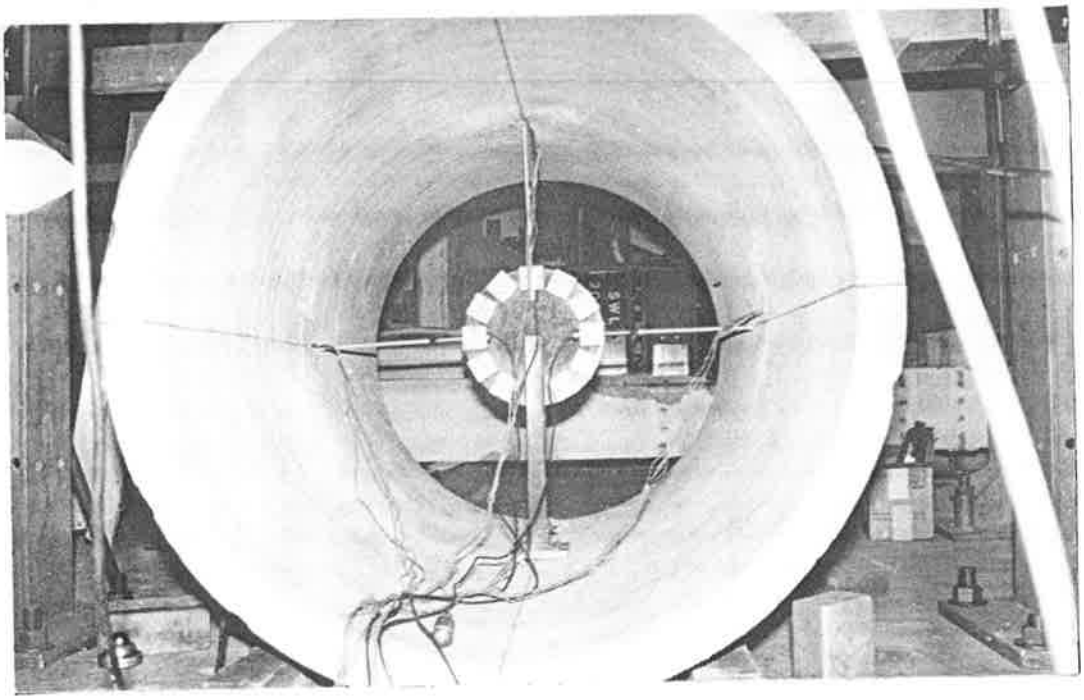

Plate 6

Three-edge bearing test, displacement measuring apparatus.

After each increment of load, readings of all the LVDT's and strain gauges were taken along with the load cell reading this information was collected and recorded by the data collection system described in 3.2.

The load was increased up to a point somewhat below the expected first cracking load of the pipe, then the pipe was unloaded in 1 kN steps. Finally it was reloaded to destruction.

Cracking progressed as follows:

14.0 kN/m	Crack 100 mm long at crown.
18.0 kN/m	Crack 200 mm long at invert.
21.4 kN/m	Crack along entire invert.
25.4 kN/m	0.15 mm crack along most of invert.
27.2 kN/m	0.15 mm crack along most of crown.
41.2 kN/m	External cracks near haunches.
73.7 kN/m	Shear failure at crown.

Diameter changes and calculated moments are shown in Figs. 35 to 40. Thrust values are not shown. Initial comparison attempts showed that thrust values computed from strains compared very poorly with those predicted from theory. This was probably because slippage of the steel brought about errors in the calculation of concrete strain and the area of compressive concrete. Because the calculated thrust in the section was the result of the relatively small difference between the large tensile and compressive forces in the steel and concrete, errors due to slippage brought about a proportionally greater error in the thrust. This did not have the same result in the calculation of moment, where the effect of the separate tensions and compressions were added.

3.4. Test of Pipe Bedded in Test Bin

3.4.1. Installation of Pipe in Test Bin

At the beginning of this study an installation suitable for testing bedded pipes under simulated loads was available at Mile End in South Australia. A detailed description of the facility has been given by Avalle, Flint & Kay, (40).

The major component of this facility was a rigid steel bin measuring internally 2 m by 4 m by 3 m high, capable of accommodating a 2 m length of pipe up to 750 mm diameter.

In order to minimise friction between the sides of the bin and the soil and pipe inside during loading, a layer of grease was applied to the internal vertical surfaces and 200 micron polythene sheeting was stuck to the grease.

To model the behaviour of the proposed type of bedding it was necessary to place a layer of soil in the bottom of the bin to act as "natural soil". Consideration was given to using compacted Hindmarsh clay which is abundant on the Adelaide Plains and which in its undisturbed state can have a modulus of up to 75 MPa according to measurements made by Kurzeme and Richards (41). However as the onset of winter rains wetted the available supplies and since it was unlikely that the high modulus of the undisturbed clay could be restored by compaction in the bin this alternative was rejected in favour of 20 mm dolomite quarry rubble.

It was not possible to use a petrol driven tamper in the confined space of the bin, so compaction of the quarry rubble was achieved by means of a 170 mm diameter steel butt mounted on a jack-hammer.

The quarry rubble was supplied to the bin by means of a bucket with a capacity of 0.1 m^3 which was lifted into the bin by the facility's gantry crane. The material was placed in 40 mm layers and compacted by

vibrating the steel butt into one area at a time. Since the device would not walk forward like a tamper, it had to be physically lifted forward each time to vibrate the next circle. The circles were overlapped so as to produce as nearly as possible a uniformly compacted layer.

The trench for the pipe and bedding was formed by placing timber formwork and continuing the compaction process each side of the void thus created. On removal of the formwork a layer of dolomite packing sand was placed at the bottom of the trench, levelled and lightly compacted. The pipe was centrally placed in the trench and then the sidefill was placed in 100 mm layers and compacted in a similar way to the quarry rubble. The placing and compacting operation of fine crushed rock alternated from one side of the pipe to the other so that lateral movement of the pipe as a whole could be minimised, this process continued until the fine crushed rock was flush with the top of the quarry rubble.

At this stage it was noticed that on one side the pipe had developed a crack 25^{o} below the haunch on the right-hand side which was entirely unexpected. The reference condition for the pipe was to be its state when bedded and buried but there was no way to find out its state of stress and deflection at this stage.

The gap between the ends of the pipe and the polythene lining of the bin was filled with a flexible rubber mastic to prevent loss of sand from the layer above. This seal was only applied to the part of the pipe end in contact with the sand as the fine crushed rock below was unlikely to escape through the 5 mm gap.

The sand filling was applied by means of a hopper travelling at a controlled rate, sand falling through 400 bushed holes, 10 mm in diameter, on to a parallel pair of dispersion screens then down into the test bin. This system placed a uniformly dense layer of sand 50 mm thick

at each pass of the hopper.

This process continued until a predetermined level was reached. The surface was then levelled to an accuracy of ±5 mm and the air bag placed on this surface. The position of the pipe and bedding in the filled bin is shown in Fig. 13. The air bag was held down by a steel lid which was in turn held down by a series of reaction beams attached to steel ties anchored to the base of the test bin.

3.4.2. Displacements

Radial displacements of the pipe wall were measured by eleven LVDT's mounted on a steel plate at the centre of the mid-section of the pipe which was firmly anchored to the pipe invert, see Fig. 14. Each LVDT was connected by a connecting rod to a steel ball glued to the inside surface of the pipe, the balls were located at 30^{o} intervals around a plane perpendicular to the pipe axis. The radial displacements obtained from the LVDT's were later adjusted to give a radial displacement for each of the balls relative to a theoretical pipe centre, a point equidistant from the crown and invert and also equidistant from the two haunches. Thus the LVDT's measured the change in the shape of the pipe rather than its absolute movement relative to the bin.

Consideration was given to installing soil pressure transducers in the pipe wall to measure normal soil pressure. However, after some testing with load cells to try and measure this quantity, this was abandoned as being too unreliable. (See Appendix B)

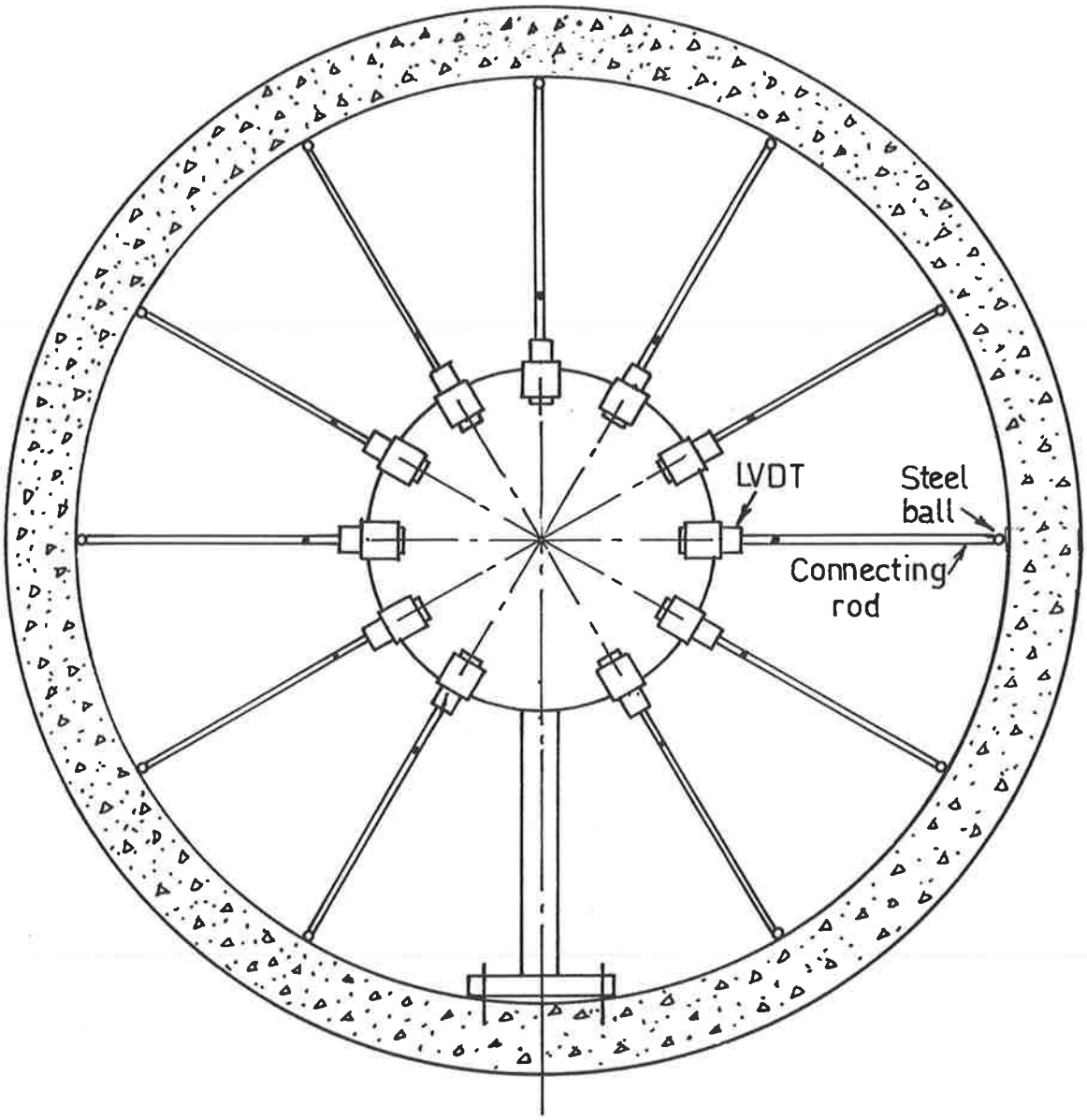

FIG. 14 BEDDED PIPE DISPLACEMENT MEASUREMENT

3.4.3. Test Procedure and Results

The surcharge on the surface of the sand was raised in increments of about 6.9 kPa (1 psi), after each increment the pressure was allowed to equilibrate and then all the strain gauges and LVDT's were read by the data collection system described in section 3.2. Observers at each end of the pipe reported the progress of the cracking. They were also equipped with feeler gauges to determine the progress of the cracking.

It had been intended to raise the pressure in equal increments to the maximum capacity of the air bag, 210 kPa, and then return the pressure in equal decrements to zero, repeating the cycle several times. However at a pressure of 171.1 kPa the air bag burst, this apparently being caused by settlement of the sand at one corner.

Because of the rapidity of the pressure drop, no readings could be taken during the pressure decrease. When the air bag burst original crack which had formed during the compaction of the sidefill had reached a width of 0.15 mm.

Cracking progressed as follows as surcharge increased:

69.8 kPa	First crack along invert and 1 o'clock.
74.9 kPa	Crack at 8 o'clock.
102.2 kPa	1 o'clock crack extended more than 50% of length of pipe.
108.8 kPa	Original 4 o'clock crack 0.15 mm wide.
122.5 kPa	4 o'clock crack wider.
164.7 kPa	Hairline crack at 8 o'clock.
171.1 kPa	Air bag burst.

Radial displacements, calculated moments and thrusts are shown in Figs. 41 to 60.

3.4.4. Plate Load Tests

Following the removal of the reaction beams, cover and air bag from the top of the test bin, a series of plate load tests was made to measure the elasticity of the contents of the bin. For the two tests that were made on the sand a metal sleeve was pushed 180 mm into the sand surface, as shown in Fig. 15, and the sand vacuumed out until a flat base was obtained at the level of the bottom of the sleeve.

A steel plate 125 mm in diameter was carefully placed on this base so as not to disturb the sand. On this was centrally placed a spherical bearing and then drill rods connected this to a motor driven mechanical jack. The two tests were made at about 700 mm each side of the mid-point of the centreline of the pipe, the base of the load plate being about a metre above the level of the crown of the pipe.

Load was measured by a load cell and the displacement of the top of the drill rod was measured by an LVDT. Readings were taken by means of the data collection system described in 3.2, but set so that readings were taken automatically at intervals of a few seconds.

Two tests were made on the sand, two on the quarry rubble and two on the fine crushed rock sidefill of the pipe. For the tests on the sand the reference datum was an inverted U-shaped piece of 50 mm water pipe with its two ends embedded into the sand well clear of the load plate. The load-deflection curves for the two tests are shown in Figs. 61 and 62.

For the tests on the other materials in the bin no other datum was available apart from the loading frame itself, which had previously had its load-deflection characteristics measured. However these characteristics were subsequently found to vary so much that the variation completely masked the load-deflection behaviour of the loaded plate, rendering these tests useless.

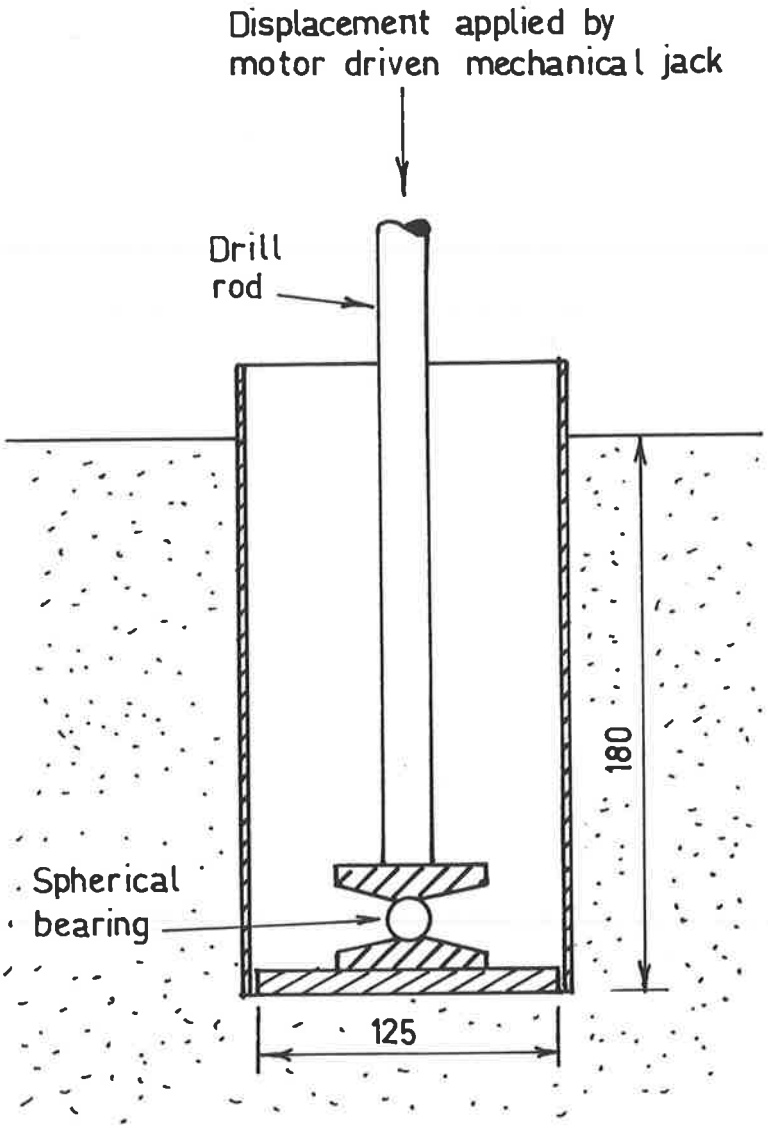

FIG.15 PLATE LOAD TEST ON RAINED SAND IN TEST BIN

The elastic modulus for the sand was calculated from the gradient of the force-deflection curves using the average of the reload curves. Once again the elastic solution for a circular rigid plate on an elastic half space was used. The presence of the 180 mm height of sand above the level of the plate's contact with the sand was ignored, this just serving to provide a surcharge on the sand below the plate so that a bearing failure would not occur at a small load.

Young's modulus was calculated to be 48 MPa for the reload curves. This is consistent with the results of oedometer tests on the rained sand at the installation reported by Avalle, Flint and Kay, (40) which yielded a constrained modulus of 54 MPa from which by assuming a Poisson's ratio of 0.3, Equation 2. gives a Young's modulus of 40 MPa.

SECTION 4: ANALYSIS AND DISCUSSION OF TEST RESULTS

4.1. Analysis of Results of Three-Edge Bearing Test

The decrease of the vertical diameter of a thin elastic pipe under line load top and bottom for its full length is given by elastic theory as:

$$\delta = 0.149 \frac{P\ r^3}{D\ l} \qquad (22)$$

Where: P = applied load

r = mean radius of pipe

l = length of pipe

D = flexural stiffness of pipe wall

$$= \frac{E\ t^3}{12\ (1-\nu^2)}$$

Where: E = elastic modulus of concrete in flexure.

t = wall thickness.

ν = Poisson's ratio of concrete (assumed to be 0.15).

Figs. 35 and 36 clearly indicate the bilinear nature of the force-deflection behaviour of reinforced concrete pipe. The initial slope of the load-vertical deflection curve (see Fig. 35) was 43.3 kN/m, which on substitution into Equation 22. gave a value of equivalent Young's modulus for the pipe in flexure as 31440 MPa. As the stress in the tensile steel reached the end of its linear range and the steel began to yield large cracks developed. As this occurred, the apparent value of Young's modulus dropped to less than 4000 MPa, however it is generally considered that concrete pipes are unserviceable in this region owing to the possibility of reinforcement corrosion in the wide cracks.

The first visible cracking occurred at the crown at a load of 14 kN/m. A crack at the invert reached a width of 0.15 mm at a load of 25.4 kN/m, this fell short of the load requirement of 32 kN/m specified in Australian Standard AS 1342 - 1973, probably because plain wire had been

used for reinforcement rather than the customary deformed wire. The lack of deformations on the wire surface allowed greater slippage between steel and concrete causing wider cracks to form. Additionally, because the final stage of the wire drawing process occurs when the deformations are rolled on, the wire used was not fully hard-drawn. This is shown by the low value of yield stress in Fig. 23.

Bending moments calculated from the strain gauge readings agreed reasonably well with those predicted by elastic theory for the haunches, see Figs. 38 and 40. However at the crown and invert, Figs. 37 and 39, moments were less than the elastic prediction until visible cracking occurred at the crown and invert, after which the calculated moments were greater than the elastic prediction. The underestimate before cracking is probably due to slippage between the steel and concrete caused by a combination of high shear in the region of the line loads and the poor bonding characteristics of plain wire. This slippage upsets the "plain sections remaining plain" assumption implicit in the calculation of moments from strains.

In addition since the strain gauges were located in holes in the pipe wall afterwards filled with fine mix concrete, the strains measured at these locations may not have been entirely representative of the rest of the section.

4.2. Analysis of Results of Test on Bedded Pipe

4.2.1. Comparison with Finite Element Prediction

The measured deflections of the test pipe were far less than those predicted by the finite element model using the elastic moduli measured in the earlier plate load tests as indicated in Table 3.

TABLE 3

Diameter changes under 171.1 kPa surcharge.			
	Actual (mm)	Predicted (mm)	Predicted/Actual
Horizontal	+0.068	+1.09	16
Vertical	-0.125	-1.20	9.6

This indicates that the moduli measured in the plate load tests were much lower than those experienced by the pipe in the bin. Höeg, (24) demonstrated that the deflection of a flexible pipe was inversely proportional to the modulus of the material around it. While this pipe was not in the usual sense flexible, the surrounding material had such a high modulus that Höeg's observation could be used to obtain a first approximation for further finite element analysis.

Subsequent trial runs of the programme were made, and on each run values of elastic modulus for the different zones were adjusted to try to obtain the deflection profile of the pipe. The best fit to the profile of the left-hand side of the pipe (see Figs. 17 and 18) was given by the moduli shown in Fig. 16. A reasonable agreement was obtained between the moments predicted by the finite element model and those calculated from the measured steel strains, in particular the moments at 12 and 3 o'clock compare favourably as shown in Fig. 19.

It is a reasonable presumption that had the pipe not cracked at the time of sidefilling the deflection profile of the right-hand side of the pipe would have been very close to a mirror image of the left.

A modulus value of 800 MPa in the fine crushed rock sidefill was required in the finite element analysis in order to obtain reasonable agreement with the measured deflections of the pipe. NAASRA, (38), (39) give modulus values of from 100 MPa to 700 MPa for this type of material when used in flexible road pavements. Under the more confined conditions

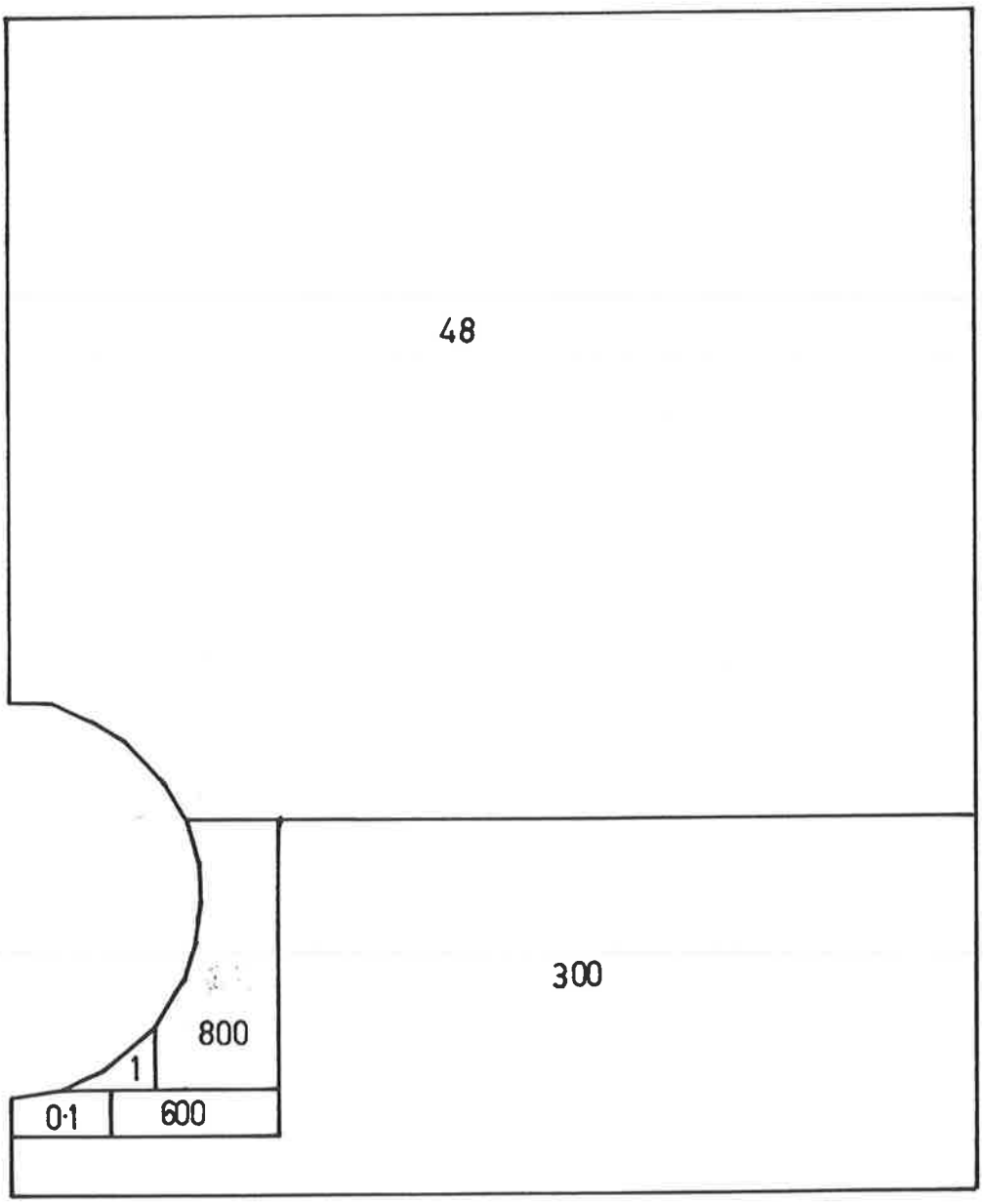

Modulus values marked within zones (MPa).
Poisson's ratio 0·3 for all zones.

FIG.16 MODULUS VALUES USED IN REVISED FINITE ELEMENT MODEL

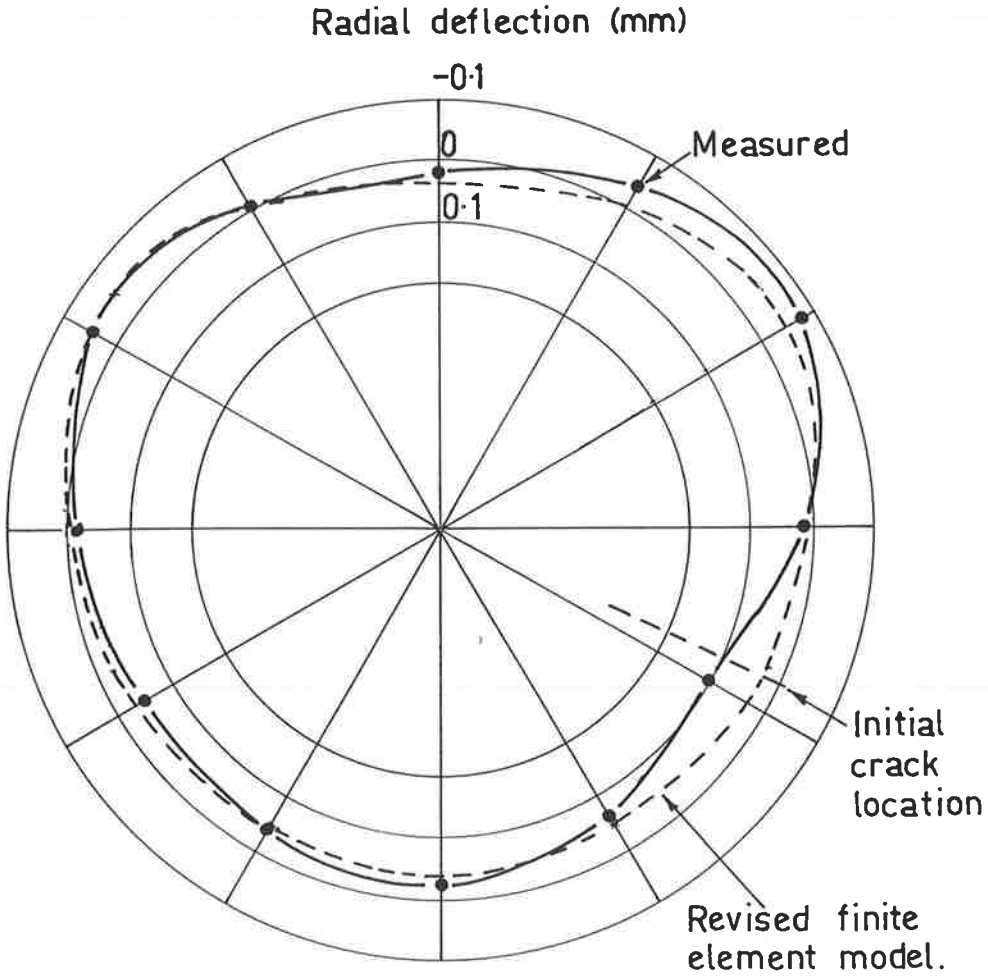

FIG.17 BEDDED PIPE TEST- RADIAL DEFLECTION PROFILE AT 819 kPa SURCHARGE

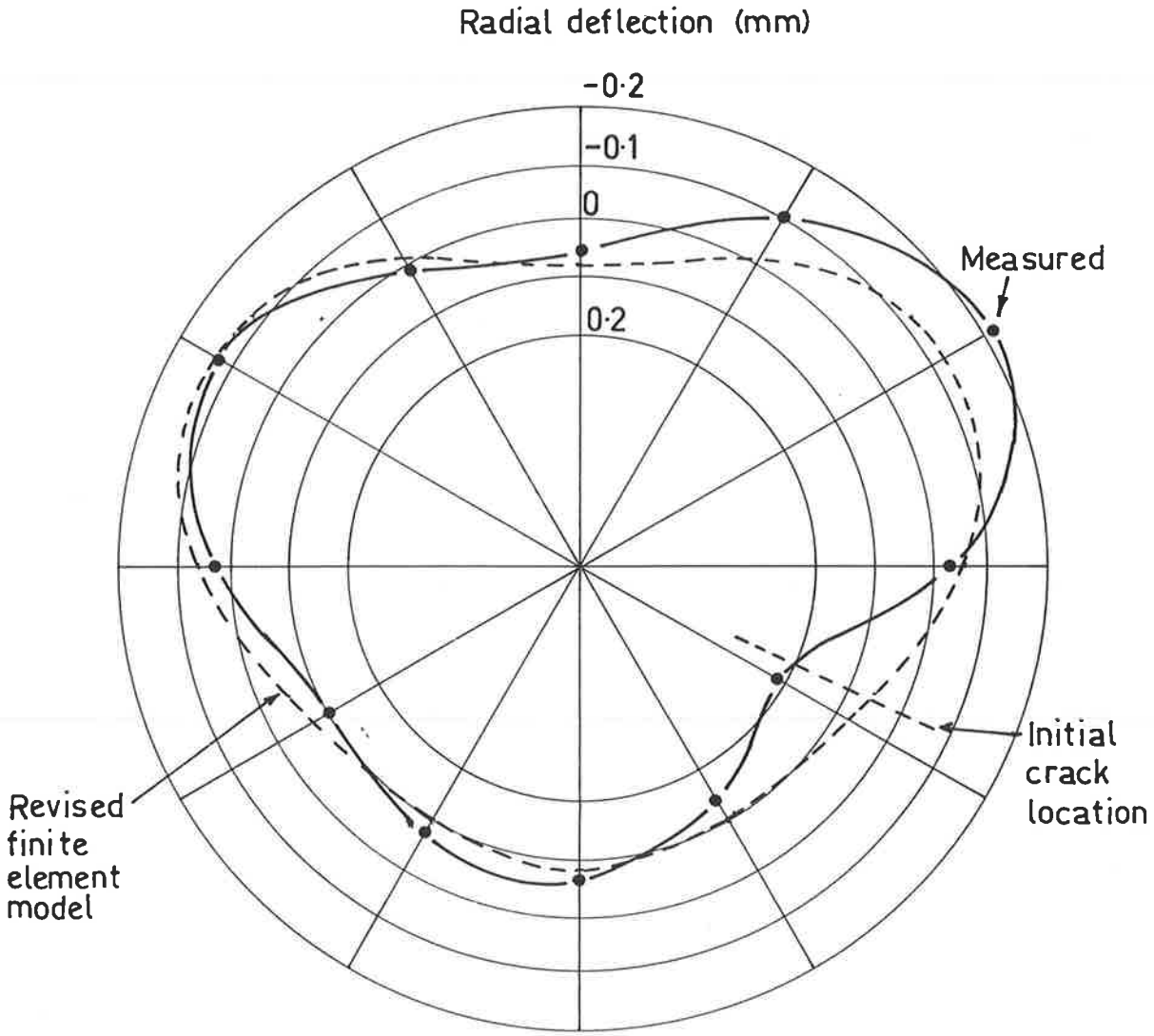

FIG.18 BEDDED PIPE TEST - RADIAL DEFLECTION PROFILE AT 171·1 kPa SURCHARGE

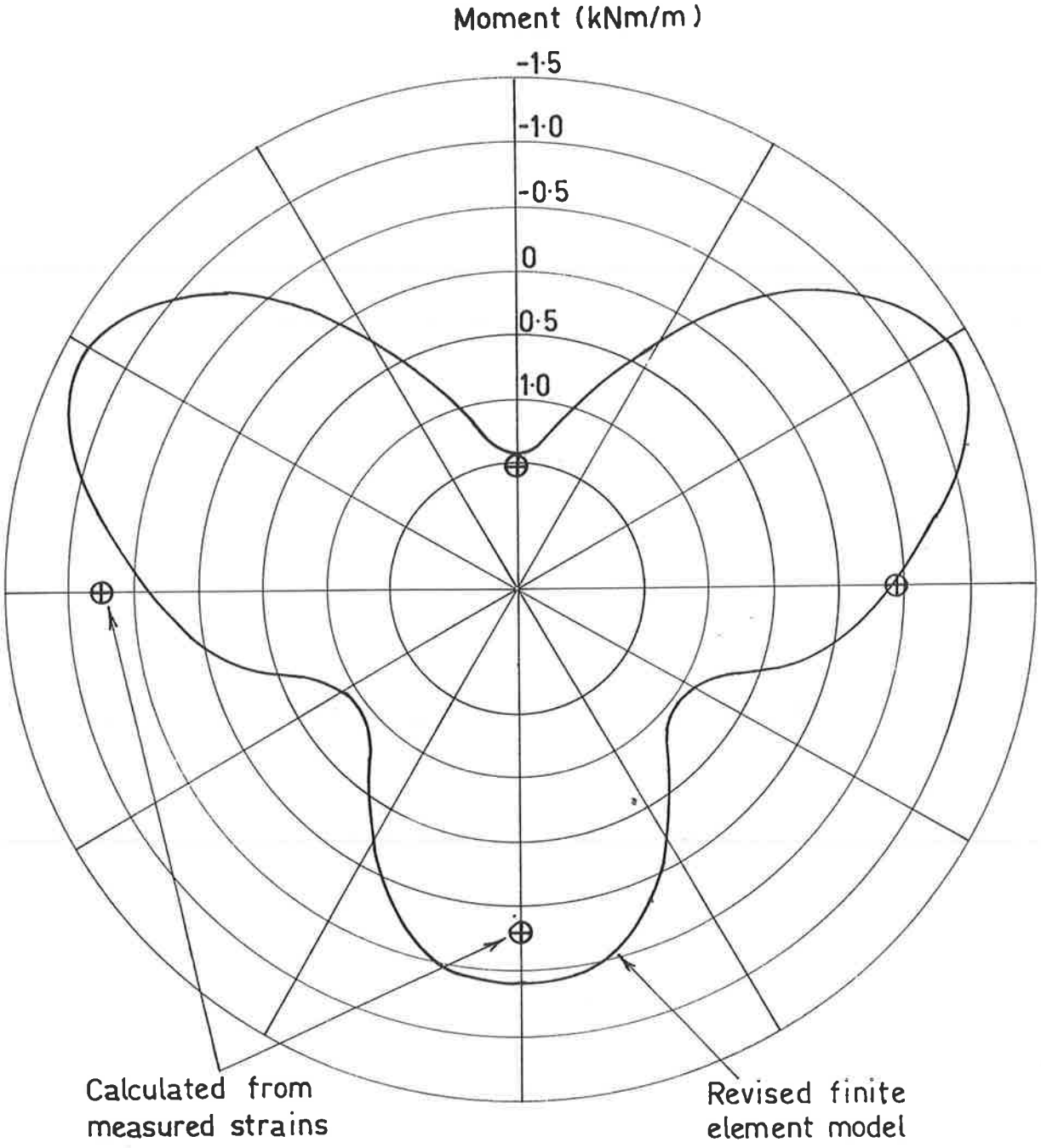

FIG.19 BEDDED PIPE TEST - MOMENT PROFILE AT 171·1 kPa SURCHARGE

adjacent to a buried pipe a modulus of 800 MPa may not be unreasonable. However it is at variance with most previously published recommendations for the design of flexible conduits. In particular ASTM D.3839-79 Table A6 gives 20.7 MPa as the average modulus of fine crushed rock of over 70% relative density, and it is notable that this is consistent with the initial tangent modulus found in the plate load tests. It appears that such small scale tests give values which are inapplicable to the problem of soil-pipe interaction.

Attempts to similarly model the behaviour of the right-hand side of the pipe failed to produce the peak in deflection 25° below the right-hand haunch. It is reasonable to assume that the original crack formed during the compaction of the sidefill which was subsequently the largest crack in the pipe had developed to the stage where the flexural stiffness of the pipe wall started to decrease. It was not possible to model this nonlinear behaviour without considerable additional programming effort and to do so would not have added to the understanding of the bedding's behaviour.

From the fact that the moment at the pipe invert was of the opposite sign to that normally encountered it was also apparent that the pipe had been lifted off the sand by the wedging action of the sidefill compaction. This had created a void under the invert which had allowed the wall to bow outwards at this point creating tension on the outer reinforcing grid. The change in the direction of moment variation with surcharge at the invert as shown in Fig. 53 may be due to the invert making contact with the bedding and so closing the void. It is probable that initially there was no contact between the pipe and bedding up to about 40° each side of the invert where the material begins to be more compacted.

From the shape of the deflection curve it may also be deduced that the bulk of the vertical load on the pipe is supported at around 30° below

the haunches. This is in sharp contrast to the observations of Spangler (43), who found a peak of normal pressure at the invert falling away to a minimum below the haunch.

4.2.2. Condition of the Pipe After Sidefill Compaction

During sidefill compaction the pipe developed a crack which followed the line of a longitudinal wire of the inner steel grid which was immediately below the surface. Had this wire not been present to initiate the crack it is probable that the crack would have formed lower on the pipe wall and at a higher load. It is evident that the hard spot at about 30^{o} which caused local deflections during application of the surcharge was also responsible for the initial cracking of the pipe.

In order to better understand the action of the sidefill compaction on the state of the pipe a comparison was made between the cracking of the pipe in the three-edge bearing test and the cracking which occurred in the pipe in the test bin.

The three-edge bearing test pipe reached a level of crown and invert cracking comparable to the initial cracking of the pipe in the test bin at a load of 21.3 kN/m.

Idealizing this loading as diametrically opposed line loads, ignoring self-weight and assuming that the pipe is a linear elastic incompressible cylinder the moment induced at the crown and invert will be:

$$M = \frac{P\ r}{\pi} = \frac{21.3 \times 0.4065}{\pi} = 2.76 \text{ kNm/m}$$

Supposing that the condition of the pipe in the bin at the completion of sidefilling can be represented by opposing horizontal line loads acting 30^{o} below the haunch, other assumptions remaining as above. Roark and Young (42), p. 221 gives the moments at the load application points as:

$$M = \frac{P\ r}{\pi} (1 - \cos^2 60^\circ) \qquad (23)$$

If it is assumed that the moment required to produce the cracks at the crown and invert of the three-edge bearing test pipe were of the same value as that which caused a longitudinal crack in the bedded pipe then the horizontal force applied to the bedded pipe immediatelv after sidefilling bv the hard spots can be estimated:

Hence assuming that the moment at the loaded line is 2.76 kNm/m the required horizontal force to produce this moment will be:

$$P = \frac{2.76\ \pi}{0.4065\ (1 - \cos^2 60^\circ)} = 28.4 \text{ kNm/m}$$

However, the vertical and horizontal diameter changes to the bedded pipe under a lateral force of this magnitude predicted bv the formulae given bv Roark and Young (42), p. 221 for a linear elastic ring are:

$$\Delta_V = + 0.0891 \frac{\omega\ r^3}{E\ I} \qquad (24)$$

$$\Delta_H = - 0.0930 \frac{\omega\ r^3}{E\ I} \qquad (25)$$

For a linear elastic cylinder E I is replaced in these equations bv D, where D = flexural stiffness of pipe wall

$$= \frac{E\ t^3}{12\ (1-\nu^2)} = \frac{31440 \times 51^3}{12\ (1-0.15^2)} = 3.56 \times 10^8 \text{ N.mm}$$

Therefore:

$$\Delta_V = + 0.0891 \times \frac{28.4 \times 406.5^3}{3.56 \times 10^8} = + 0.48 \text{ mm}$$

$$\Delta_H = -0.0930 \times \frac{28.4 \times 406.5^3}{3.56 \times 10^8} = -0.50 \text{ mm}$$

Assuming that the pipe was circular before bedding the horizontal diameter would be expected to be 1 mm shorter than the vertical diameter. This difference is consistent with measurements taken of the pipe after sidefilling was completed, the surface roughness of the concrete however, prevented these measurements from being very precise.

4.2.3. Ratio of Average Lateral Pressure to Vertical Pressure

Average diameter change under maximum load = 0.097 mm

Roark and Young (42), p. 228 give the following formula for the diameter change of an elastic ring under uniform lateral stress as:

$$\Delta_H = -\Delta_V = 0.1667 \frac{\omega r^4}{E I} \qquad (26)$$

Substituting D for E I as before, and applying a uniform vertical stress of 1.2 x 171.1 kPa:

$$\Delta_H = -\Delta_V = \frac{0.1667 \times 0.1711 \times 1.2 \times 406.5^4}{3.56 \times 10^8} = 2.625 \text{ mm}$$

But since deflection only averages 0.097 mm, therefore lateral pressure must account for an opposite deflection of 2.625 - 0.097 = 2.528 mm. This would require a lateral pressure of 198 kPa.

Therefore, for such a large vertical pressure to produce so small a deflection, the ratio between the average horizontal and vertical pressures on the pipe must be:

$$\frac{q_H}{q_V} = \frac{0.198}{0.205} = 0.964$$

Finite element analysis indicates a similar ratio of pressures acting on the pipe.

4.2.4. Mobilization of Lateral Soil Pressure

In (1) and (43) Spangler has stated that since a rigid pipe deforms only slightly under vertical load the sides do not move outwards far enough to develop any appreciable passive resistance. With a pipe that has been sidefilled with ordinary soil with little compaction this is no doubt true but in order to explain the small deflections of the test pipe substantial lateral pressure must be involved.

Calculations assuming the pipe to be an elastic ring show that an average lateral pressure 96% of the vertical pressure would be needed to give such small diameter changes in the pipe. Since the pipe wall is virtually incompressible, diameter changes are brought about by the differences of pressure in different directions. Looked at in this way it is the 4% difference between the average vertical and the horizontal soil pressures which is responsible for the diameter changes observed.

Assuming that the vertical stress in the soil adjacent to the side of the pipe is equal to the applied surcharge, while the lateral soil stress at the side of the pipe is about 96% of the vertical soil stress on the pipe, itself 1.2 times the surcharge, then the ratio of horizontal to vertical stress at the side of the pipe will be approximately 1.15 . Bowles (44), gives the following ratios for various soil conditions shown in Table 4.

TABLE 4

Soil Condition	Usual range of $\frac{q_H}{q_V}$
Active	0.33 - 0.22
At rest	0.4 - 0.6
Passive	3 - 14

A ratio of 1.15 then places the case between "at rest" and "passive".

4.2.5. Vertical Load on Pipe

From Figs. 58 and 60 it can be seen that the increase in load as calculated from the strain gauge readings is highly asymmetrical, the left-hand haunch having approximately four times as much thrust as the initially cracked right-hand haunch. Adding the haunch thrusts together, the resultant is 1.2 times the air bag surcharge on the plan area of the pipe. The finite element analysis also predicts that the vertical soil stress on the horizontal plane level with the crown of the pipe is about 1.2 times the surcharge. The total thrust on the haunches predicted by the finite element model is 1.17 times the surcharge on the plan area of the pipe. Despite the poor measurements of thrust given for the three-edge bearing test by calculation from the strains (see 3.3.2.), those calculated for the bin test are more credible in view of their closeness to the finite element predictions. The usual assumptions made in the calculation of soil loads on pipes on Australian Standard AS 1342 Class B beddings under embankments, that is projection ratio = 0.7, and settlement ratio = 0.7, lead to a soil load of 1.5 times the weight of the soil prism above the pipe. Therefore, the partial trench bedding, in addition to improving lateral support to the pipe, reduces the concentration of load on the pipe by increasing the vertical stiffness of the material each side of the pipe.

4.2.6. Calculation of Marston-Spangler Load Factor

Taking the more conservative value of the additional vertical load on the pipe as 1.2 times the surcharge on the plan area of the pipe, it is possible to calculate a bedding factor for this bedding assuming that field cracking be limited to 0.15 mm.

Assuming that the total vertical load on the pipe is 1.2 times the surcharge on its plan area, plus the weight of the prism of sand above the pipe, at the 0.15 mm crack load:

Load on pipe = 1.2 x 108.8 x 0.864 + 17.4 x 1.3 x 0.864

= 177.4 + 19.5 kN/m = 132.3 kN/m

Under the three-edge bearing test the 0.15 mm crack was reached at a load of 25.4 kN/m

The bedding factor is then given by the ratio of:

$$\frac{\text{Cracking load on bedding}}{\text{Cracking load on 3-edge test}} = \frac{132.3}{25.4} = 5.2$$

In accepting this value of bedding factor of 5.2, several things must be bourne in mind which tend to make this figure conservative:

1. Only the initial crack which formed during sidefill compaction reached a width of 0.15 mm, and that crack grew only slightly larger as the surcharge reached a level of 171.1 kPa. First cracks are normally expected at the invert or crown.

2. Other cracks about the crown and haunches were still very narrow even at the highest applied surcharge and these may be regarded as being typical of the cracks which would have been formed had not an initial crack been present.

3. Due to the very high stiffness of the sidefill, the capacity for movement of the haunches is very slight and it is very unlikely that sufficient movement would ever occur under a realistic load to produce an ultimate flexural failure.

4. The fact that a pipe has cracks exceeding 0.15 mm in width does not

mean that the pipe is no longer serviceable, the value of 0.15 mm is an arbitrary figure itself very conservative intended to prevent steel corrosion. In the U.S.A. ASTM C76M - 1982 allows cracks up to 0.3 mm while the California Department of Transportation allows cracks of up to 2.5 mm under non-aggressive bedding conditions.

4.2.7. Comparison With Mountainhouse Creek Zone 8 Results

The Mountainhouse Creek test in the U.S.A. included pipes bedded in partial trenches, Zone 7 of this test used a shaped bedding while Zone 8 used a flat sand bed, see Refs. (33) and (34).

Three-edge bearing tests of the pipes used showed cracks nearly 0.01" (0.254 mm) wide under loads of 10750 lb/ft (157 kN/m).

For the pipe bedded under Zone 8 conditions a 0.01" (0.254 mm) crack width was reached at a fill height of 51 ft (15.5 m), the effective density provided by the soil stressmeters was 120 lb/ft^3 (18.9 kN/m^3).

$$\text{Load on pipe} = 120 \times 51 \times 8.33 \text{ lb/ft}$$

$$= 50979 \text{ lb/ft (744 kN/m)}$$

$$\text{Bedding factor} = \frac{50979}{10750} = 4.74$$

Despite the intial cracking, the Mile End test appears to have given a slightly better result that the Mountainhouse Creek test for 2 reasons:

1. The Dimension Ratio (D/t) for the Mile End pipe was 14.9 as against 10.5 for Mountainhouse Creek, this increased flexibility increased the lateral soil pressure and so reduced the moment in the pipe wall.

2. The Mile End pipe projected out of the compacted sidefill by only 30% of its external diameter, whereas the Mountainhouse Creek pipe projected by 40% of its external diameter.

CONCLUSIONS

Applicability of Finite Element Method

Agreement between the initial finite element analysis of the pipe's response and the experimental results was poor. The main reasons for this were the poor estimates of bedding modulus given by the plate load tests, and the unexpected formation of a longitudinal crack during the compaction of the sidefill. By a process of trial and error, a revised finite element model was produced which gave deflections closely matching those obtained experimentally, the bending moments matched the experimental results quite closely for two of the four quadrant points while at the other they matched only in sign and not magnitude.

It should be noted that whereas the main criterion in designing a flexible culvert is the diameter change which can be calculated relatively easily on the basis of an average modulus around the pipe, the cracking performance of a rigid concrete pipe is dependant on the distribution of bending moment around its circumference. However the distribution of bending moment is influenced considerably by localized responses following the onset of initial cracking. Therefore it is more difficult to use the finite element method to predict the fill height which will cause a concrete pipe to crack to a specified width than it is to predict the fill height that will shorten the vertical diameter of a flexible pipe by a specified amount.

Nevertheless, given the details of modulus around the pipe, the finite element method should in principle be capable of predicting pipe cracking loads with considerably greater accuracy than the existing methods based on the work of Marston and Spangler.

Suitability of Plate Load Test for Modulus Measurement

It is apparent that when used on compacted crushed rock or quarry rubble the plate load test greatly underestimates the elastic modulus. The most likely reason for this is that when the area of the surface of the material under test has a deflection imposed upon it by the plate, severe shear stresses occur around the edge of the plate causing local shear failure. Despite the efforts made in the laboratory tests to prevent bearing failure by applying a surcharge around the plate, this seems nevertheless to have occurred. A similar type of failure must have occurred on those plate load tests made through the pipe wall. When a pipe deflects under load the deflection varies gradually around the circumference without abrupt changes and so the shear stresses are far less. For this reason it is felt that plate load tests are unsuitable for measuring the moduli of granular materials unless proper confinement can be provided.

Suitability of Linear Elastic Analysis

On the basis of the results obtained from this test programme it is doubtful that any significant practical value could be obtained from a more complex model than from a simple linear elastic model. The significance of both the magnitude and the distribution of an average linear value for soil modulus is overwhelming.

These results appear to demonstrate that future research should place a major emphasis on the measurement of soil modulus and its variability around the pipe.

Desirability of High Compaction of Sidefill

At the beginning of this study it was inferred from the various mathematical analyses of buried pipes that the more rigid is the sidefill the less the pipe will deflect and so the greater will be the fill height

which the pipe can support. The mathematical analyses however, make the assumption that the side support for the pipe is of a uniform stiffness.

In the case of the bedding tested this was far from the truth, the stiffest part of the sidefill was concentrated around a small arc at about 30^{o} below the haunch on each side of the pipe. This lateral support did in fact reduce the radial deflections of the pipe as anticipated, but since the force which it imposed was so concentrated it also contributed, after the initial cracking, to the pipe's early cracking to a width of 0.15 mm. This suggests that a high sidefill modulus needs to be uniform in order to gain the maximum benefit from the additional effort expended. For future testing more care should be given to the attainment of a uniform modulus in the sidefills and care should be taken to minimize dynamic load effects on the pipe.

Recommendations

1. According to the draft Australian Standard 86013, the required strength of pipe for a projection ratio of 0.3 and a given height of embankment, should be determined using an earth load equal to 1.4 times the weight of the prism of soil above the pipe and a bedding factor of 4.0 to obtain the equivalent three-edge bearing test load. Provided that reasonable installation practices are adopted this will give a conservative design. This test indicated that a vertical load ratio of 1.2 and a bedding factor of 5.2 corresponded to a field crack of 0.15 mm. implying a factor of safety of 1.5 in the draft standard. It should be noted that a field crack of 0.15 mm under non-aggressive conditions is quite insignificant.

2. Because of the irregular shape of the bending moment profile, only pipes with a double cage of circular reinforcement should be used with this type of bedding.

3. Consideration should be given to the strength requirements of the pipe to prevent premature cracking of the pipe caused by the lateral load imposed by the compaction equipment during the placement and compaction of the sidefill.

REFERENCES

1. Spangler, M.G. and Handy, R.L. "Soil Engineering", 4th Edition, Harper & Row, New York, 1982.

2. Winterkorn, H.F. and Fang, H.Y. "Foundation Engineering Handbook", Van Nostrand Reinhold Company, New York, 1975, p.149

3. Janbu, N. "Soil Compressibility as Determined by Oedometer and Triaxial Tests", Proc. European Conference on Soil Mechanics and Foundation Engineering, Weisbaden, Vol.1. 1963 pp.19-25.

4. Osterberg, J.O. Discussion of "Field Compaction" by R.R. Phillippe. Proc. Conference on Soil Stabilization, Massachussetts Institute of Technology, 1952, pp.167-168

5. Espinosa, J.H.S., Krizek, R.J. and Corotis, R.B. "Regression Analysis of Soil Compressibility", Transportation Research Record, 1975.

6. Kondner, R.L. "Hyperbolic Stress-Strain Response: Cohesive Soils", Journal of the Soil Mechanics & Foundation Division, ASCE, Vol.89 No. SM1, Proc. Paper 3429, 1963, pp.115-143.

7. Kondner, R.L. and Zelasko, J.S. "A Hyperbolic Stress-Strain Formulation for Sands", Proc. 2nd Pan American Conference on Soil Mechanics and Foundation Engineering, Brazil, Vol.1, 1963, pp.289-324.

8. Kondner, R.L. and Zelasko, J.S. "Void Ratio Effects on the Hyperbolic Stress-Strain Response of a Sand", Laboratory Shear Testing of Soils, ASTM STP No.361, Ottawa, 1963.

9. Kondner, R.L. and Horner, J.M. "Triaxial Compression of a Cohesive Soil with Effective Octahedral Stress Control", Canadian Geotechnical Journal, Vol.2, No.1, 1965, pp.40-52.

10. Duncan, J.M. and Chang, C.Y. "Nonlinear Analysis of Stress and Strain in Soils", Journal of the Soil Mechanics and Foundation Division, ASCE, Vol.96, No.SM5, 1970, pp.1629-1653.

11. Krizek, R.J. and Atmatzidis, D.K. "Assessment of Soil Constitutive Models for Numerical Analysis of Buried Concrete Pipe Systems", Concrete Pipe and the Soil-Structure System, ASTM STP No.630, M. Bealey and J.D. Lemons, Editors, ASTM, 1977, pp.76-90.

12. Krizek, R.J. and Corotis, R.B. "Synthesis of Soil Moduli from Different Types of Laboratory and Field Tests", Proc. of the Speciality Conference on In-Situ Measurement of Soil Properties, ASCE, Raleigh, North Carolina, Vol.1, 1975, pp.225-240.

13. Krizek, R.J. and McQuade, P.V. "Behaviour of Buried Concrete Pipe", Journal of the Geotechnical Division, ASCE, Vol.104, No.GT7, 1978, pp.815-836.

14. Krizek, R.J. and Kay, J.N. "Material Properties Affecting Soil-Structure Interaction of Underground Conduits", Highway Research Record, No. 413, 1972, p.13-29.

15. Krizek, R.J., Corotis, R.B. and Wenzel, T.H. "Soil-Structure Interaction of Concrete Pipe Systems", Proc. National Structural Engineering Conference on Methods of Structural Analysis, Madison, Wisconsin, ASCE, Vol.2, 1976, pp.607-643.

16. Hognestad, E. "A Study of Combined Bending And Axial Load in Reinforced Concrete Members", Engineering Experiment Station Bulletin No. 399, University of Illinois, 1951.

17. Desavi, P. and Krishnan, S. "Equation for the Stress-Strain Curve of Concrete", ACI Journal, Proceedings Vol.61, No.3, 1964.

18. Kay, J.N. and Hain, S.J. "A Design Method for Buried Concrete Pipe", Report No. R21, Department of Civil Engineering, University of Adelaide, October 1979.

19. Kay, J.N. and Hain, S.J. "Design Method for Concrete Under High Fills", Transportation Research Record No. 878, 1982, pp.29-33.

20. Katona, M.G. "Discussion and Application of CANDE Computer Program to Reinforced Concrete Culverts", Concrete and the Soil-Structure

System, ASTM, STP No. 630, M. Bealey and J.D. Lemons, Eds, ASTM, 1977, pp.17-40.

21. Wenzel, T.H. and Parmelee, R.A. "Computer-Aided Structural Analysis and Design of Concrete Pipe", op cit pp. 105-118.

22. Krizek, R.J., Parmelee, R.A., Kay, J.N. and Elnaggar, H.A. "Structural Analysis and Design of Pipe Culverts". National Cooperative Highway Research Program, Report No. 116, 1971.

23. Burns, J.Q. and Richard, R.M. "Attenuation of Stresses for Buried Cylinders", Proc. Symposium on Soil-Structure Interaction, University of Arizona, Tucson, 1964, pp. 378-392.

24. Höeg, K. "Stresses Against Underground Structural Cylinders", Journal of the Soil Mechanics and Foundation Division, ASCE, Vol. 94, No. SM4, 1968, pp. 833-858.

25. Kay, J.N. and Krizek, R.J. "Adaptation of Elastic Theory to the Design of Circular Culverts", Civil Engineering Transactions, Institution of Engineers, Australia, April 1970.

26. Selig, E.T., McVay, M.C. and Chang, C.S. "Finite-Element Modeling of Buried Concrete Pipe Installations", Transportation Research Record, No. 878, 1982, pp. 17-23.

27. Katona, M.G., Smith, J.M., Odello, R.J. and Allgood, J.R. "CANDE: A Modern Approach for the Structural Design of Buried Pipe Culvert", Civil Engineering Laboratory, Port Hueneme, California, technical report to Federal Highway Administration, October 1976.

28. Katona, M.G. and Smith, J.M. "CANDE: User Manual", Civil Engineering Laboratory, Port Hueneme, California, technical report to Federal Highway Administration, October 1976.

29. Parmelee, R.A. "A New Design Method for Concrete Pipe", Concrete Pipe and the Soil-Structure System, ASTM STP No. 630, M. Bealey and J.D. Lemons, Eds., ASTM, 1977, pp. 119-130.

30. Kay, J.N. and Abel, J.F. "Implementation of Finite Element Studies

for the Design of Buried Circular Culverts", Symposium on Finite Elements in Engineering, University of Adelaide, 1976.

31. Davis, R.E., Bacher, A.E. and Obermuller, J.C. "Concrete Pipe Culvert Behavior - Part 1", Journal of the Structural Division, ASCE, Vol. 100, ST3, 1974, pp. 599-614.

32. Davis, R.E. and Bacher, A.E. "Concrete Pipe Culvert Behavior - Part 2", Journal of the Structural Division, ASCE, Vol. 100, ST3, 1974, pp. 615-630.

33. Davis, R.E. and Bacher, A.E. "Structural Behavior of a Concrete Pipe Culvert - Mountainhouse Creek (Part 1)", California Division of Highways, Report R & D No. 4-71, April 1971.

34. Davis, R.E., Bacher, A.E. and Evans, E.E. "Structural Behavior of a Concrete Pipe Culvert - Mountainhouse Creek (Part 2)", California Department of Transportation, Report FHWA-CA-ST-4121-75-8, September 1975.

35. Truesdell, C. "Hypo-elasticity", Journal of Rational Mechanics and Analysis, Vol. 4, 1955, pp. 83-133.

36. Corotis, R.B., Farzin, M.H. and Krizek, R.J. "Non-linear Stress-Strain Formulation for Soils", Journal of the Geotechnical Engineering Division, ASCE, Vol. 10, No. GT9, 1974, pp. 993-1008.

37. Poulos, H.G. and Davis, E.H. "Elastic Solutions for Soil and Rock Mechanics", Wiley, New York, 1974.

38. "Structural Design of Road Pavements - A Guide" Draft prepared by the MEC Working Group, NAASRA, Australia, July 1985. p. 50.

39. "Interim Guide to Pavement Thickness Design", NAASRA, Australia, 1979, p. 53.

40. Avalle, D.L., Flint, R.C.L. and Kay, J.N. "A Test Facility for Buried Conduits and Arches", Civil Engineering Transactions, Institution of Engineers, Australia, 1985, pp. 384-389.

41. Kurzeme, M. and Richards, B.G. "Earth Pressure Observations on a

Retaining Wall in Expansive Clay, Gouger Street Mail Exchange, Adelaide", Rpt No.17, CSIRO, Australia, 1974.

42. Roark, R.J. and Young, W.C "Formulas for Stress and Strain", McGraw-Hill, New York, 1975.

43. Spangler, M.G. "The Supporting Strength of Rigid Pipe Culverts", Bulletin 112, Engineering Experiment Station, Iowa State College, 1933.

44. Bowles, J.E. "Foundation Analysis and Design", McGraw-Hill Kogakusha, Tokyo, 1968, p. 267.

45. Hadala, P.F. "The Effect of Placement Method on the Response of Soil Stress Gauges", Proc. International Symposium on Wave Propagation and Dynamic Properties of Earth Materials, University of New Mexico, Albuquerque, 1967, pp. 255-263.

46. Wrench, B.P. "Plate Load Tests for the Measurement of Modulus and Bearing Capacity of Gravels", Die Siviele Ingenieur in Suid-Afrika, September 1984, pp. 429-437.

47. "SAP4 - A Structural Analysis Program for Static and Dynamic Response of Linear Systems", by Bathe, K.J., Wilson, E.L., Peterson, F.E., University of California, Berkeley.

48. "ELASPIPE", by John F. Abel, Department of Structural Engineering, Hollister Hall, Cornell University, Ithaca, New York, 1977.

49. Bacher, A.E. "Design of Thin Wall Reinforced Concrete Pipes Using Dimension Ratio (DR)", presentation to Second Bridge Engineering Conference, Transportation Research Board, Minneapolis, Minnesota, 24-27th September 1984.

APPENDIX A

Methods Used for Obtaining Various Relative Densities of Fine Crushed Rock Under Laboratory Conditions

As mentioned in 2.3. the maximum and minimum dry densities of the fine crushed rock were made using the methods laid down in Australian Standard AS 1289 E 5.1 - 1977. The maximum dry density obtained for this material was 2272 kg/m^3, while the minimum was 1529 kg/m^3.

The method described in AS 1289 E 5.1.4(d) for obtaining minimum dry density is to pour the material in question from a scoop into the measuring container without allowing the material to fall freely through the air. The fine crushed rock was placed in this manner into the tub described in 2.2 and the surface levelled off.

After weighing, the tub was taken about 100 m on a rubber tyred trolley to the testing laboratory where, immediately before being placed on the testing machine, measurements were taken to allow the volume and hence the relative density of the material to be calculated. At this point the dry density was found to be 1841 kg/m^3 from which a relative density was of 51.8% was calculated using Eq. 21. It appears that settlement had taken place during transit due to the vibration of the trolley and this had raised the relative density.

For the second plate load test the tub was refilled and vibrated under a steel plate which imposed an average pressure of 1.56 kPa on the surface of the contents. On being weighed and measured as before the dry density was found to be 1990 kg/m^3 from which the relative density was found to be 70.9%.

For the third test the material was vibrated in the same way but under a 50 kg concrete weight which imposed an average surcharge of 5.65 kPa, this batch reached a dry density of 2085 kg/m^3 or relative density of

81.6%.

In order to reach a relative density of around 100% the wet placement method described in AS 1289.E 5.1.5 was used. The tub was filled with fine crushed rock previously saturated with water, this was placed on a vibrating table and vibrated under a surcharge of 5.65 kPa. The excess water was removed as it collected at the surface and the vibration was continued until no further consolidation was observed. This produced the maximum dry density of 2272 kg/m^3.

APPENDIX B

Measurements of Soil Stress Against Outside of Pipe

Attempts to measure the normal soil stress on the outside surface of buried pipes have been fraught with difficulty in previous studies. The main problem is that in order to truly measure the pressure, that portion of the surface over which the force is evaluated must be of the same rigidity and surface texture as any other portion of the pipe's external surface around it. Load cells at nominal load capacity will typically deflect 0.08 mm while a 160 mm diameter Carlson type stressmeter will deflect by 0.0016 mm or about 1/50 th of a load cell's deflection.

Previous experience of the Mountainhouse Creek researchers, (34), p 18, had suggested to them that Carlson stressmeters provided consistently valid soil pressure measurements on concrete structures. Unfortunately these stressmeters were unsuitable for this study as their large size and the number required would have greatly weakened the pipe, the large flat measuring surface of the gauge would not have matched the curved surface of the pipe so that the readings could not have been trusted in any case. Hadala (45) concluded that "..using a single gauge to measure the magnitude of stress is, for practical purposes, fruitless, and the use of at least a three-gauge cluster is required to obtain ±20 percent accuracy.." In addition the cost of these gauges was in 1985, A$1000 each.

However a test was made using a load cell set up in the pressure vessel shown in Fig. 20 and using the type of sand already in the Mile End test installation. The load cell was in contact with a 100 mm diameter steel disk which was mounted flush with a surrounding steel plate under a 100 mm thick layer of sand. The top surface of the sand was loaded by means of air pressure acting on a flexible rubber membrane. The pressure registered on the load cell was only about 2/3 of that applied to the surface of the sand, but the relationship was nonlinear, see Fig. 63.

Since the exact proportion of the soil pressure that will appear on the disk will vary with the modulus of the soil, Fig. 63 could not simply be used to calibrate the load cell against the free field soil pressure.

Another device used was an Interfels hydraulic mechanical stress transducer type SC50. This unit is intended to be placed inside a concrete member under load and being supposedly of the same compressibility as the concrete, to give an accurate measure of the stress in the member. The device in this case was embedded in a 30 mm layer of mortar under a 100 mm layer of sand loaded by air pressure on a rubber membrane as shown in Fig. 21. Fig. 64 shows that the results of loading the transducer in this configuration were highly irregular and showed a large amount of hysteresis on unloading and reloading. Possibly this was due to the fact that the device was intended for use at stresses up to 5 MPa whereas in the case of this test only 210 kPa was applied.

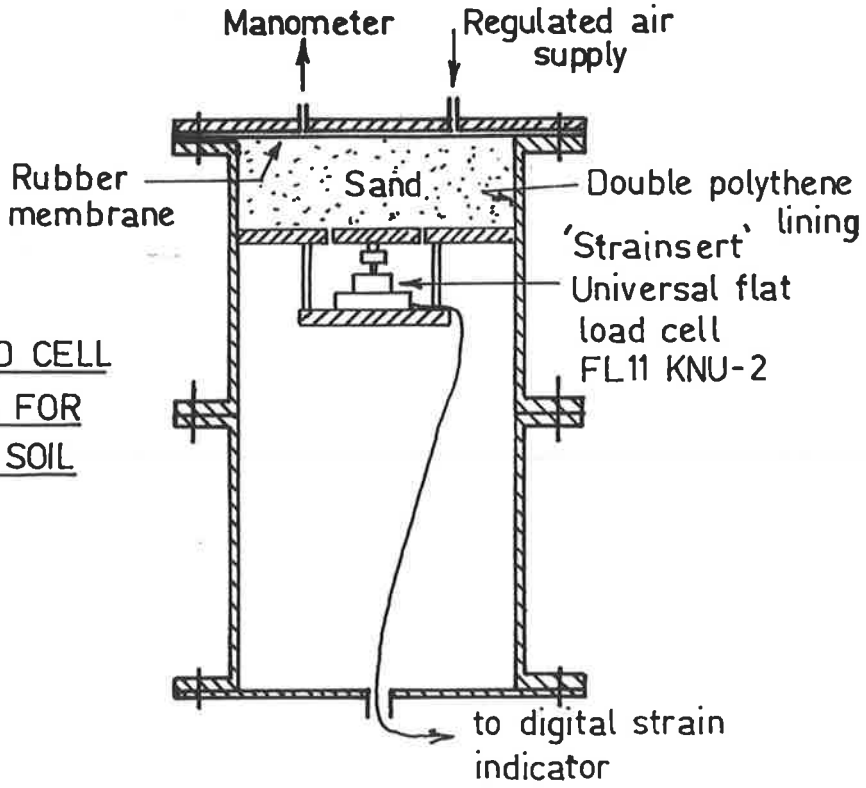

FIG.20 LOAD CELL IN TEST RIG FOR MEASURING SOIL STRESS

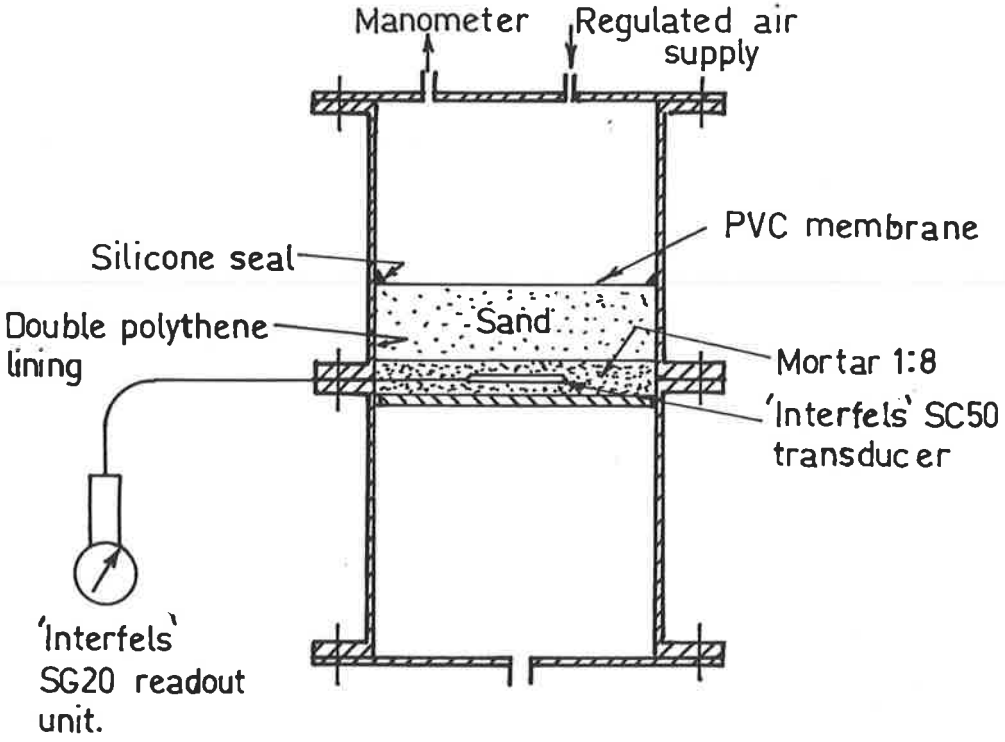

FIG.21 TEST OF INTERFELS TRANSDUCER

APPENDIX C

Derivation of Equations for Calculation of Pipe Circumferential Bending Moments and Thrusts from Measured Steel Strains

Sign convention: tensile stresses, strains and forces are positive.

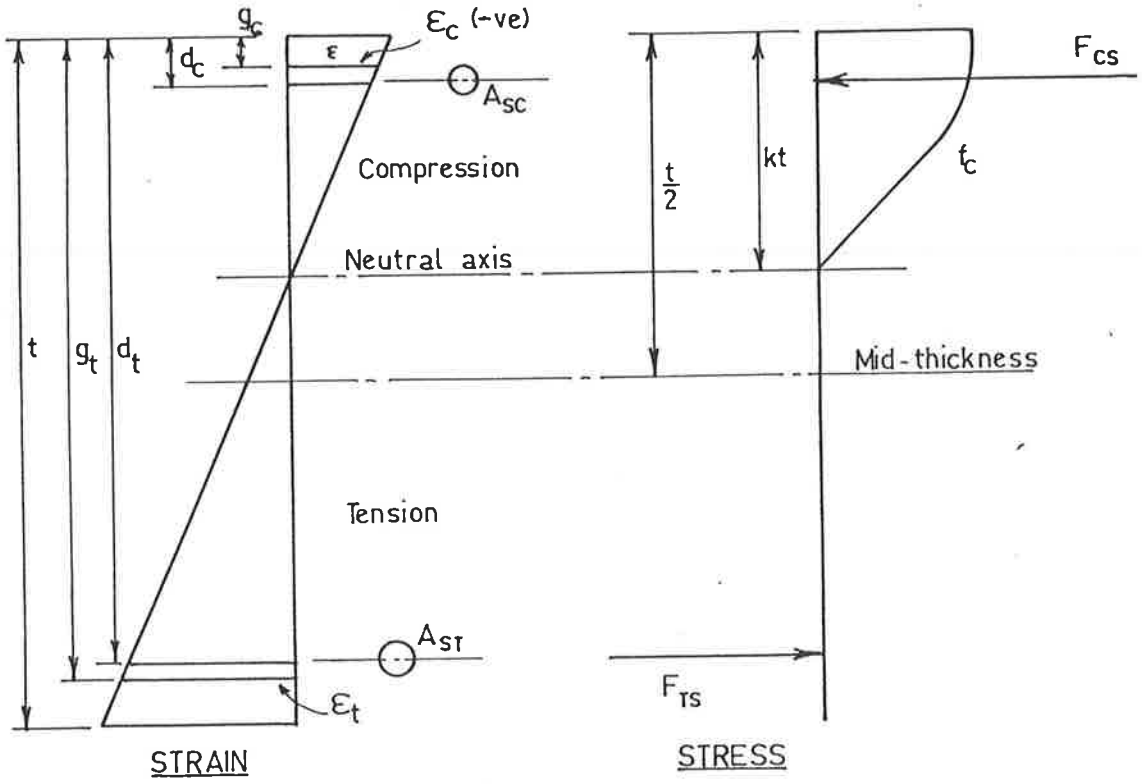

FIG. 22 - STRAIN AND STRESS DIAGRAMS FOR PIPE WALL

From Fig. 22, by similar triangles the depth from the extreme compressive fibre to the neutral axis is given by:

$$k\,t = \frac{\epsilon_C\, g_T - \epsilon_T\, g_C}{\epsilon_C - \epsilon_T} \qquad (27)$$

Strain at the centroid of the compressive steel:

$$\epsilon_{SC} = \epsilon_C \left(\frac{k\,t - d_C}{k\,t - g_C} \right) \qquad (28)$$

Strain at the centroid of the tensile steel:

$$\epsilon_{ST} = \epsilon_T \left(\frac{d_T - k\,t}{g_T - k\,t} \right) \qquad (29)$$

A stress-strain curve was measured for the hard-drawn wire used in the pipe, see Fig. 23. This was represented in the computer programme as a

series of straight lines.

Thus tensile steel force: $F_{TS} = A_{TS} \times f_T$

and compressive steel force: $F_{CS} = A_{CS} \times f_C$

Using the relationship of Desavi and Krishnan (17) to describe both the ascending and descending arms of the stress-strain curve for concrete:

$$\sigma = \frac{E_i \epsilon}{1 + \left(\frac{\epsilon}{\epsilon_o'}\right)^2} \qquad (17)$$

where σ_{uc} = compressive strength of the concrete (50 MPa)

ϵ_o' = strain at $\sigma = \sigma_{uc}$ (0.0025)

$E_i = \Delta\sigma/\Delta\epsilon$ at $\sigma = 0$ (40,000 MPa)

Values shown in brackets are typical values for concrete pipe used in the calculations, and the resulting stress-strain curve is plotted in Fig. 24. No tests were made to verify the values for the pipes used or the accuracy of the relationship, however this model gave a better fit to the results than did a linear model.

Strain in concrete at a distance x above neutral axis: $\epsilon = \beta x$

where:

$$\beta = \frac{\epsilon_T - \epsilon_C}{g_C - g_T}$$

therefore from Equation 17.:

$$\sigma = \frac{E_i \beta x}{1 + \left(\frac{\beta x}{\epsilon_o'}\right)^2} \qquad (30)$$

integrating Equation 30. over compressive zone to get concrete force:

$$F_{CC} = \int_0^{kt} \sigma \, dx$$

$$= \int_0^{kt} \frac{E_i \beta x}{1 + \left(\frac{\beta x}{\epsilon_o'}\right)^2} dx$$

$$F_{CC} = E_i \beta \left[\frac{\epsilon_o'^2}{2\beta^2} \log_e \left(1 + \left\{ \frac{\beta k t}{\epsilon_o'} \right\}^2 \right) \right] \qquad (31)$$

Moment of concrete force about neutral axis:

$$M_{NA} = - \int_0^{kt} \sigma x \, dx$$

$$= - \int_0^{kt} \frac{E_i \beta x^2}{1 + \left(\frac{\beta x}{\epsilon_o'}\right)^2} dx$$

$$M_{NA} = - E_i \beta \left[k t \frac{\epsilon_o'^2}{\beta^2} - \frac{\epsilon_o'^3}{\beta^3} \operatorname{artan} \left\{ \frac{k t \beta}{\epsilon_o'} \right\} \right] \qquad (32)$$

concrete moment about mid-thickness of wall:

$$M_{CC} = M_{NA} - F_{CC} \left(\frac{t}{2} - k t \right) \qquad (33)$$

total moment about mid-thickness of wall:

$$M = -F_{CS} \left(\frac{t}{2} - d_c \right) + F_{TS} \left(d_T - \frac{t}{2} \right) + M_{CC} \qquad (34)$$

total thrust:

$$F = - F_{CS} - F_{TS} - F_{CC} \qquad (35)$$

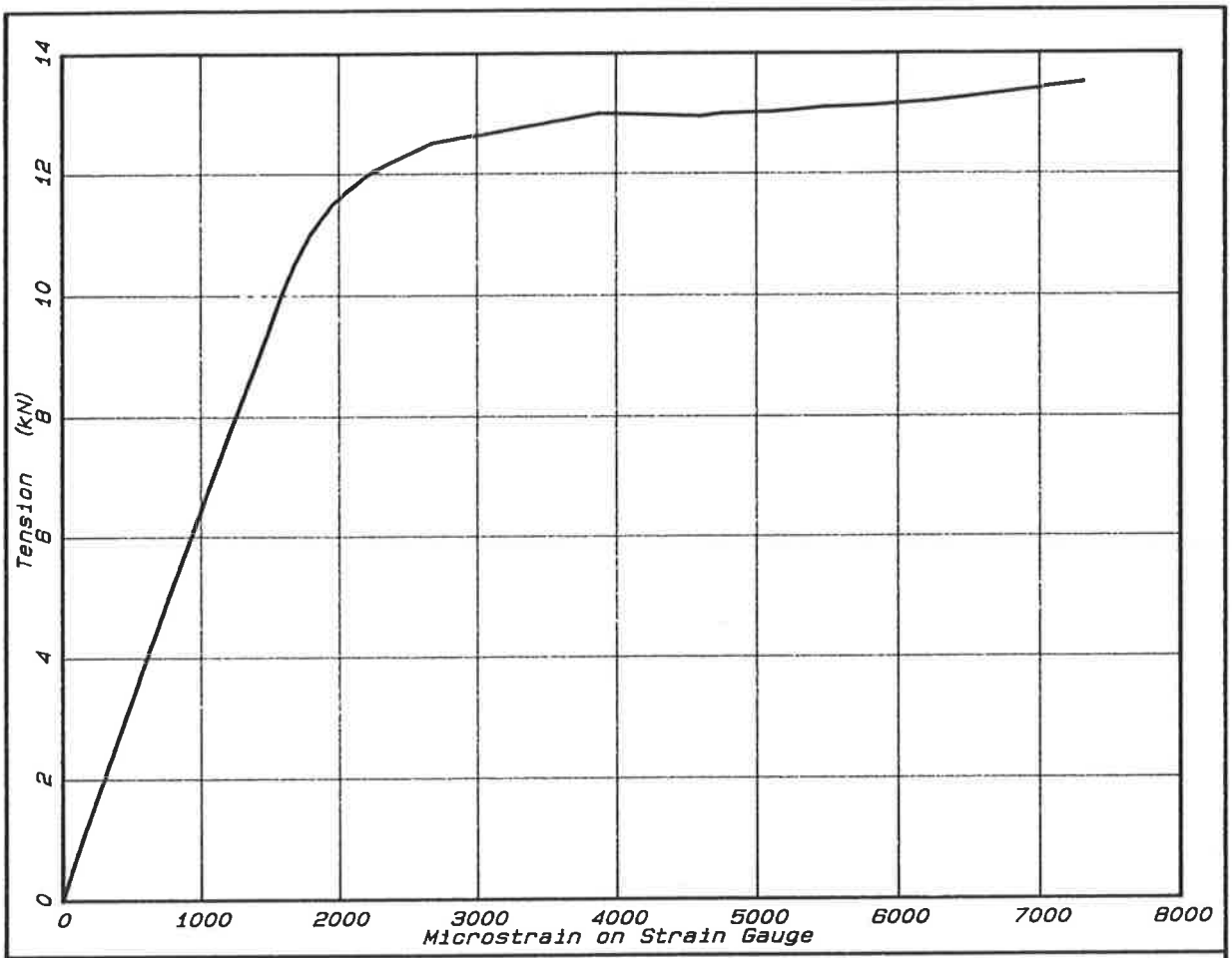

FIG.23 - STRESS-STRAIN CURVE FOR 6.23 mm DIA HARD-DRAWN WIRE

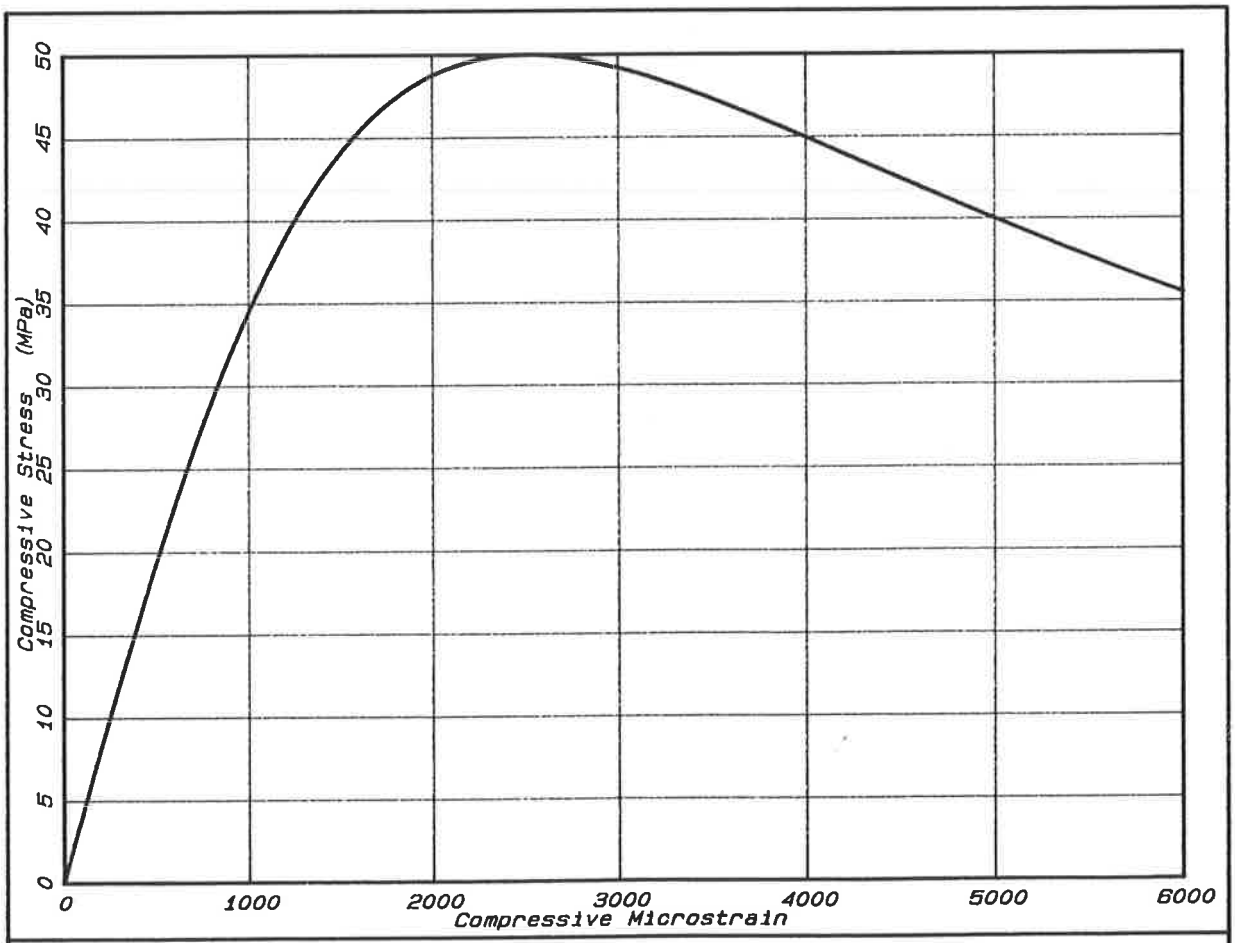

FIG.24 - ASSUMED STRESS-STRAIN RELATIONSHIP FOR CONCRETE
INITIAL SLOPE = 40000 MPa, ULT. COMPRESSIVE STRENGTH = 50 MPa

APPENDIX D

Graphs of Experimental Results

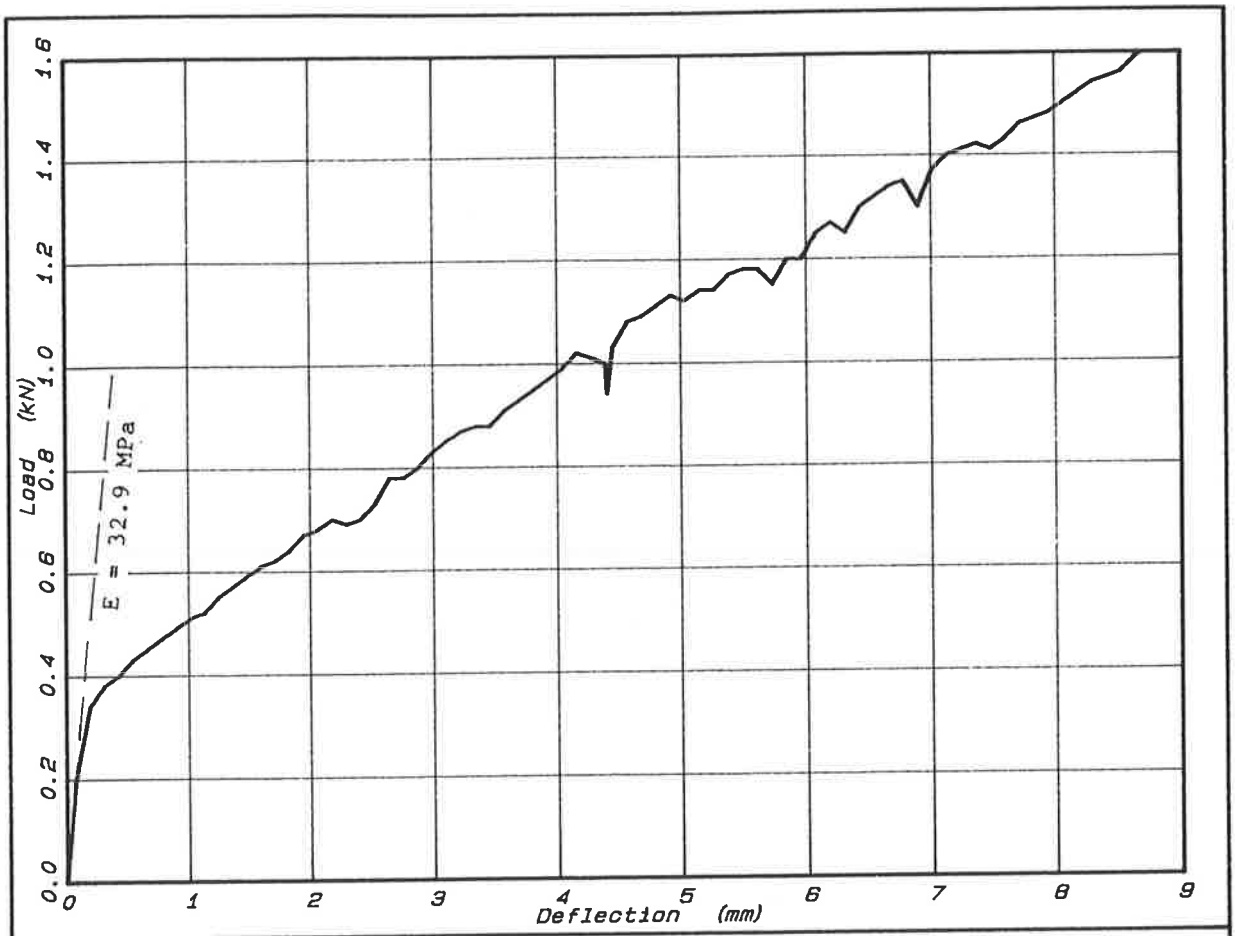

FIG. 25 - TRIAL BEDDING AT POORAKA
PLATE LOAD TEST AT LOCATION No. 1 USING 75 mm DIAMETER PLATE

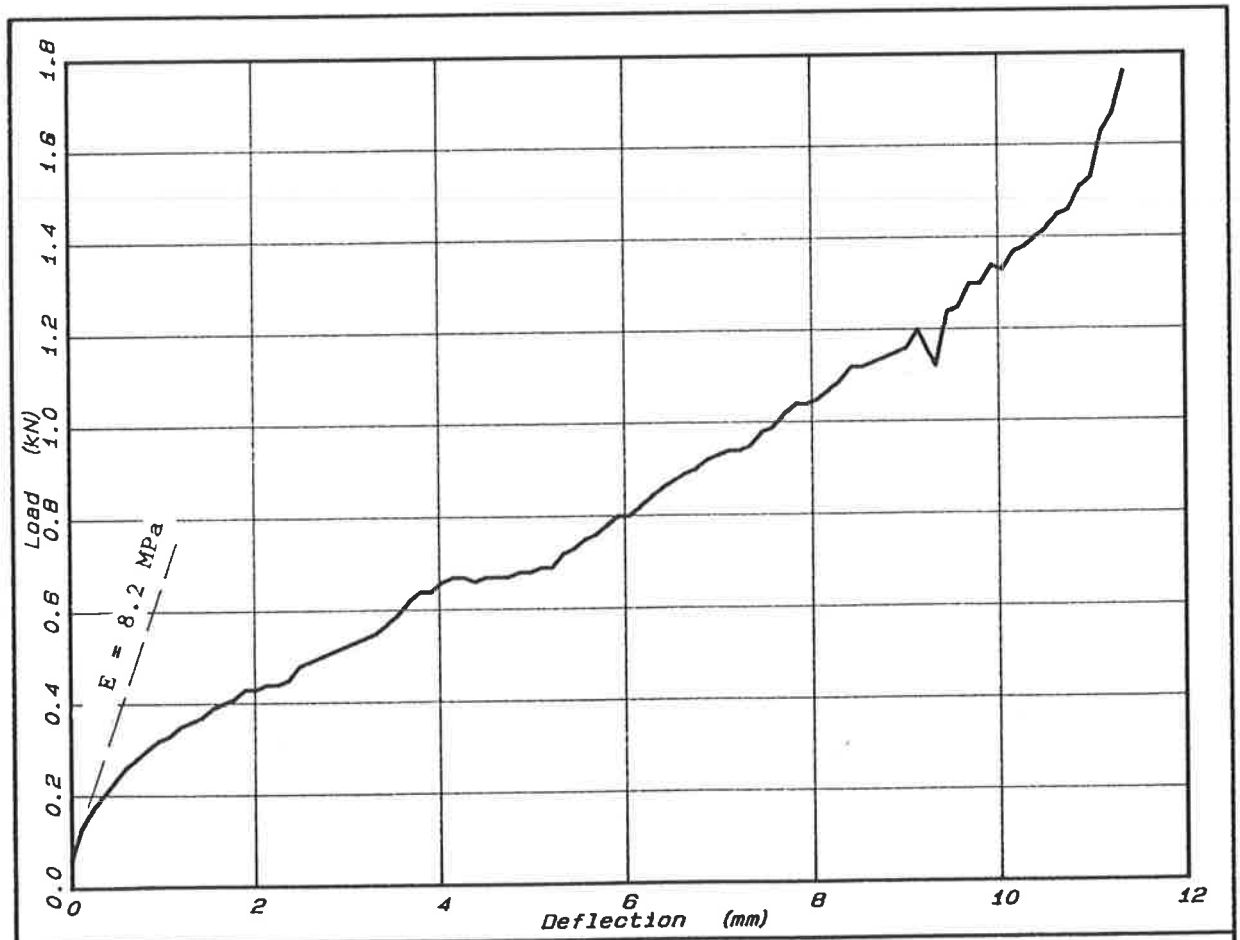

FIG. 26 - TRIAL BEDDING AT POORAKA
PLATE LOAD TEST AT LOCATION No. 2 USING 75 mm DIAMETER PLATE

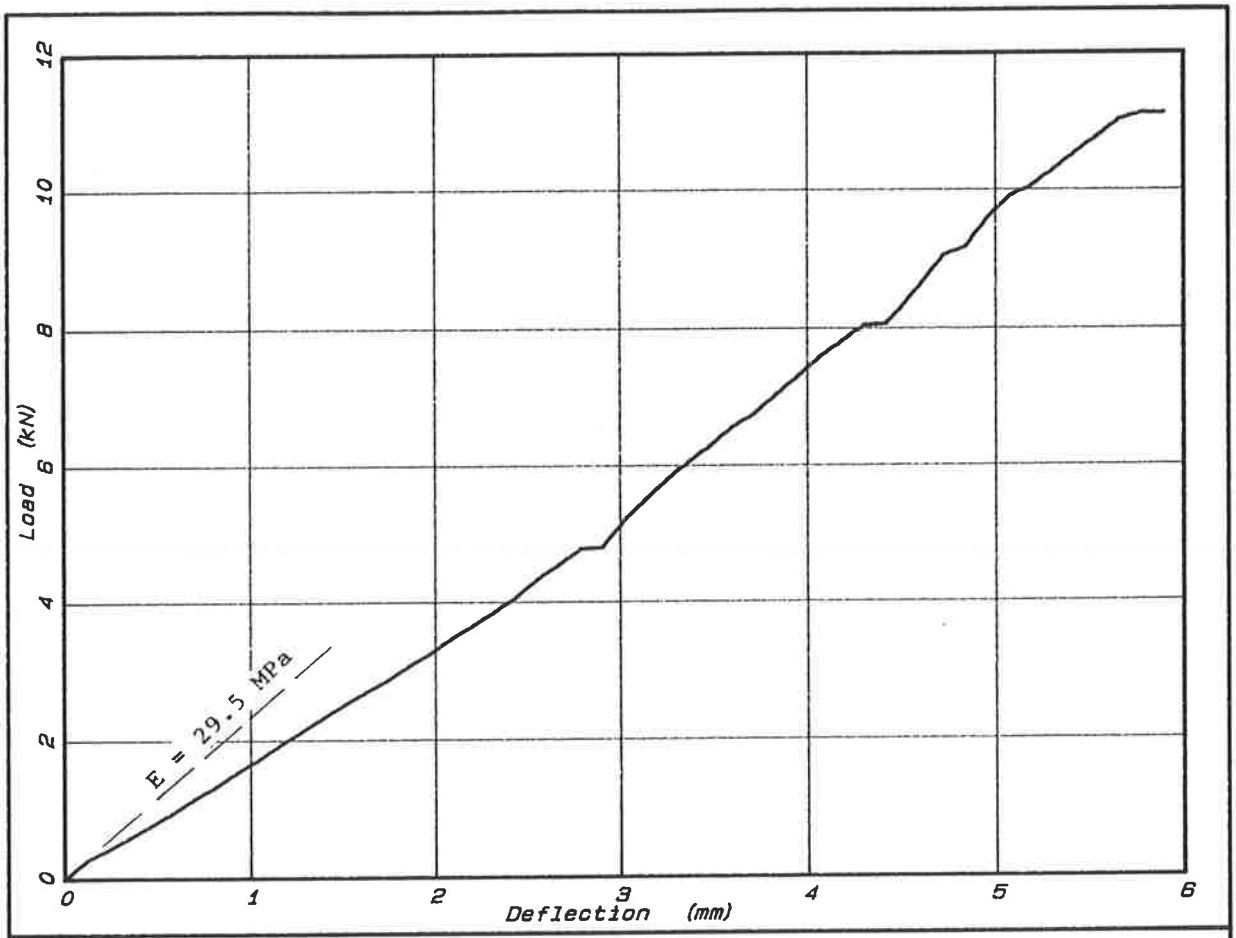

FIG. 27 - TRIAL BEDDING AT POORAKA
PLATE LOAD TEST AT LOCATION No. 3 USING 75 mm DIAMETER PLATE

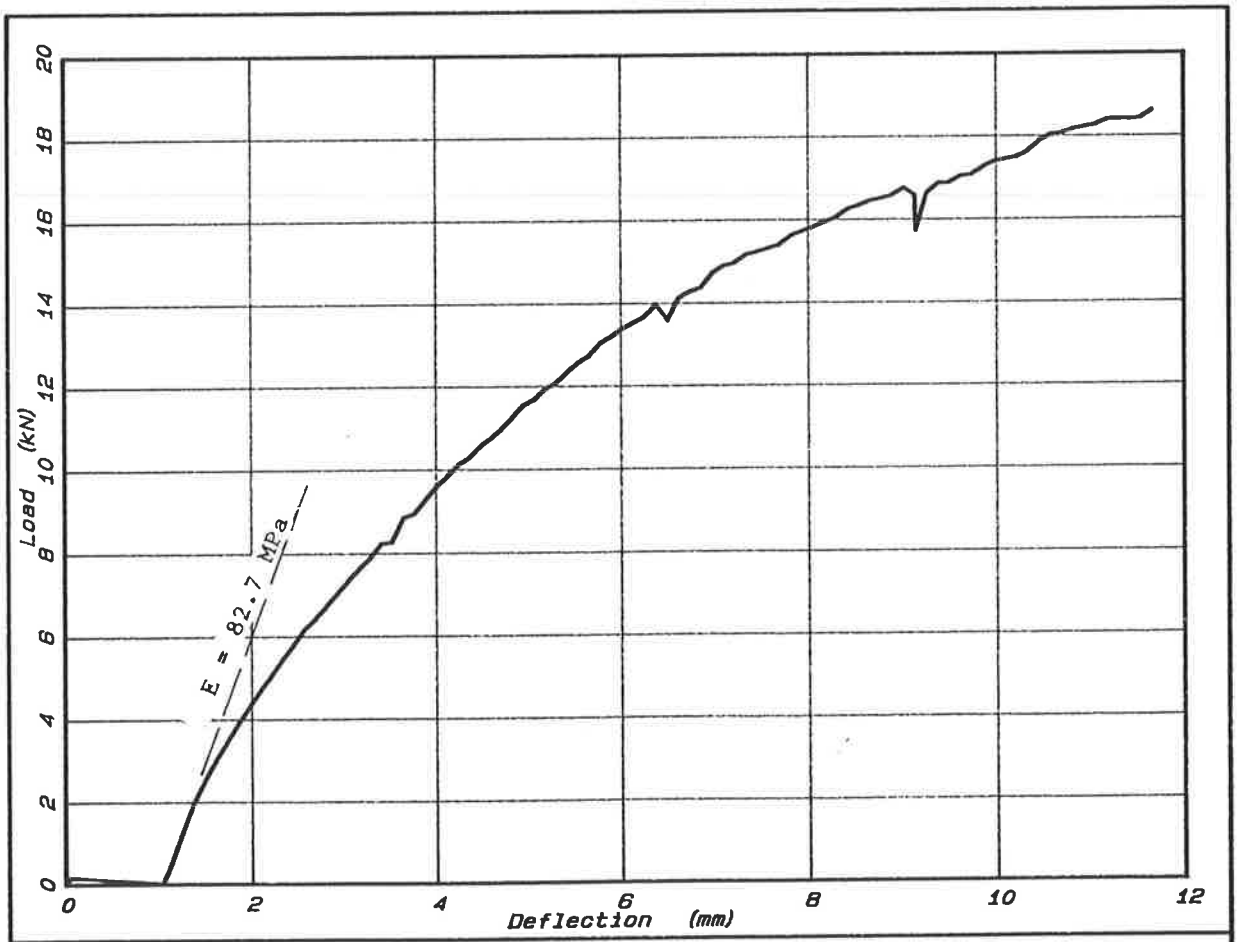

FIG. 28 - TRIAL BEDDING AT POORAKA
PLATE LOAD TEST AT LOCATION No. 4 USING 75 mm DIAMETER PLATE

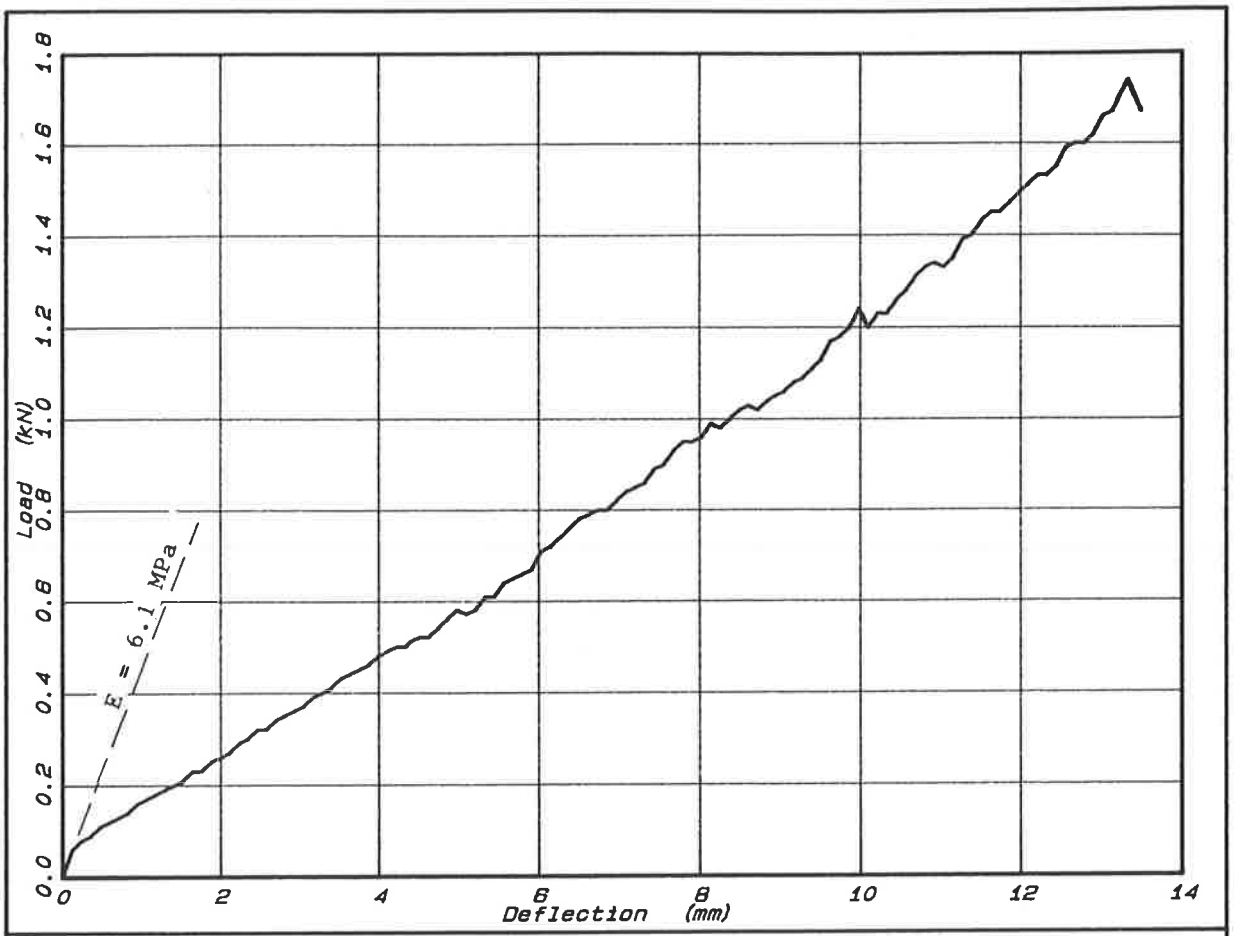

FIG. 29 - TRIAL BEDDING AT POORAKA
PLATE LOAD TEST AT LOCATION No. 5 USING 75 mm DIAMETER PLATE

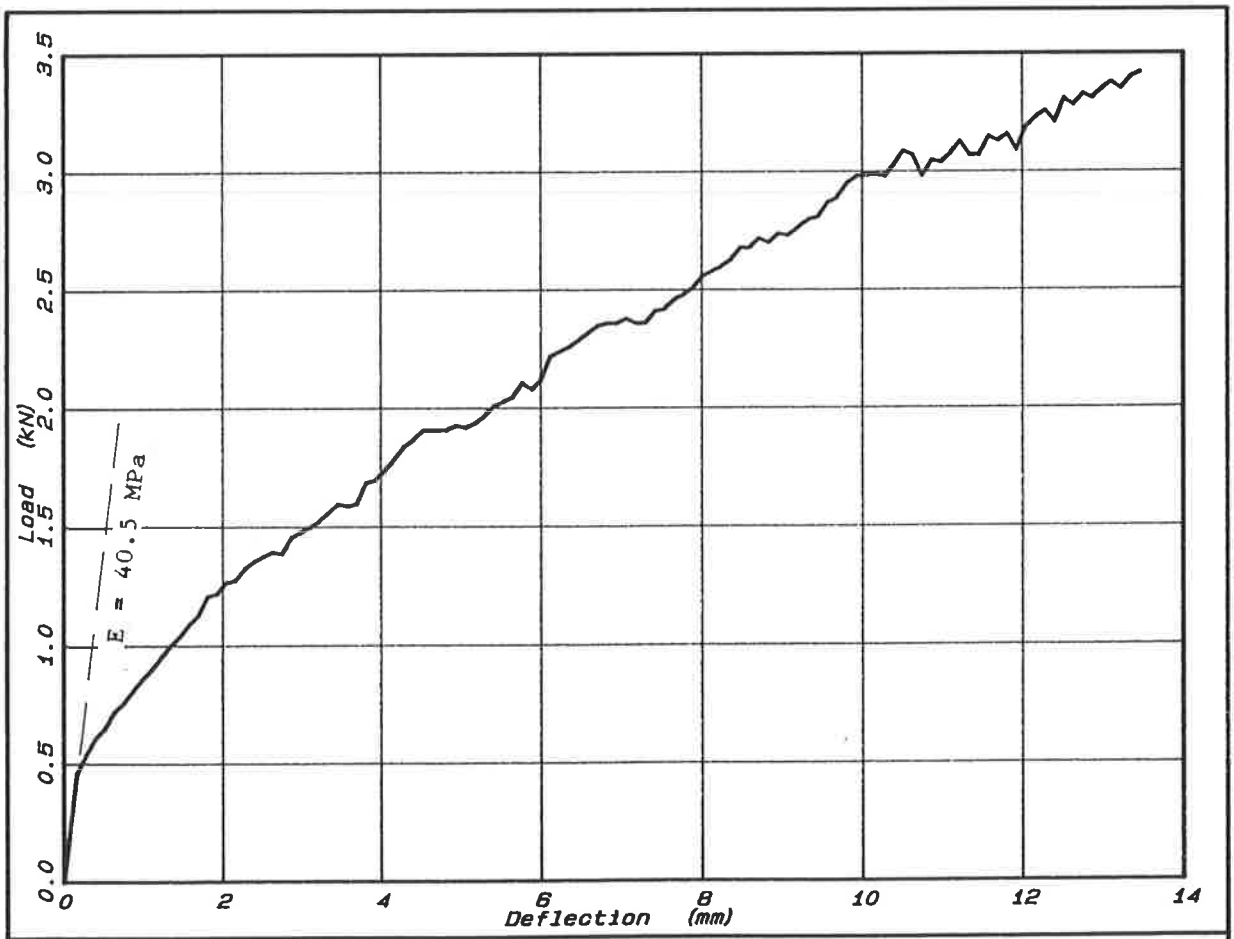

FIG. 30 - TRIAL BEDDING AT POORAKA
PLATE LOAD TEST AT LOCATION No. 6 USING 75 mm DIAMETER PLATE

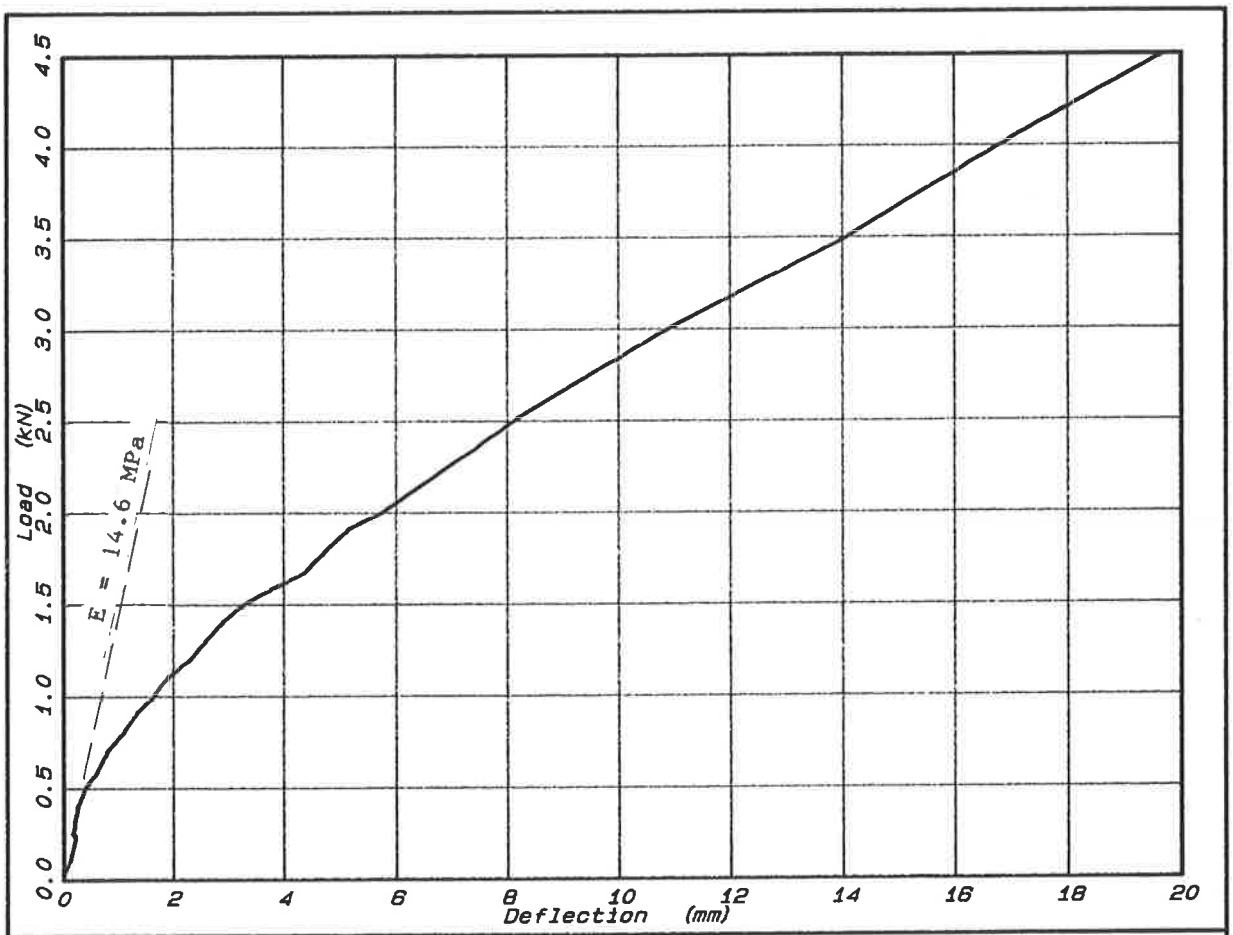

FIG. 31 - FINE CRUSHED ROCK AT 51.8% RELATIVE DENSITY
LABORATORY PLATE LOAD TEST USING 99 mm DIAMETER PLATE

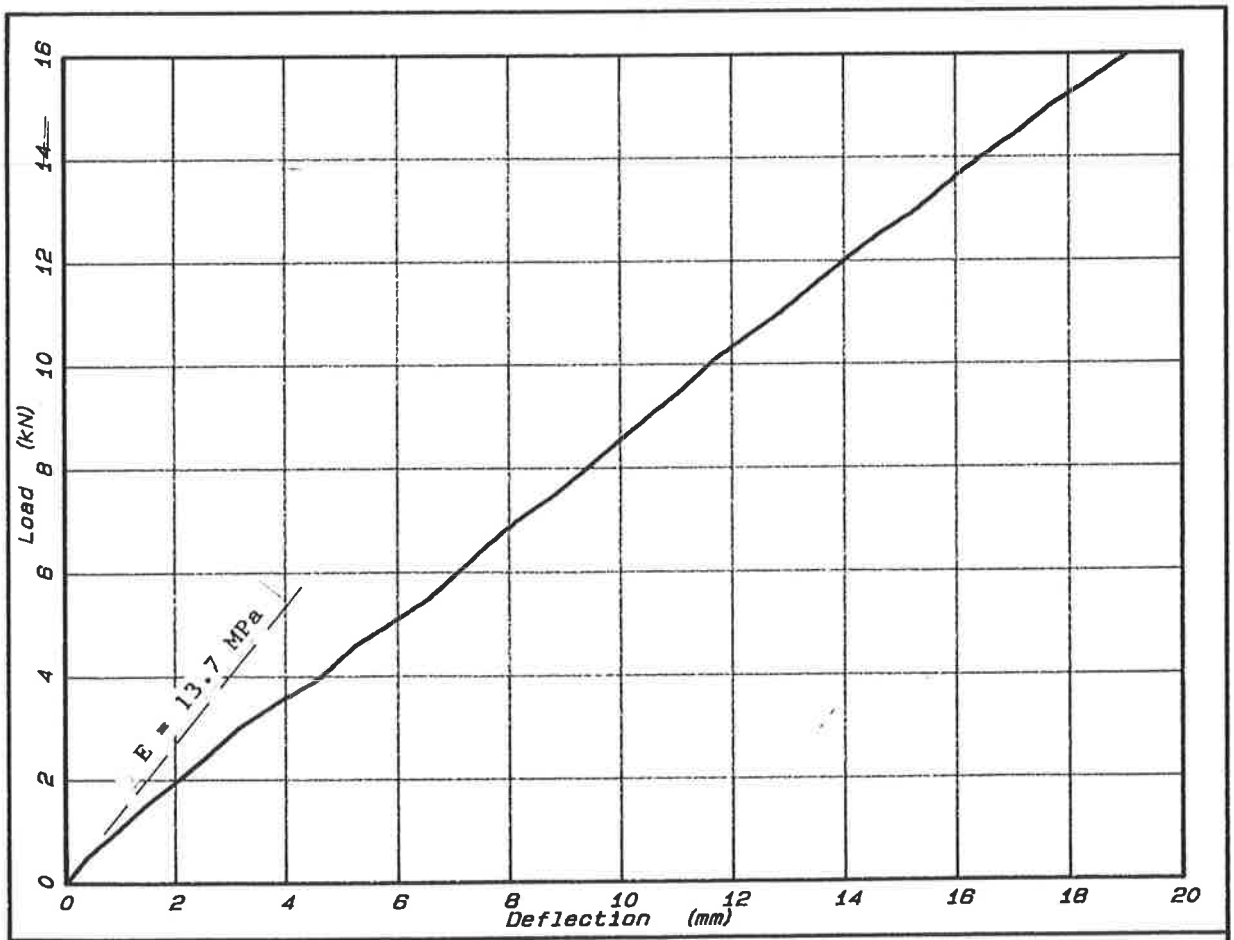

FIG. 32 - FINE CRUSHED ROCK AT 70.9% RELATIVE DENSITY
LABORATORY PLATE LOAD TEST USING 99 mm DIAMETER PLATE

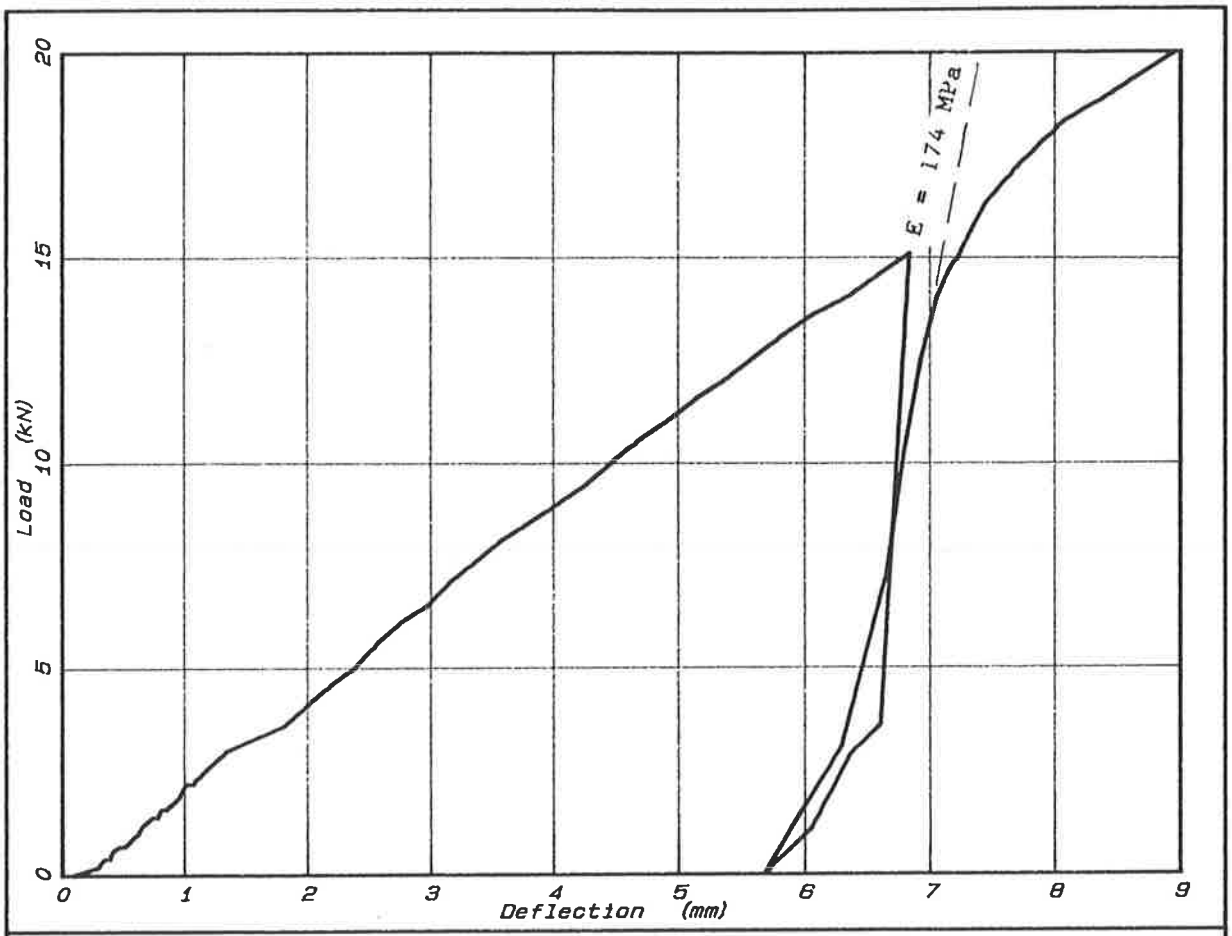

FIG.33 - FINE CRUSHED ROCK AT 81.6% RELATIVE DENSITY
LABORATORY PLATE LOAD TEST USING 99 mm DIAMETER PLATE

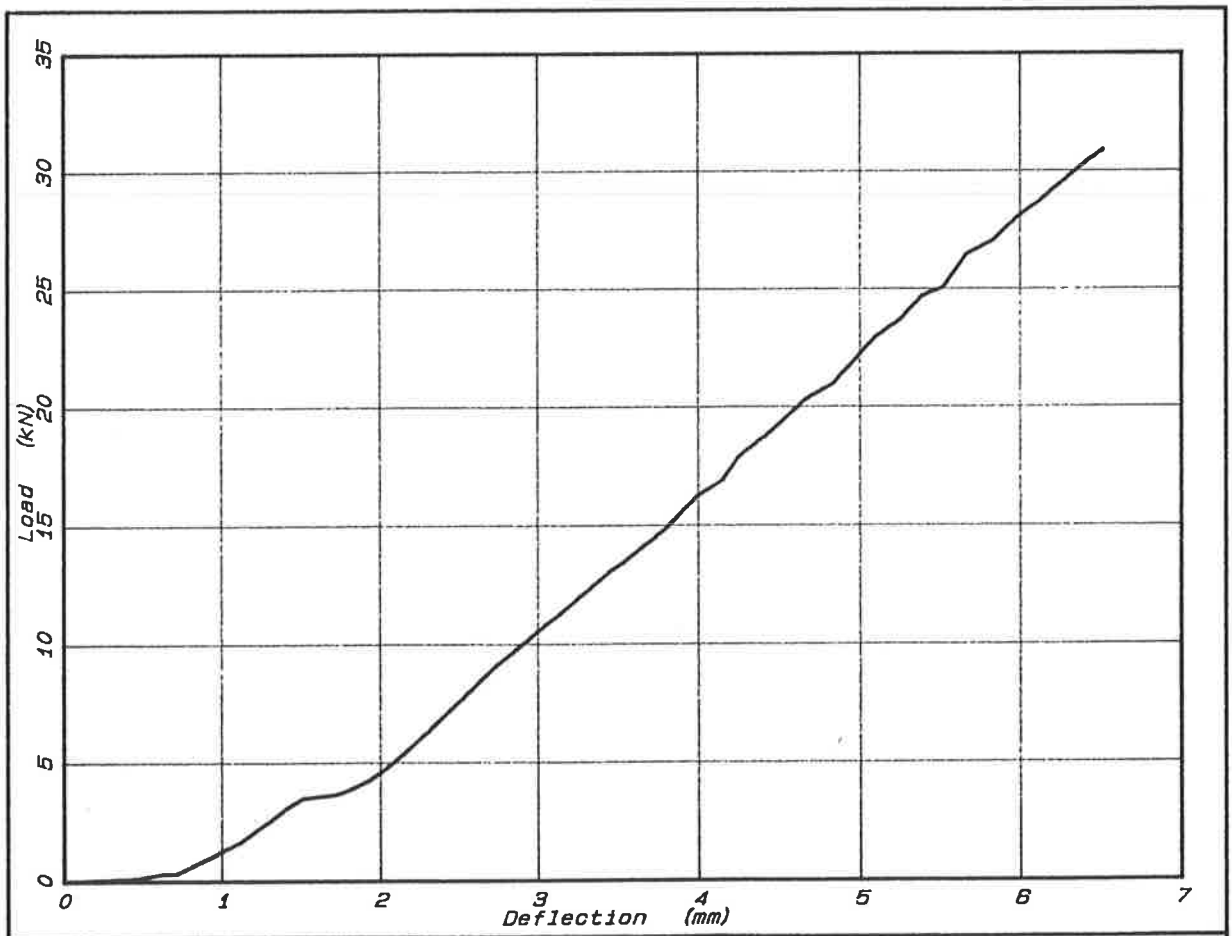

FIG.34 - FINE CRUSHED ROCK AT 100% RELATIVE DENSITY
LABORATORY PLATE LOAD TEST USING 99 mm DIAMETER PLATE

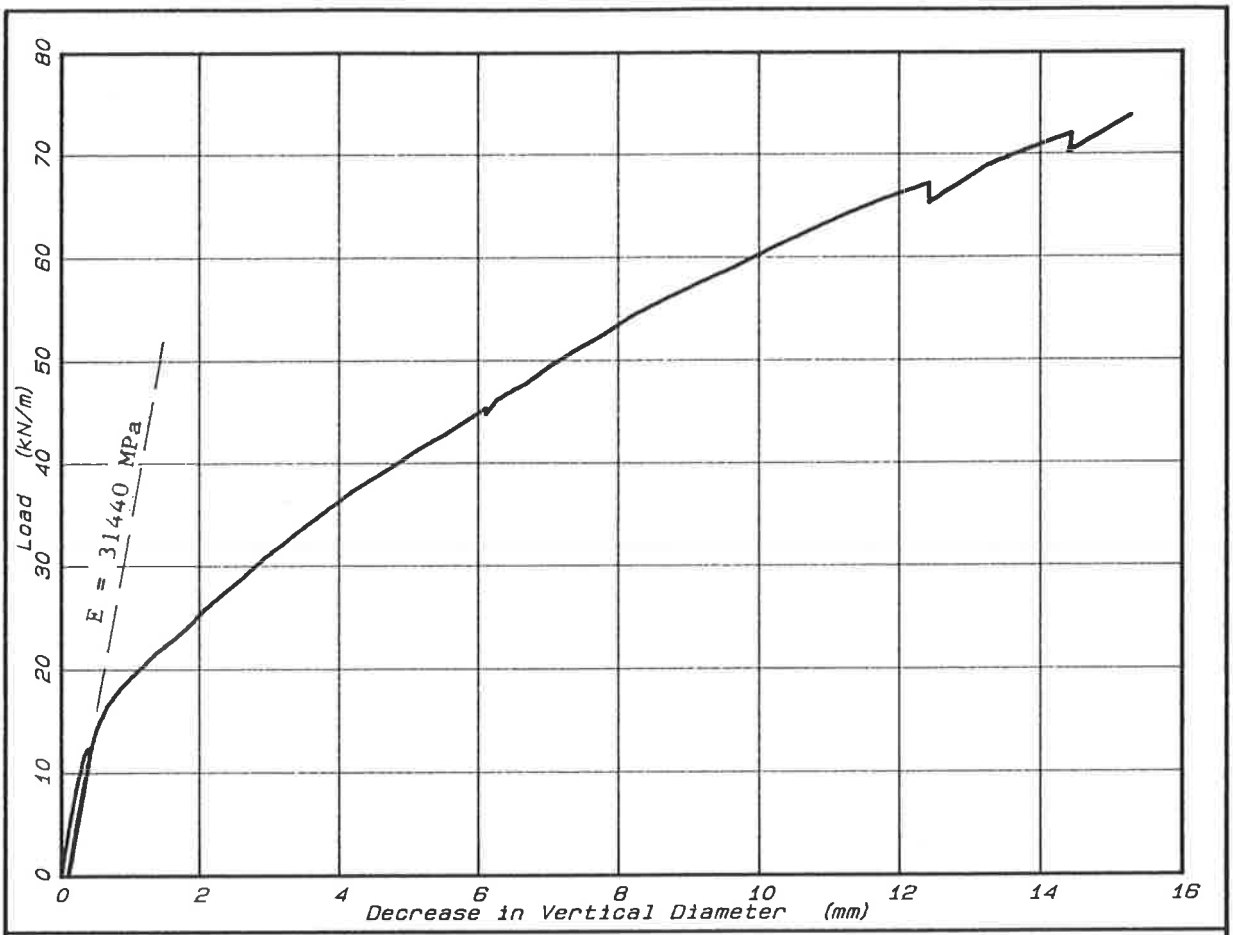

FIG. 35 - THREE-EDGE BEARING TEST
VERTICAL DIAMETER DECREASE VS LOAD

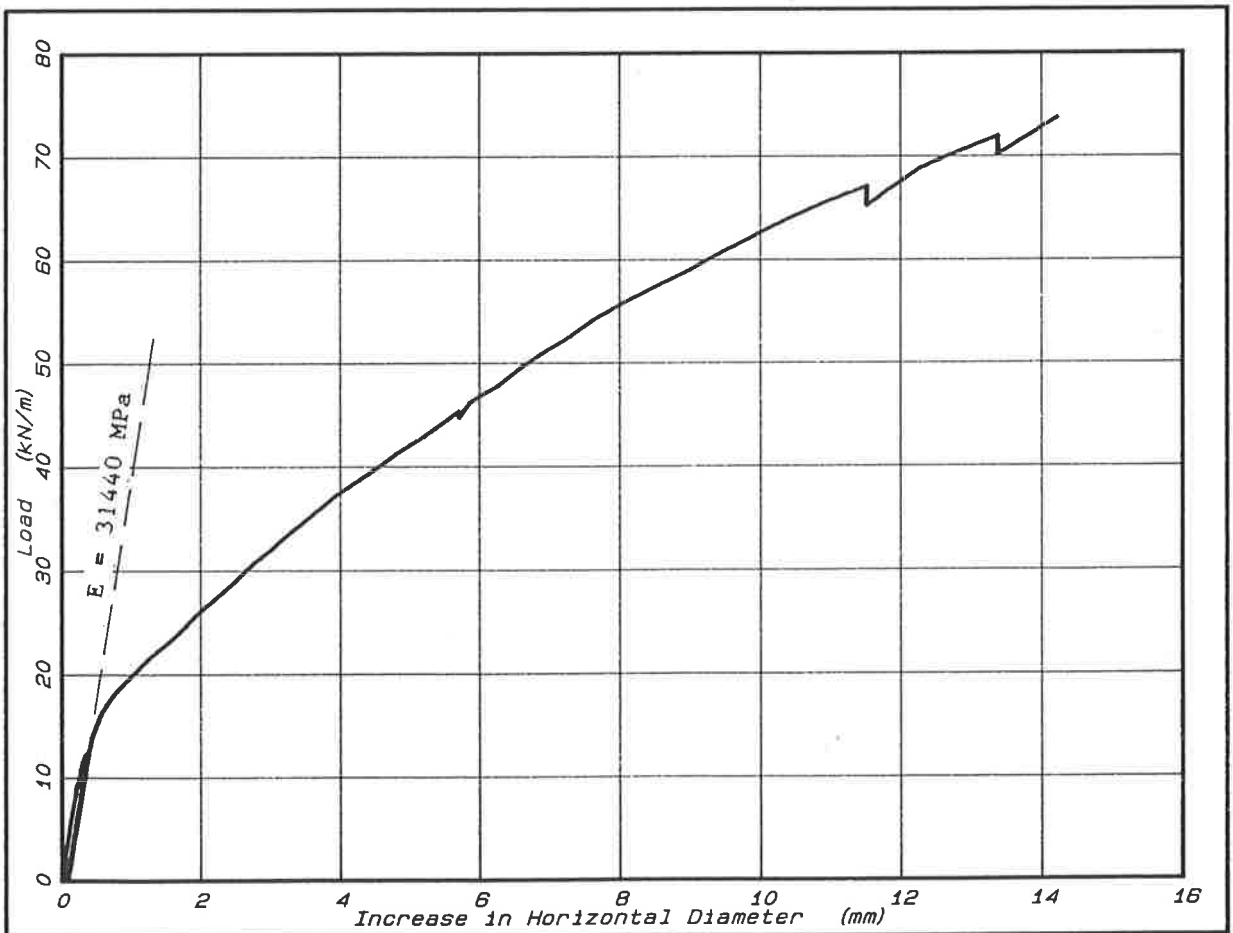

FIG. 36 - THREE-EDGE BEARING TEST
HORIZONTAL DIAMETER INCREASE VS LOAD

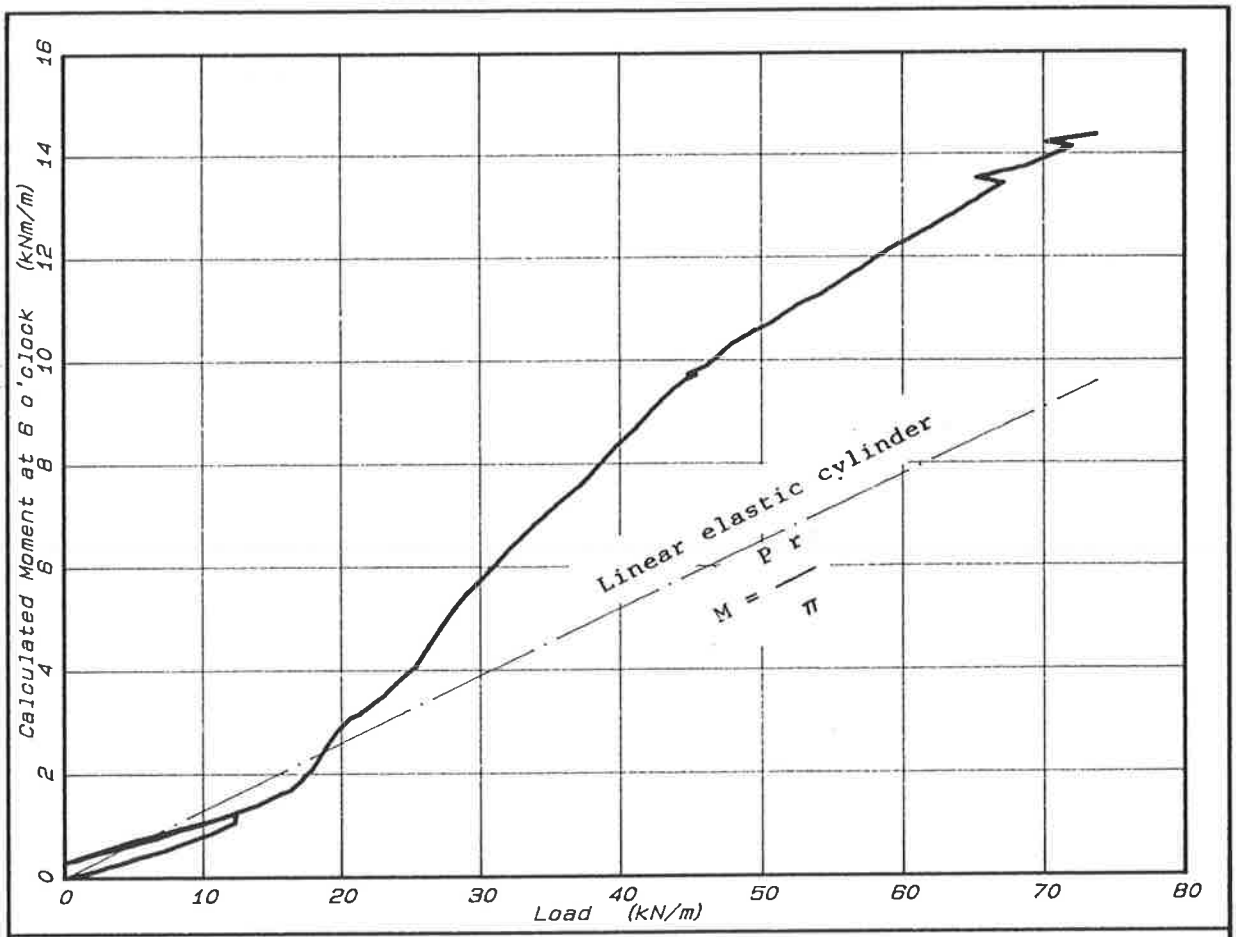

FIG. 37 - THREE-EDGE BEARING TEST
MOMENT AT 6 O'CLOCK VS LOAD (+ve M compresses outer face)

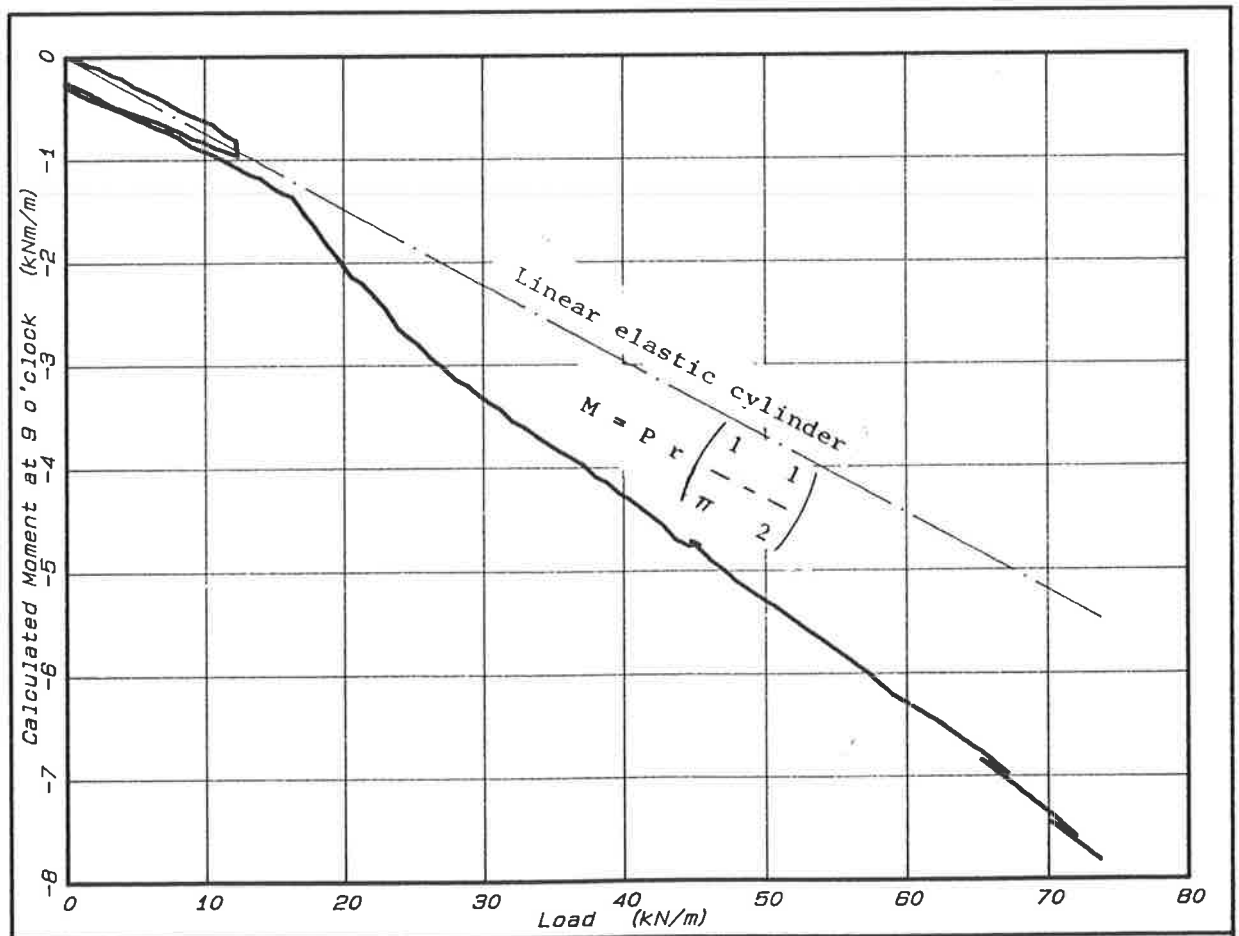

FIG. 38 - THREE-EDGE BEARING TEST
MOMENT AT 9 O'CLOCK VS LOAD (+ve M compresses outer face)

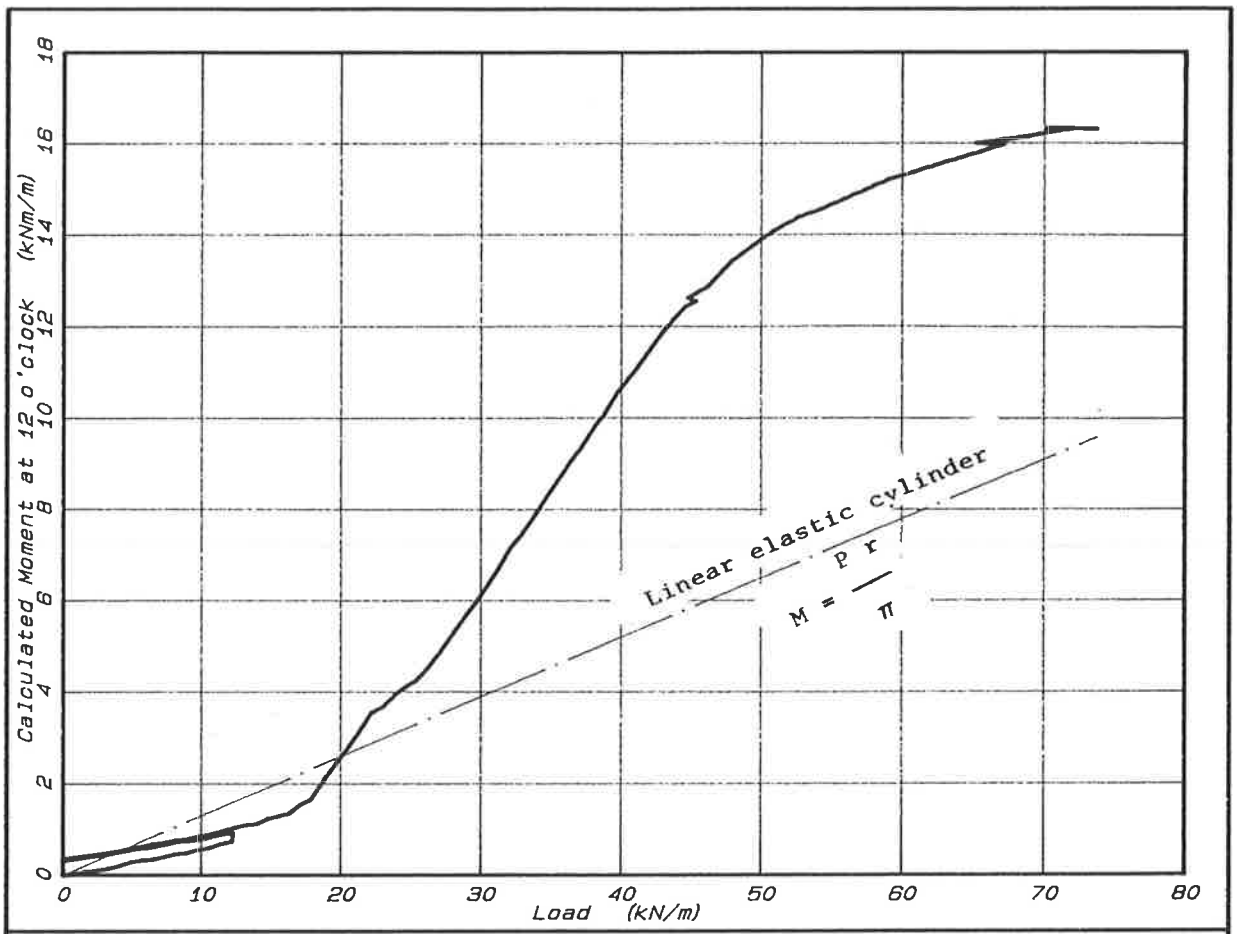

FIG. 39 - THREE-EDGE BEARING TEST
MOMENT AT 12 O'CLOCK VS LOAD (+ve M compresses outer face)

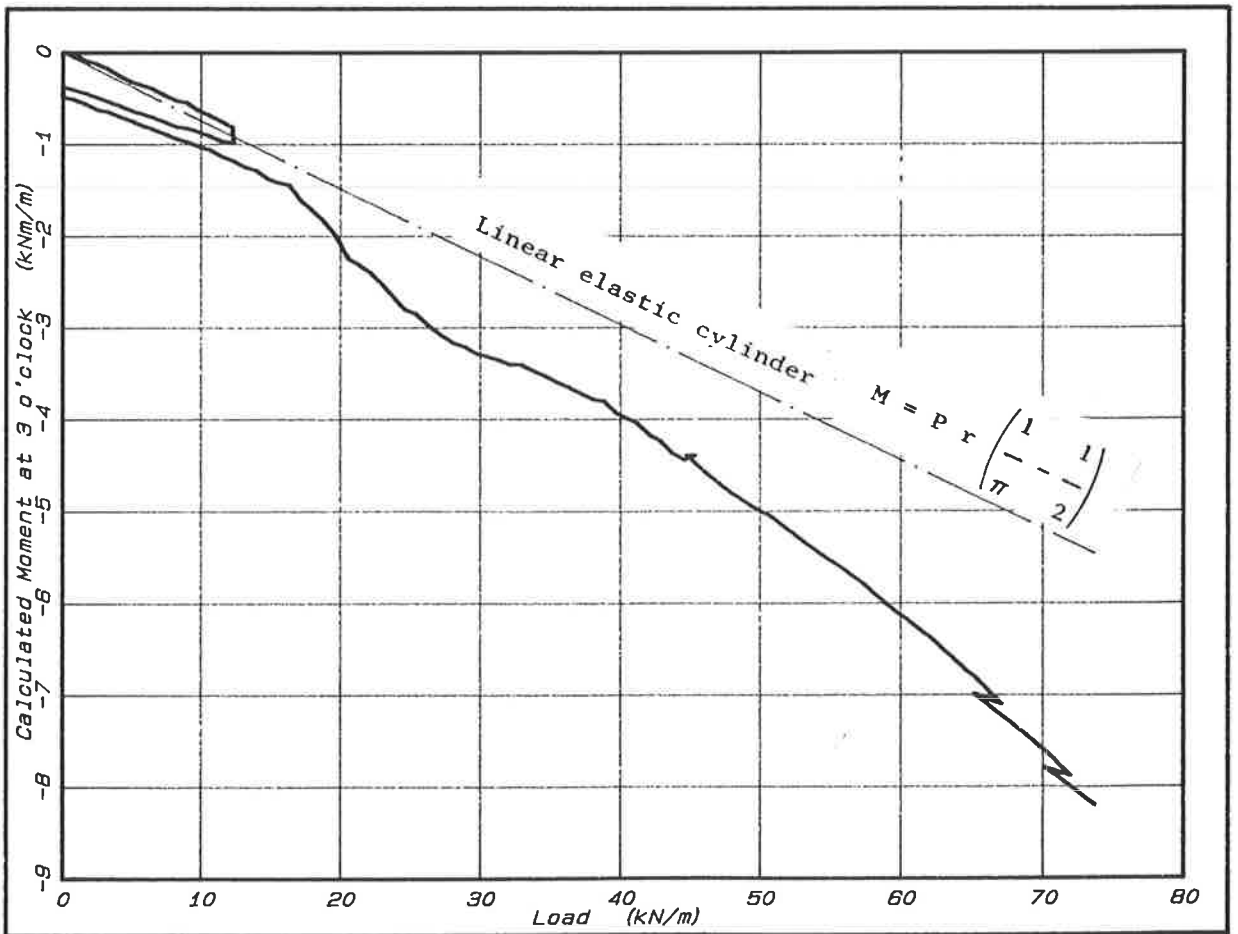

FIG. 40 - THREE-EDGE BEARING TEST
MOMENT AT 3 O'CLOCK VS LOAD (+ve M compresses outer face)

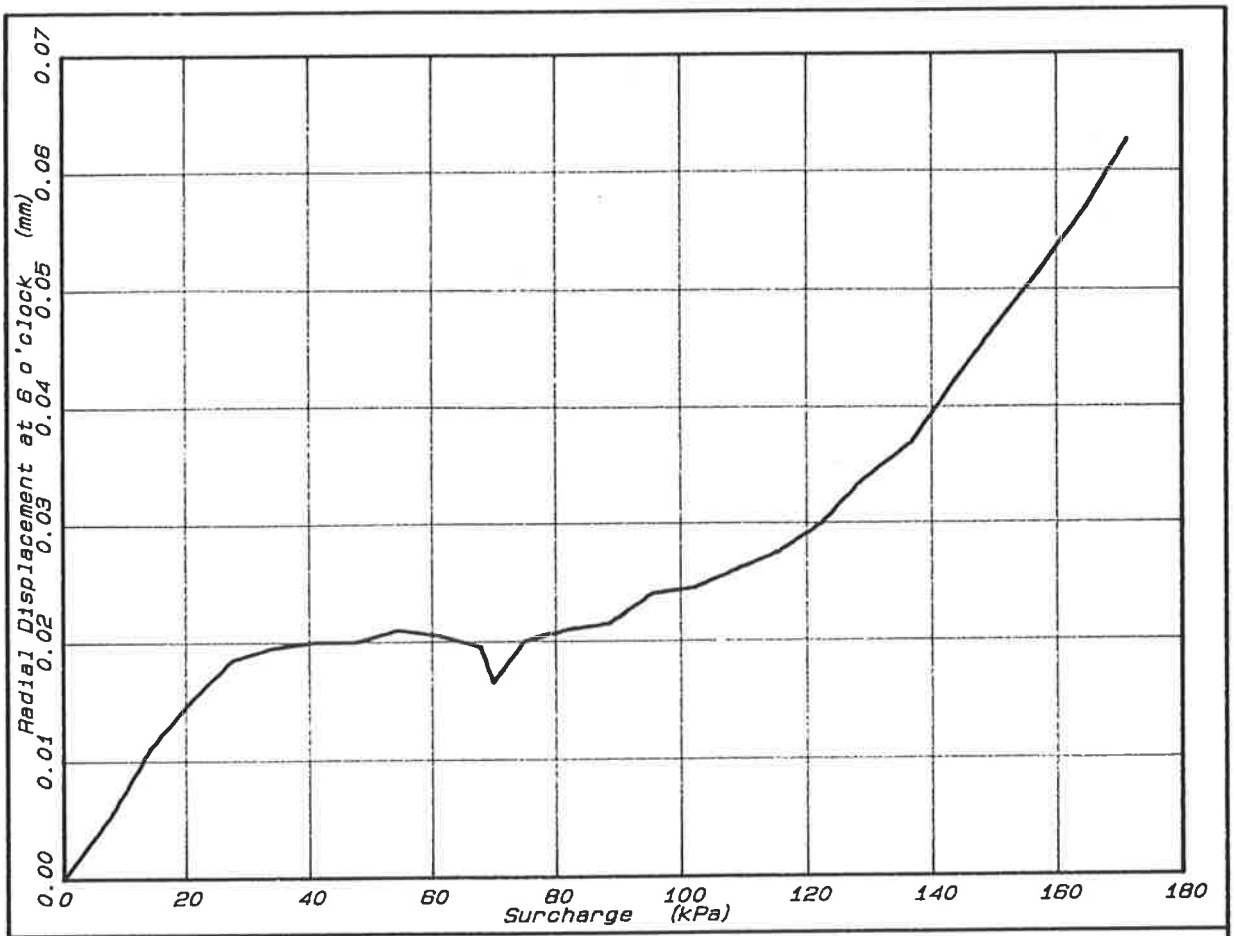

FIG. 41 - MILE END TEST BIN - BEDDED PIPE TEST
RADIAL DISPLACEMENT AT 6 O'CLOCK VS SURCHARGE (+ve towards centre)

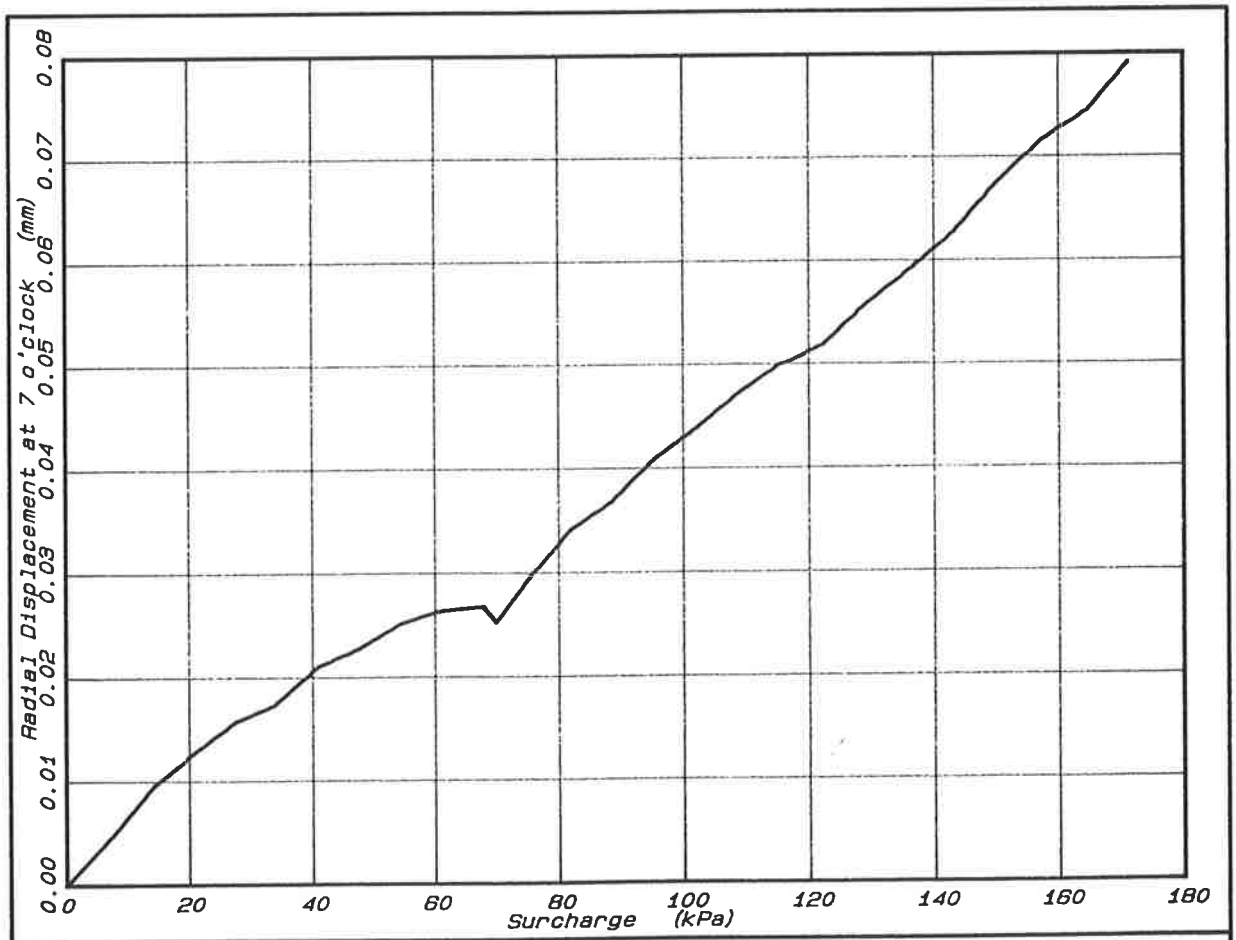

FIG. 42 - MILE END TEST BIN - BEDDED PIPE TEST
RADIAL DISPLACEMENT AT 7 O'CLOCK VS SURCHARGE (+ve towards centre)

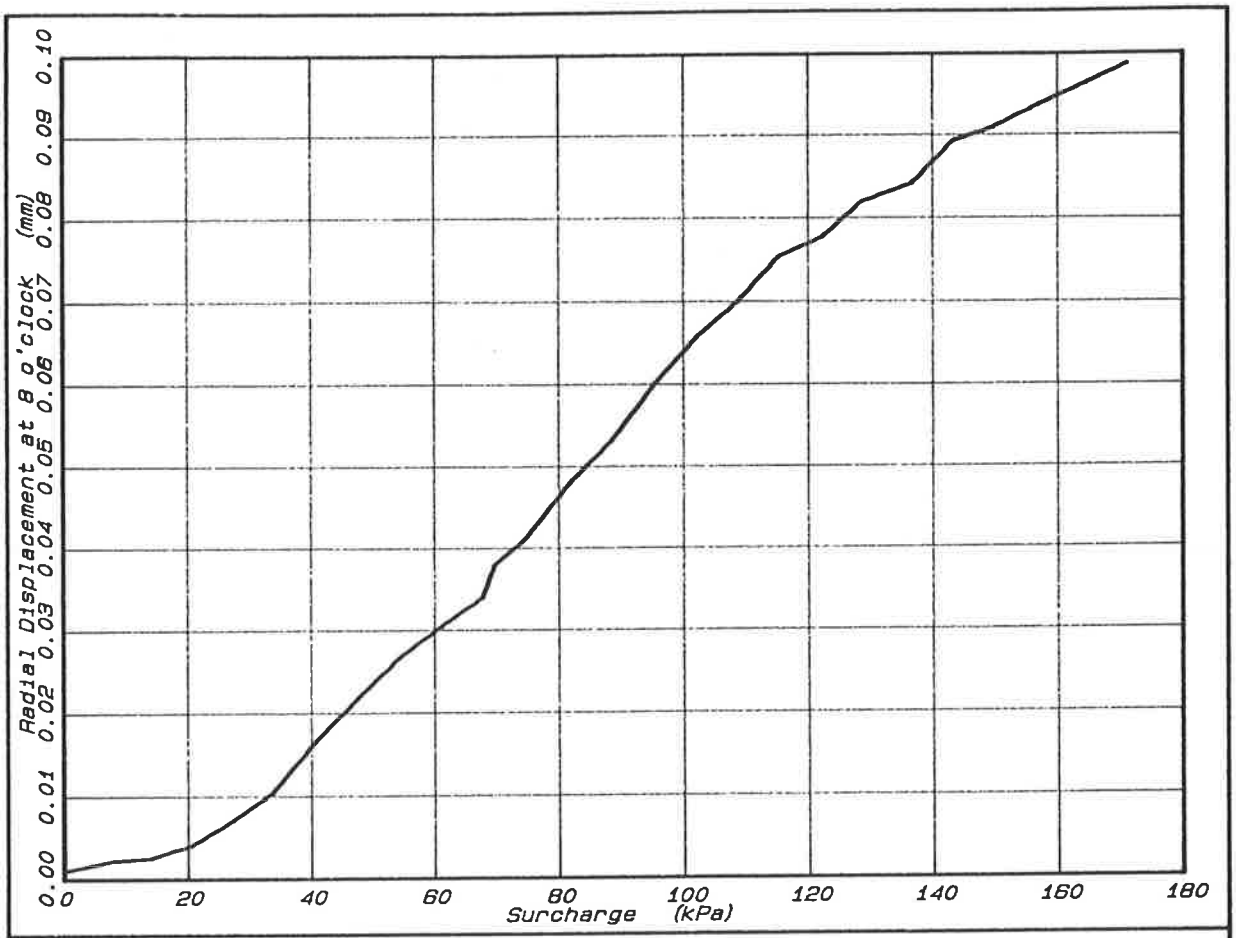

FIG.43 - MILE END TEST BIN - BEDDED PIPE TEST
RADIAL DISPLACEMENT AT 8 O'CLOCK VS SURCHARGE (+ve towards centre)

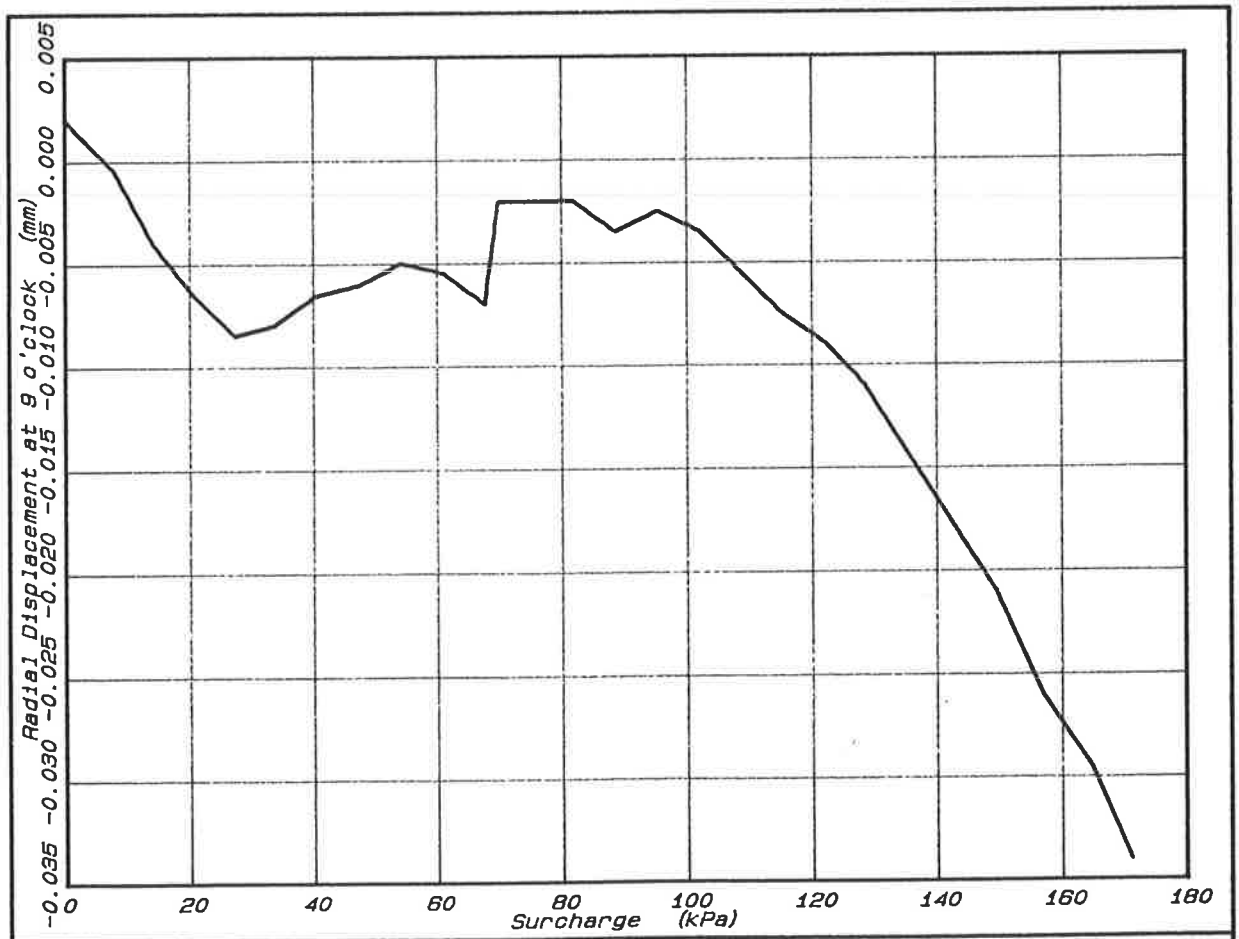

FIG.44 - MILE END TEST BIN - BEDDED PIPE TEST
RADIAL DISPLACEMENT AT 9 O'CLOCK VS SURCHARGE (+ve towards centre)

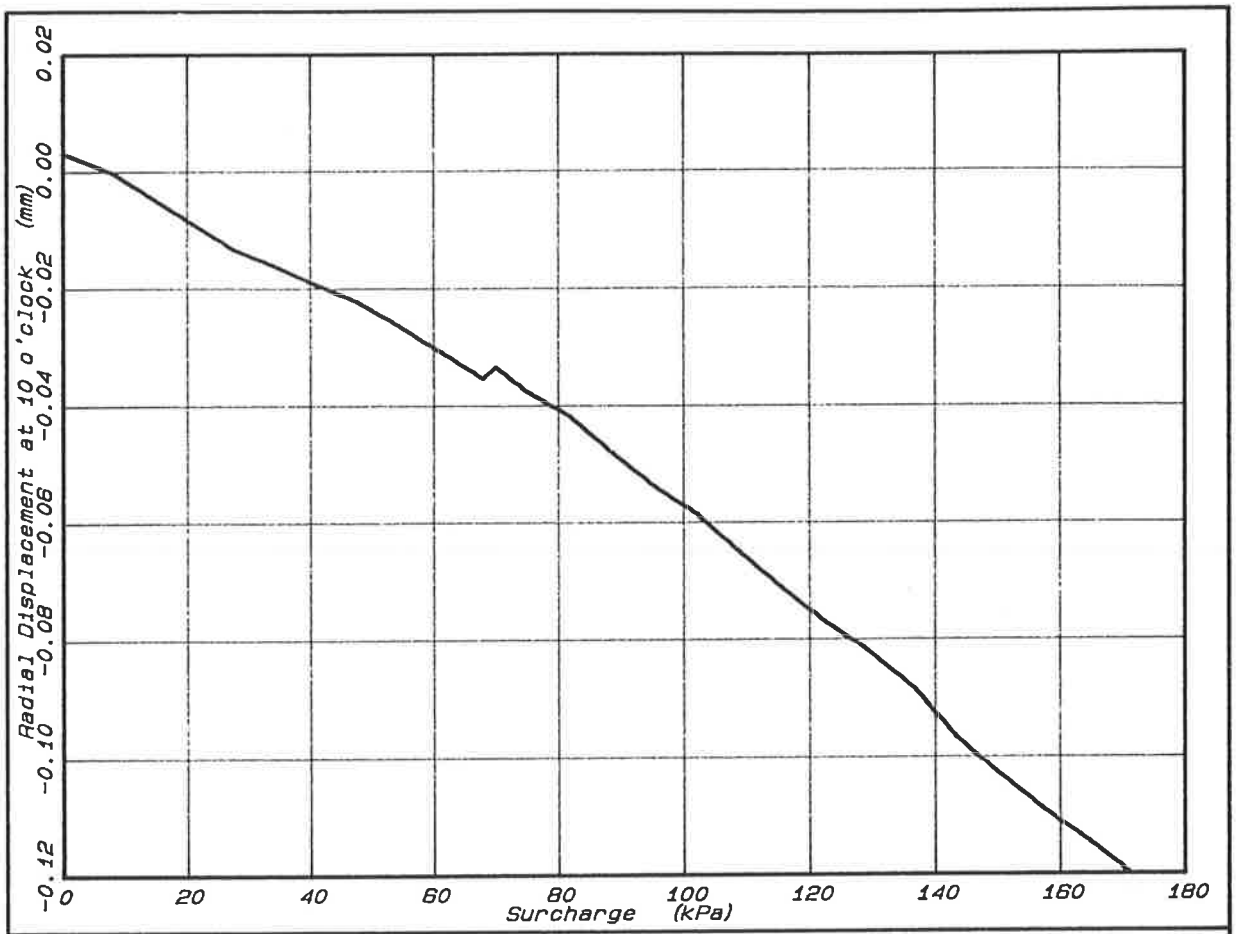

FIG. 45 - MILE END TEST BIN - BEDDED PIPE TEST
RADIAL DISPLACEMENT AT 10 O'CLOCK VS SURCHARGE (+ve towards centre)

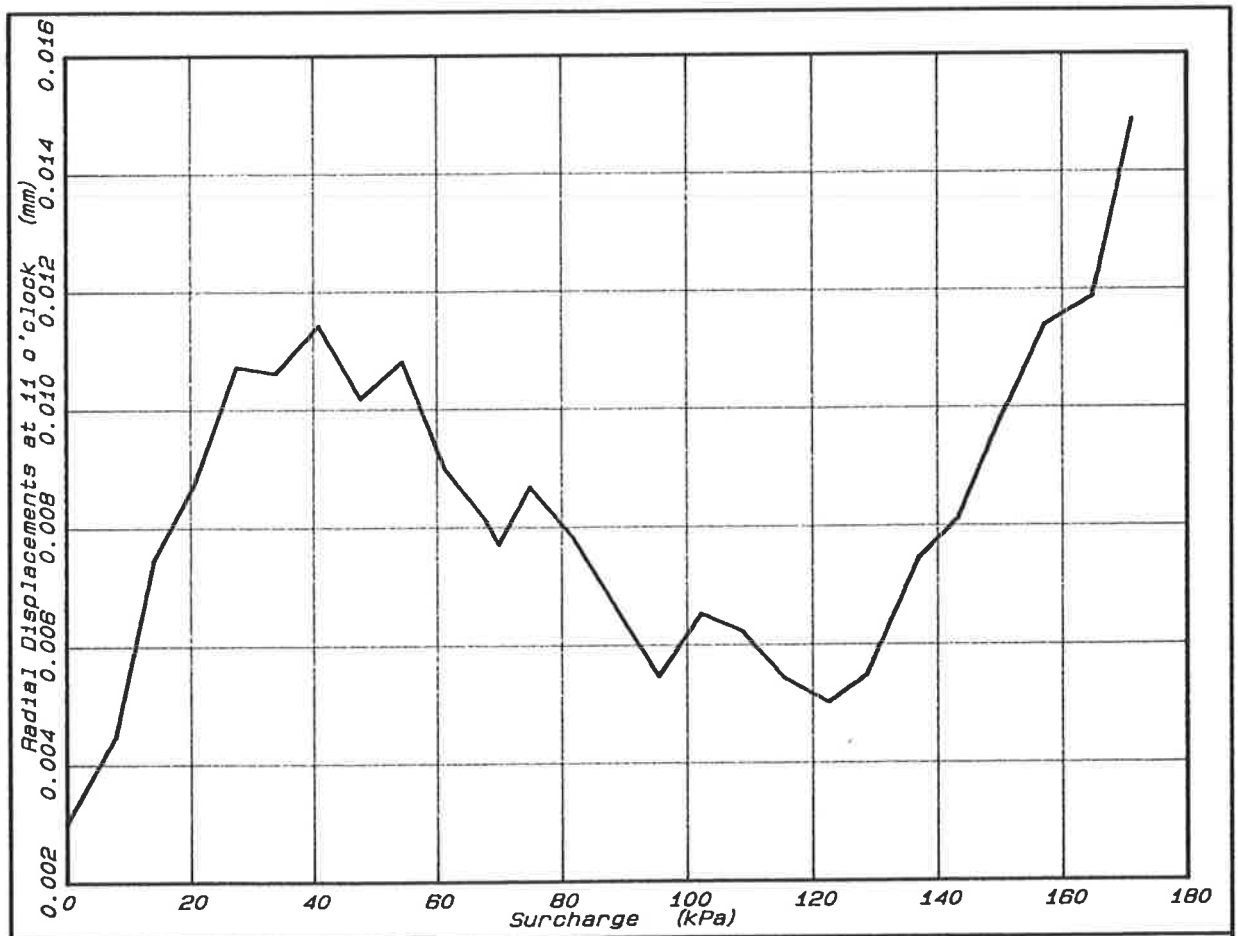

FIG. 46 - MILE END TEST BIN - BEDDED PIPE TEST
RADIAL DISPLACEMENT AT 11 O'CLOCK VS SURCHARGE (+ve towards centre)

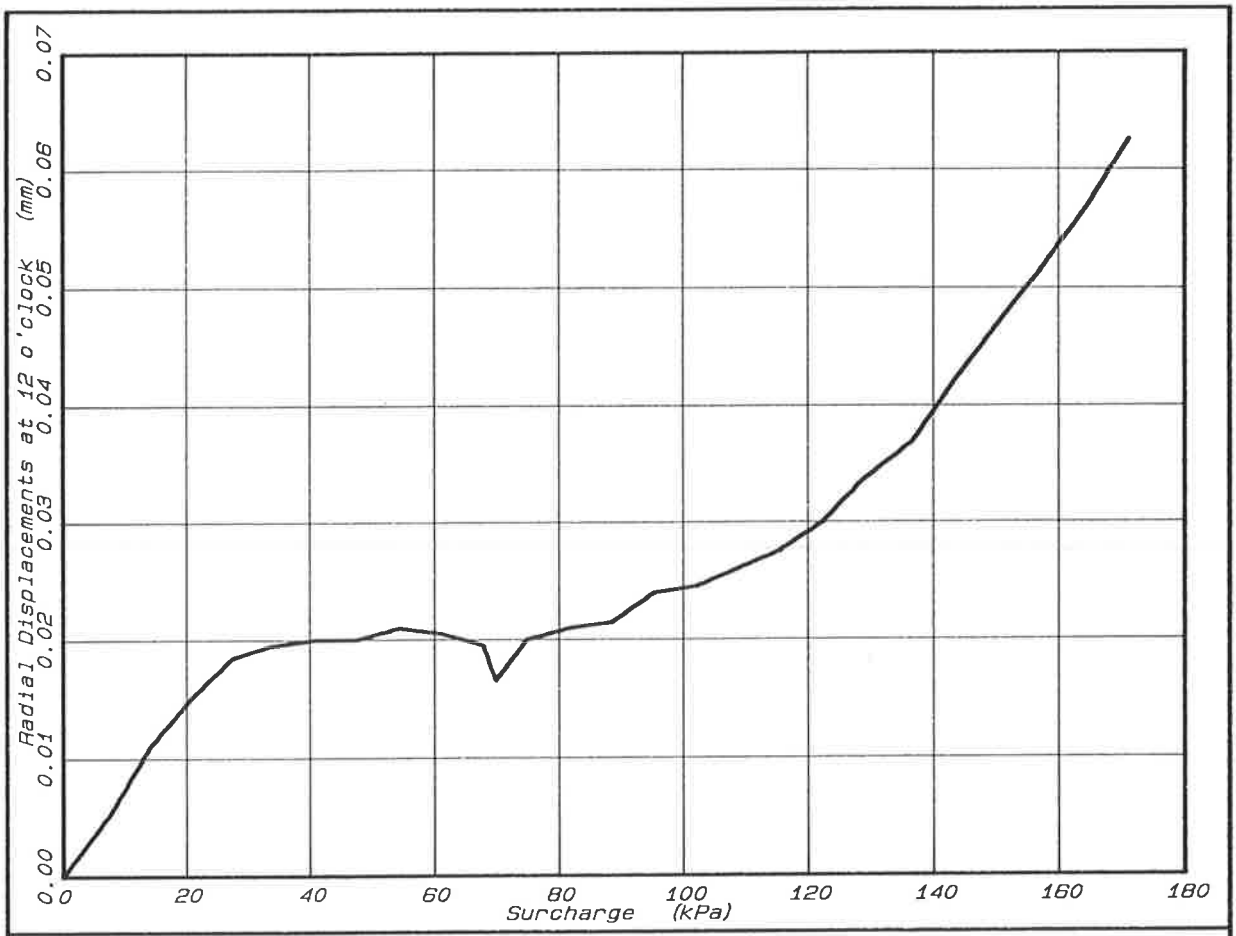

FIG. 47 - MILE END TEST BIN - BEDDED PIPE TEST
RADIAL DISPLACEMENT AT 12 O'CLOCK VS SURCHARGE (+ve towards centre)

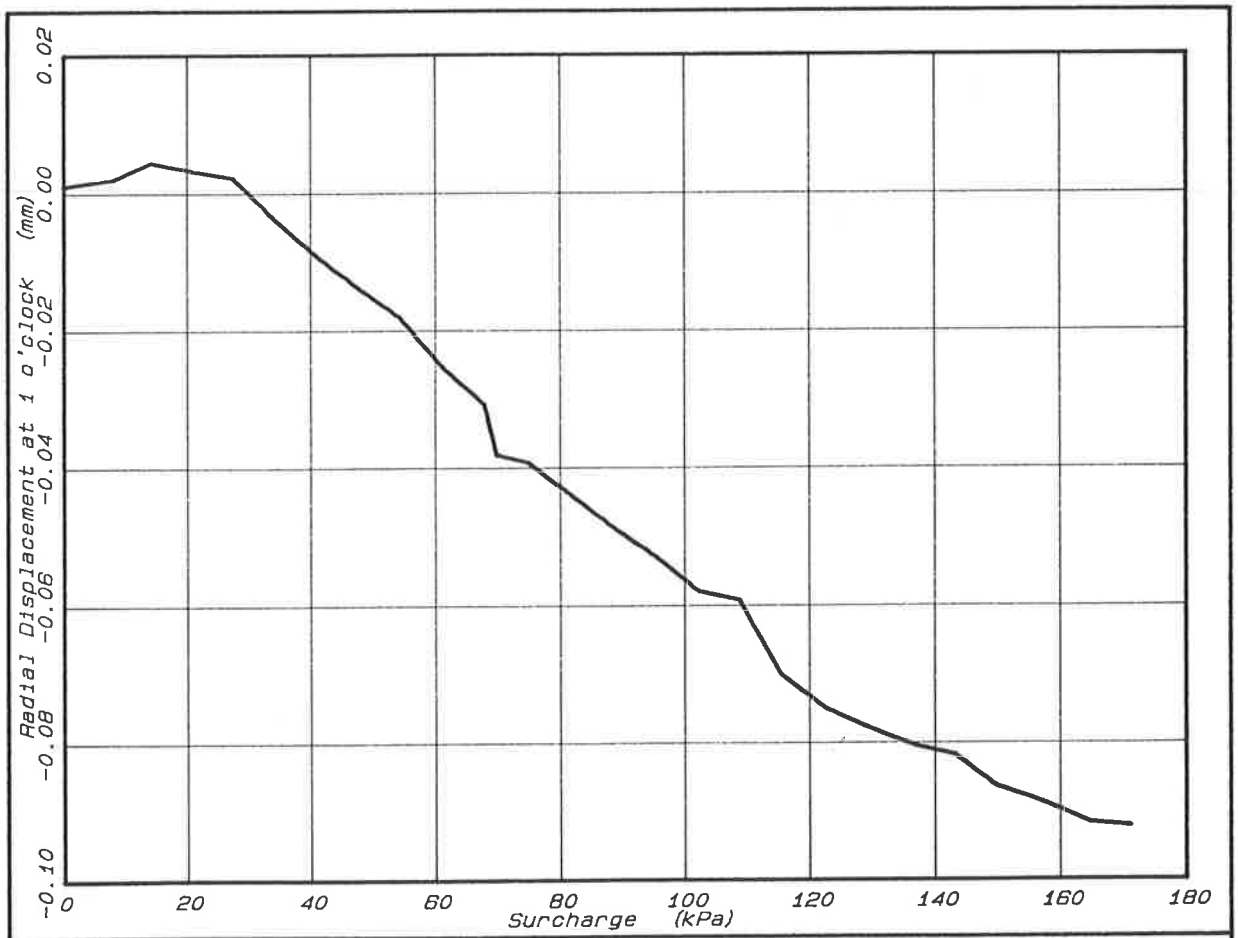

FIG. 48 - MILE END TEST BIN - BEDDED PIPE TEST
RADIAL DISPLACEMENT AT 1 O'CLOCK VS SURCHARGE (+ve towards centre)

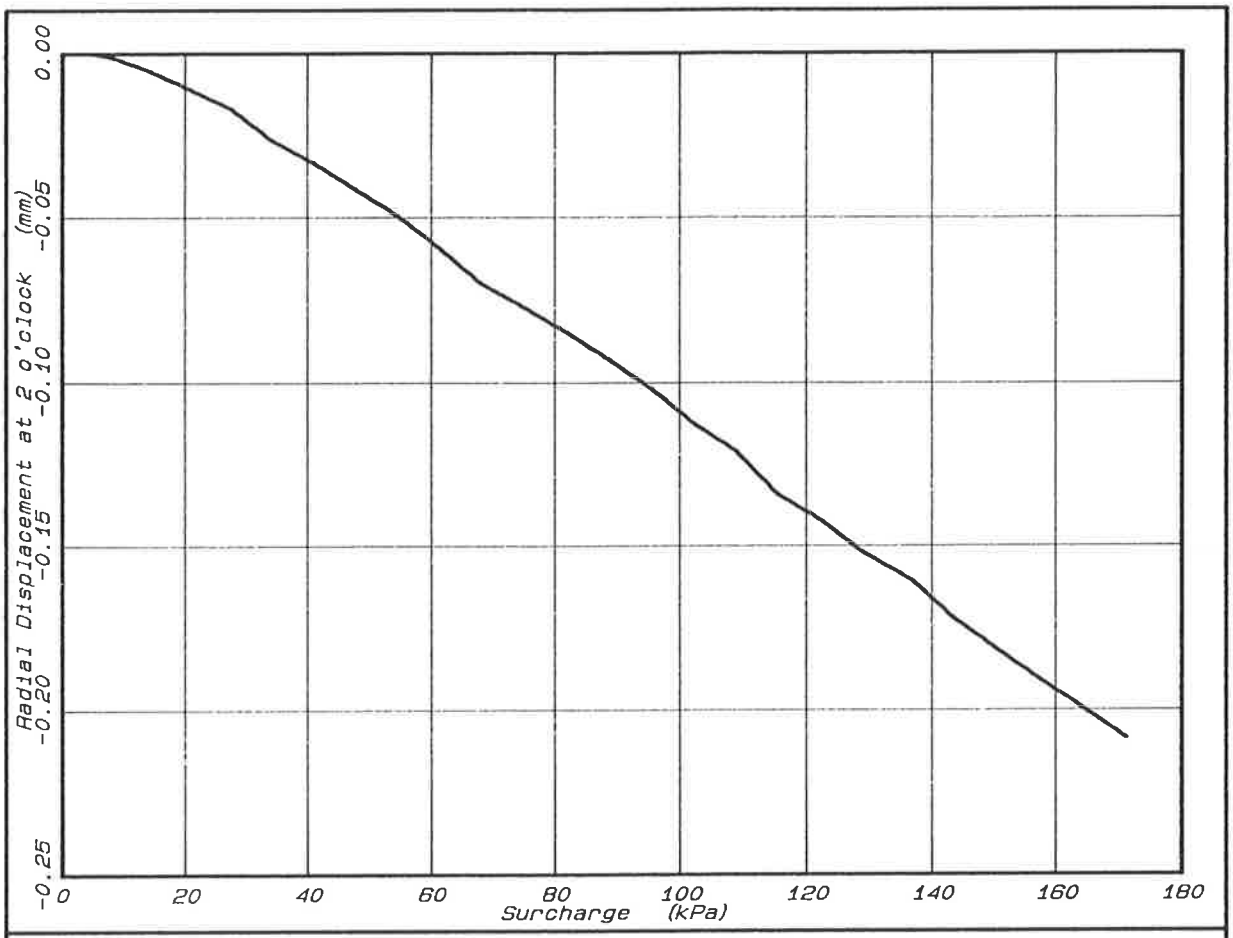

FIG. 49 - MILE END TEST BIN - BEDDED PIPE TEST
RADIAL DISPLACEMENT AT 2 O'CLOCK VS SURCHARGE (+ve towards centre)

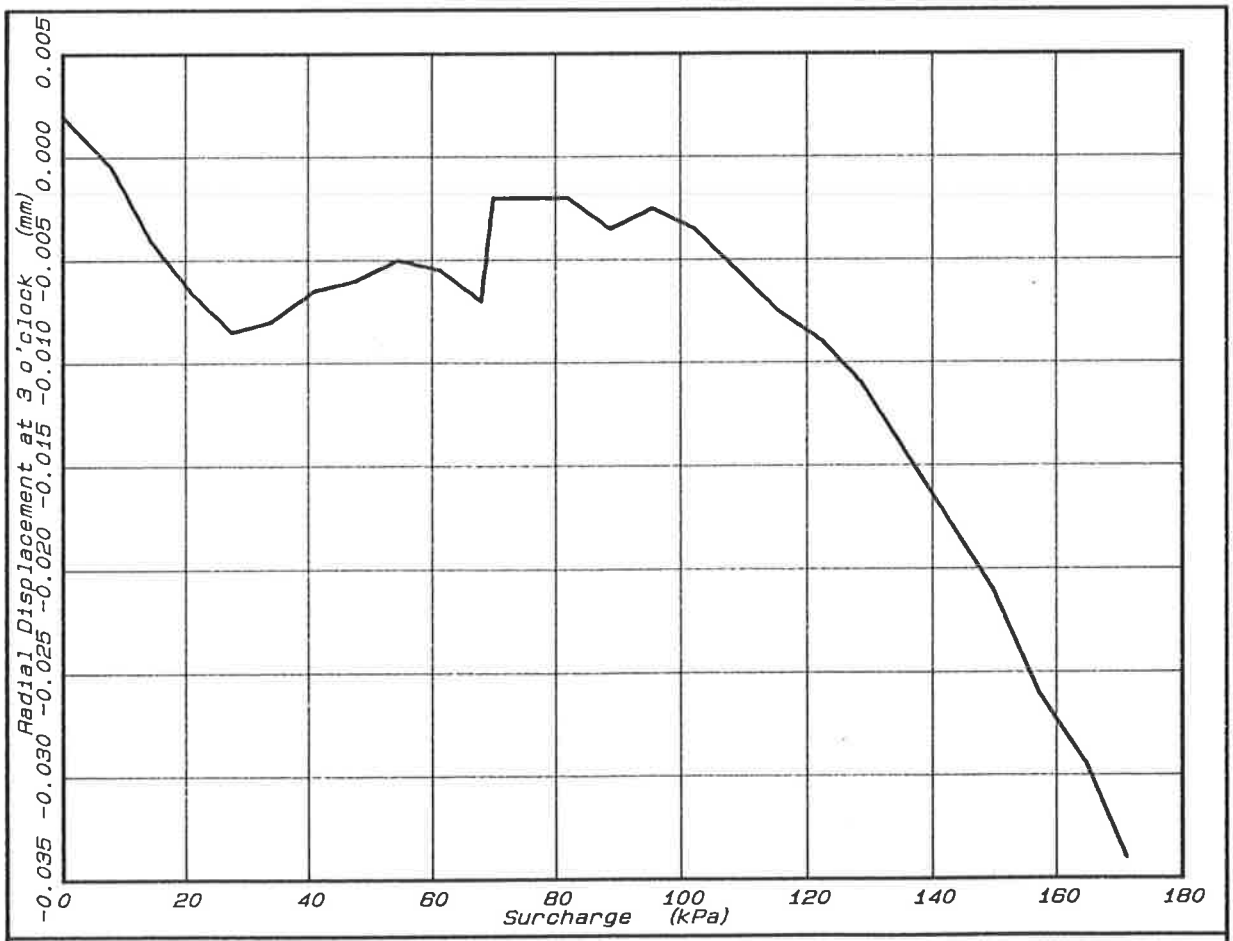

FIG. 50 - MILE END TEST BIN - BEDDED PIPE TEST
RADIAL DISPLACEMENT AT 3 O'CLOCK VS SURCHARGE (+ve towards centre)

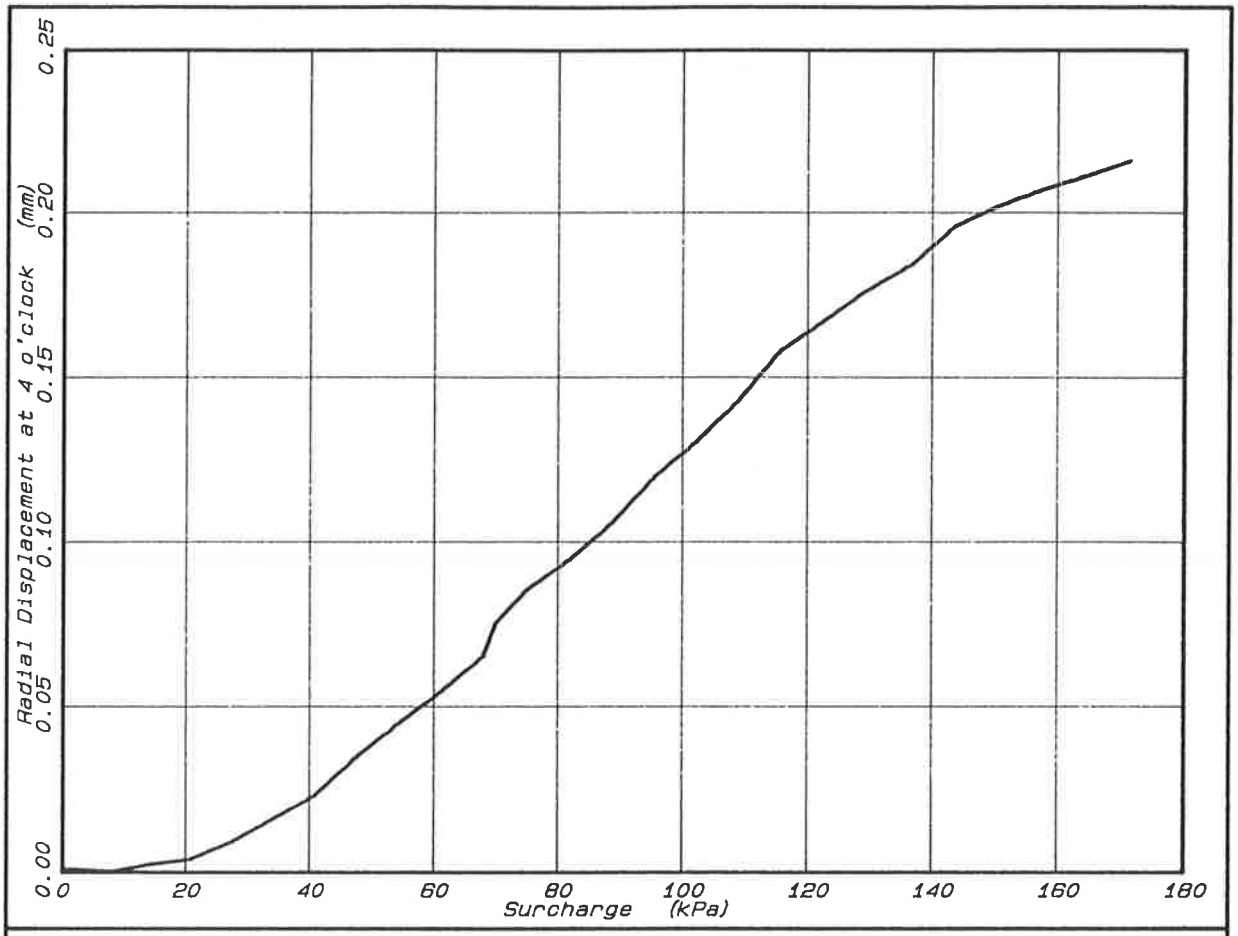

FIG. 51 - MILE END TEST BIN - BEDDED PIPE TEST
RADIAL DISPLACEMENT AT 4 O'CLOCK VS SURCHARGE (+ve towards centre)

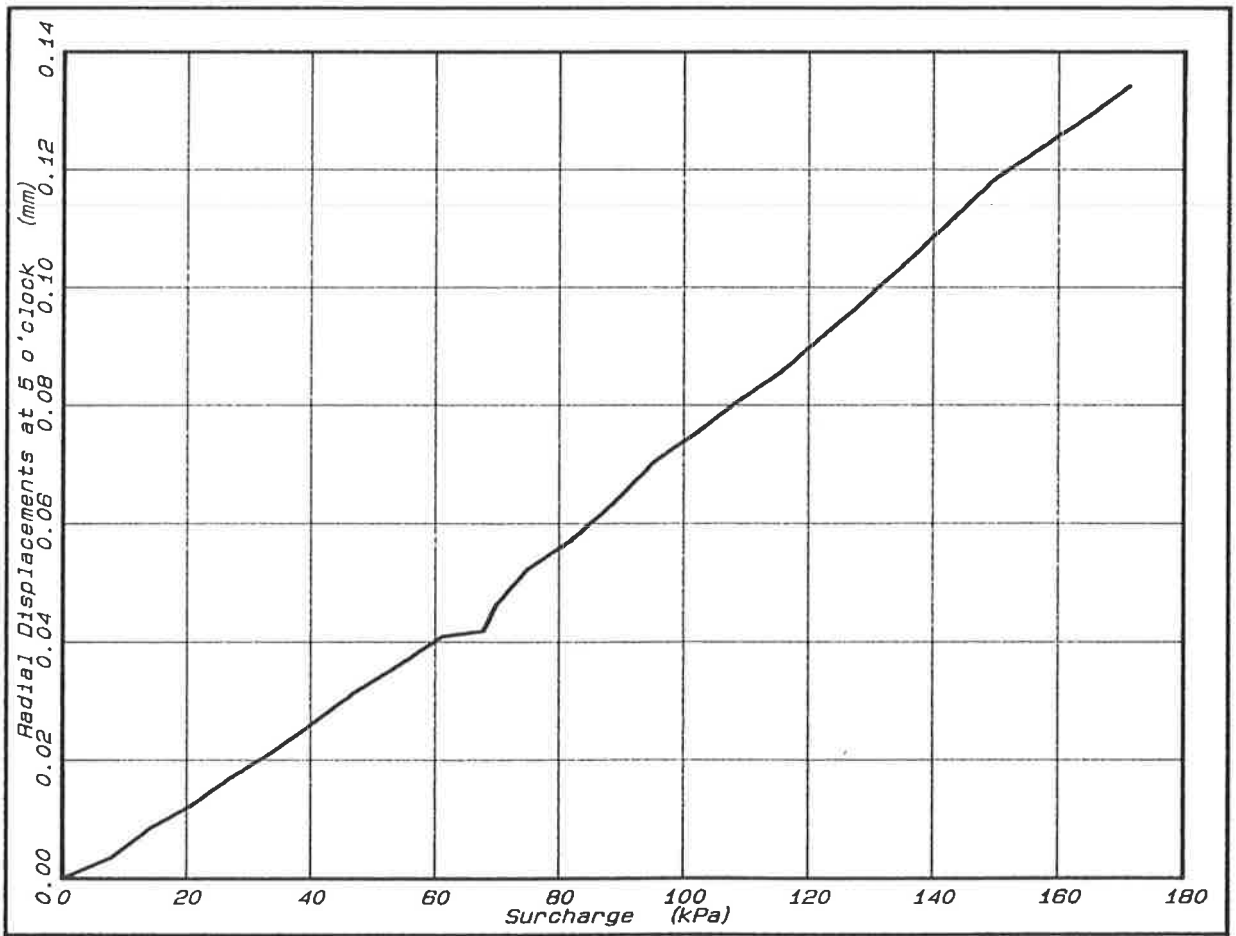

FIG. 52 - MILE END TEST BIN - BEDDED PIPE TEST
RADIAL DISPLACEMENT AT 5 O'CLOCK VS SURCHARGE (+ve towards centre)

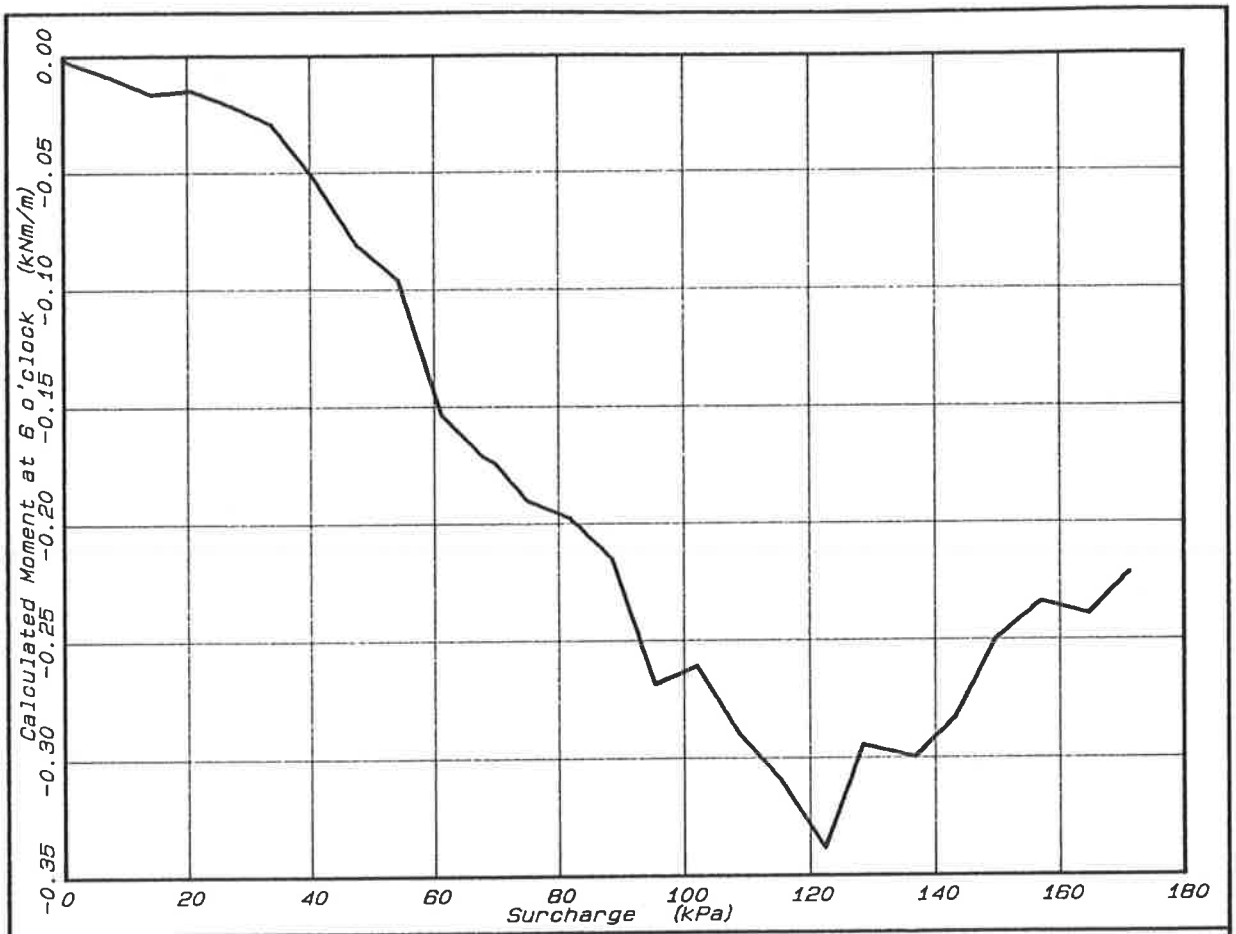

FIG.53 - MILE END TEST BIN - BEDDED PIPE TEST
MOMENT AT 6 O'CLOCK VS SURCHARGE (+ve M compresses outer face)

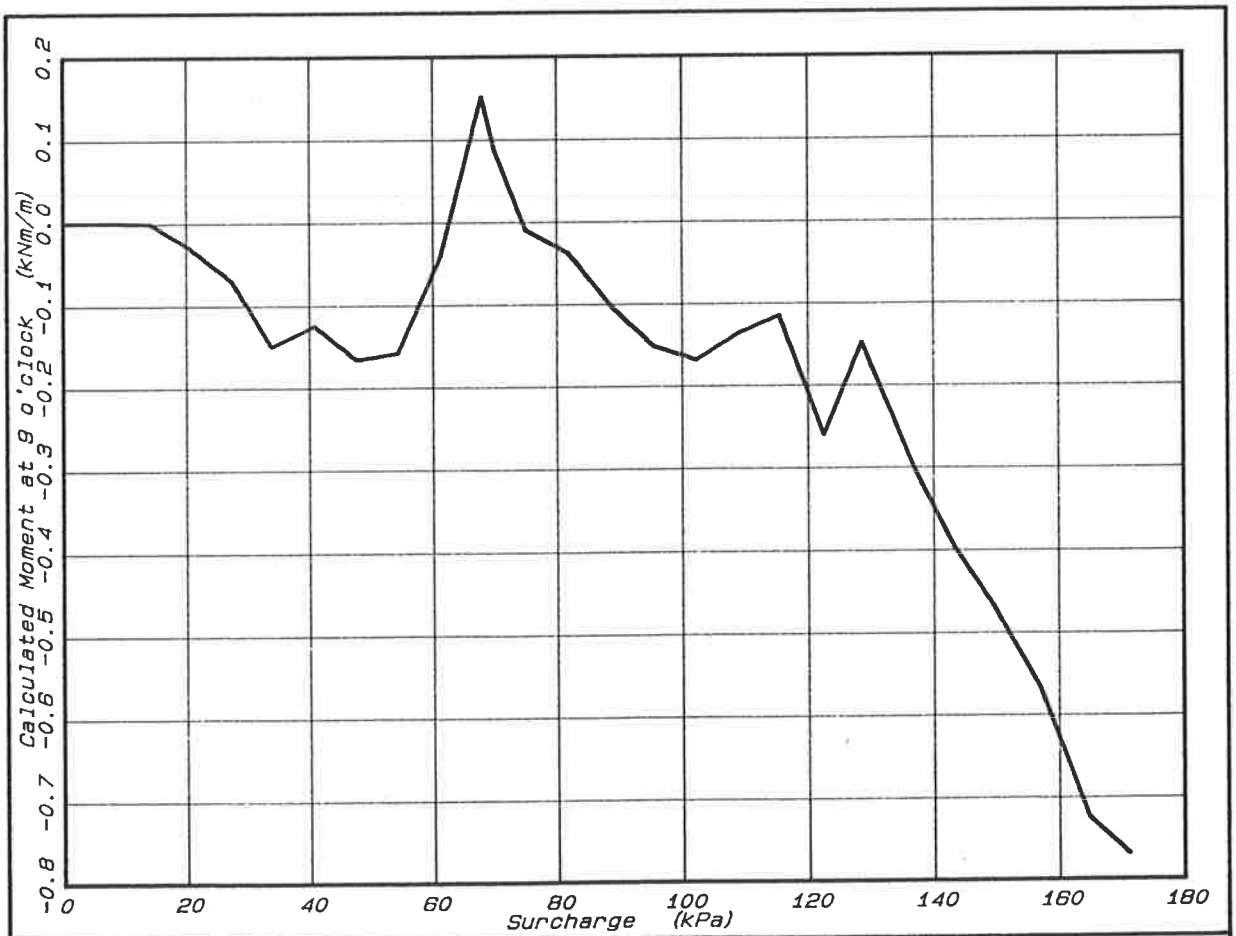

FIG. 54 - MILE END TEST BIN - BEDDED PIPE TEST
MOMENT AT 9 O'CLOCK VS SURCHARGE (+ve M compresses outer face)

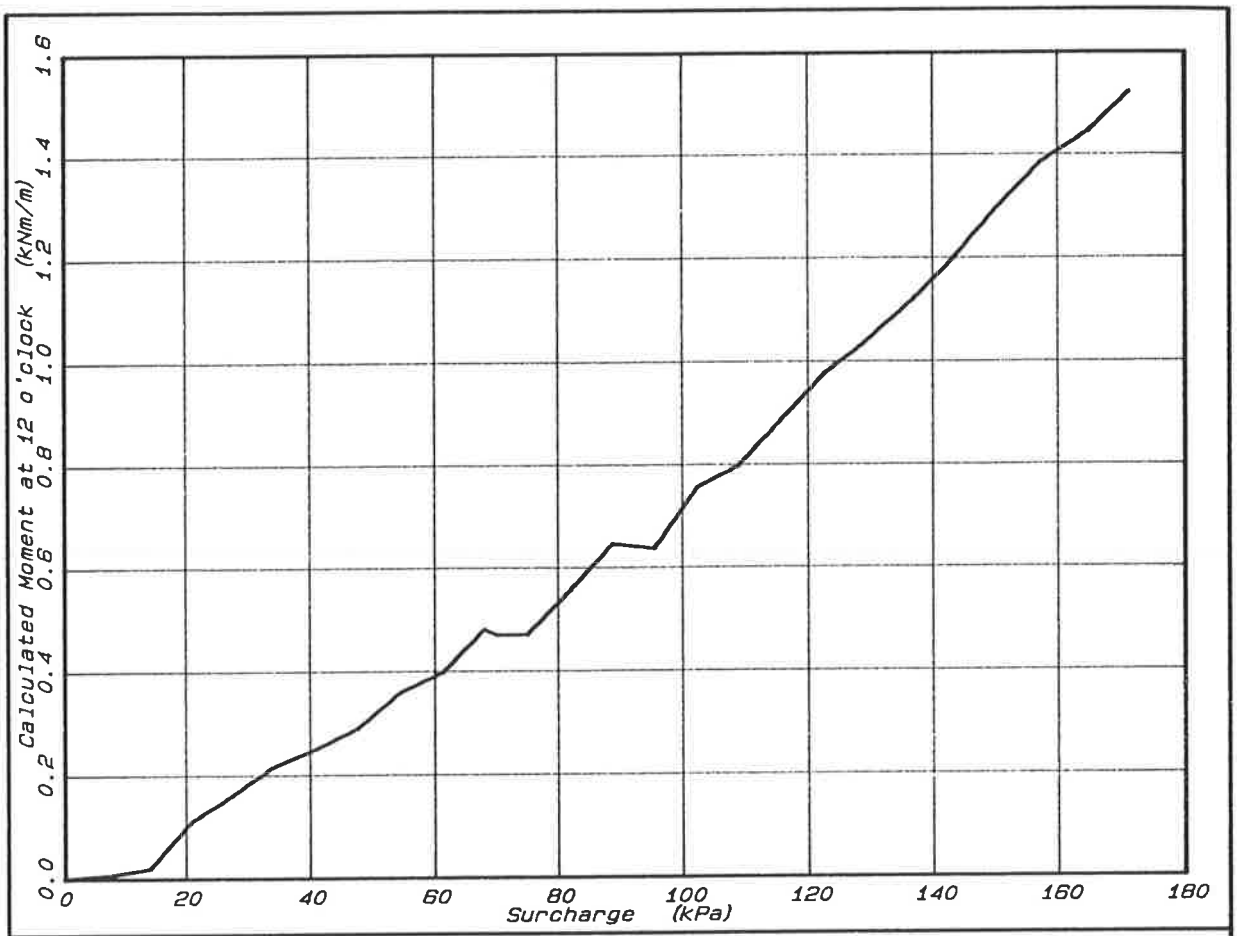

FIG.55 - MILE END TEST BIN - BEDDED PIPE TEST
MOMENT AT 12 O'CLOCK VS SURCHARGE (+ve M compresses outer face)

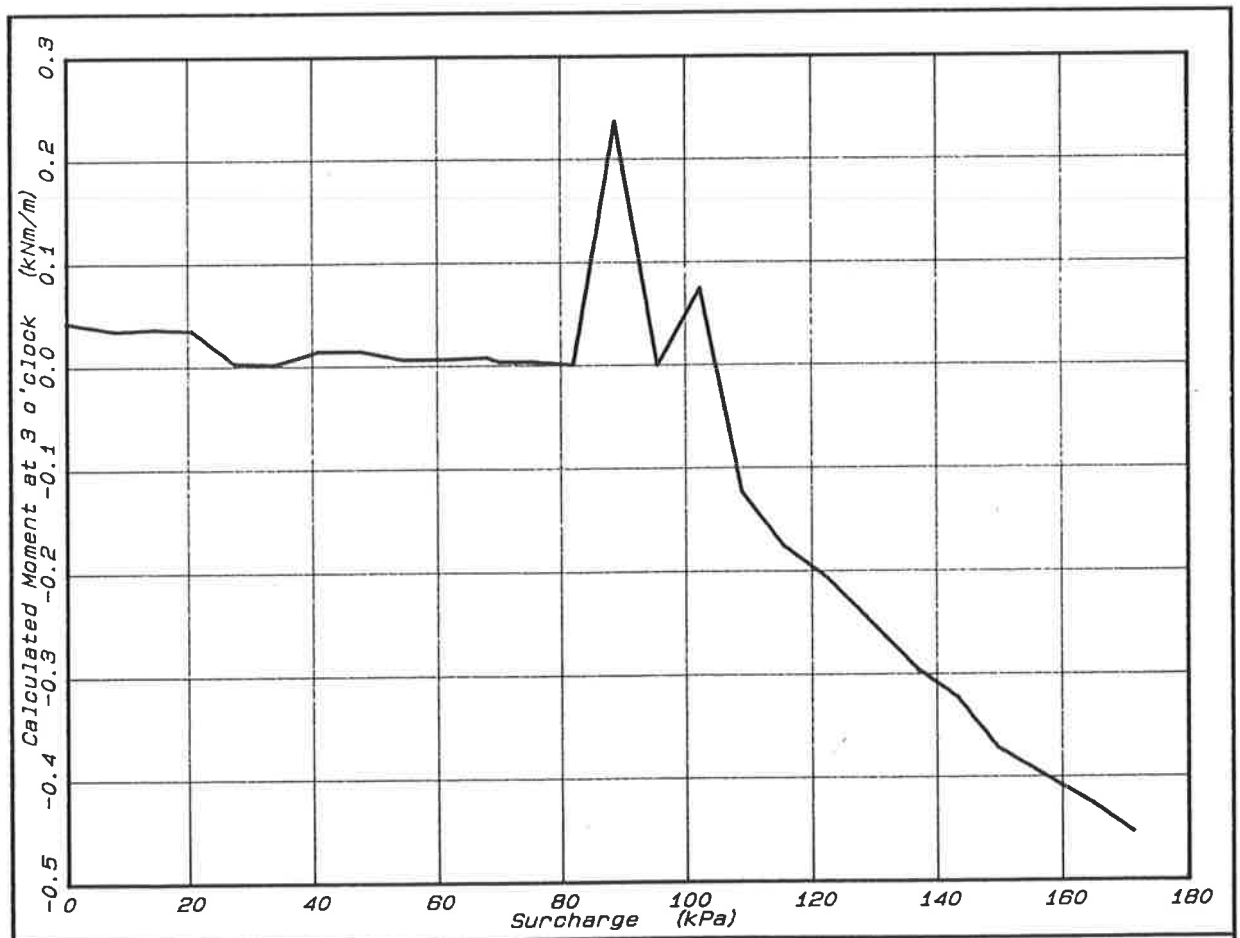

FIG.56 - MILE END TEST BIN - BEDDED PIPE TEST
MOMENT AT 3 O'CLOCK VS SURCHARGE (+ve M compresses outer face)

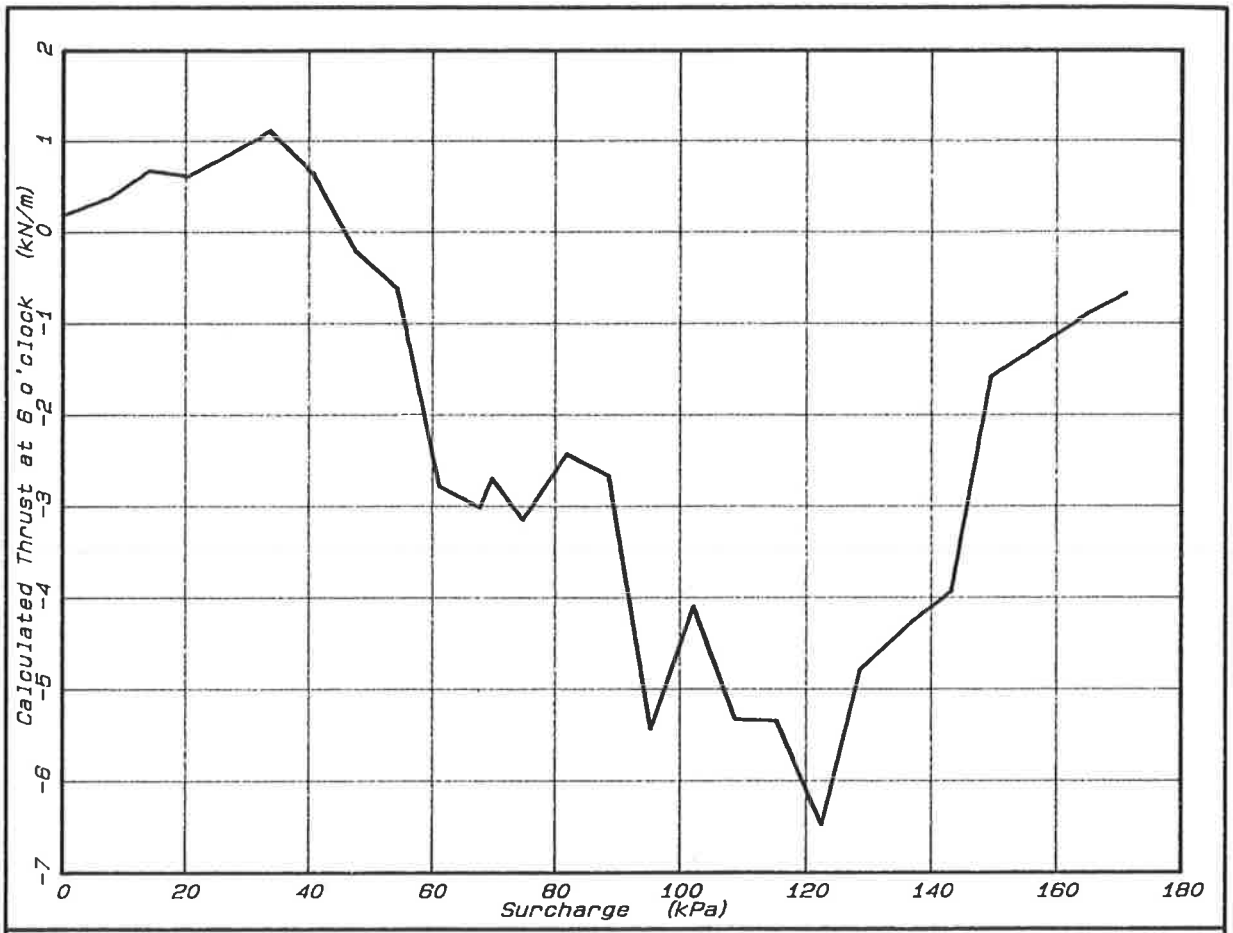

FIG. 57 - MILE END TEST BIN - BEDDED PIPE TEST
THRUST AT 6 O'CLOCK VS SURCHARGE

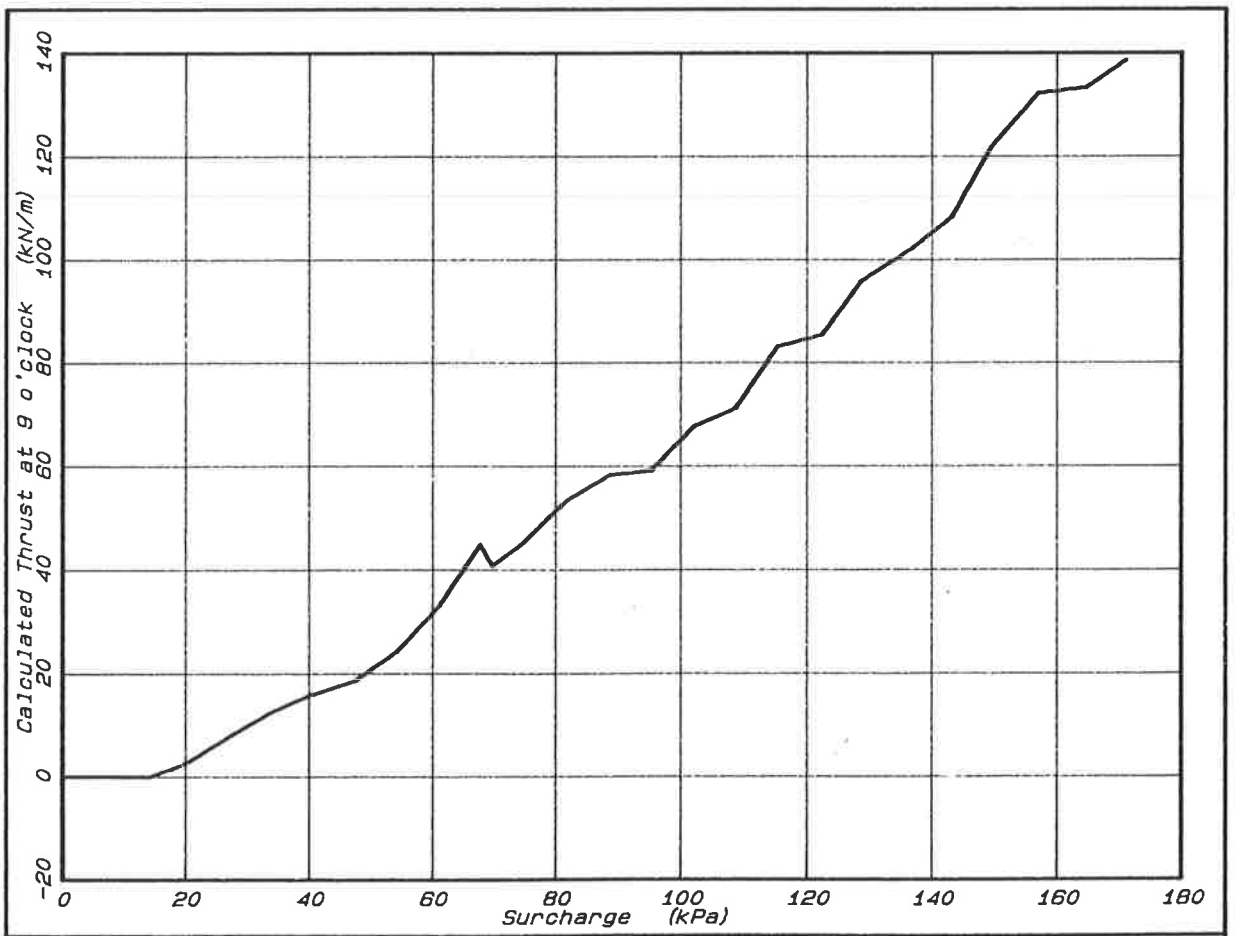

FIG. 58 - MILE END TEST BIN - BEDDED PIPE TEST
THRUST AT 9 O'CLOCK VS SURCHARGE

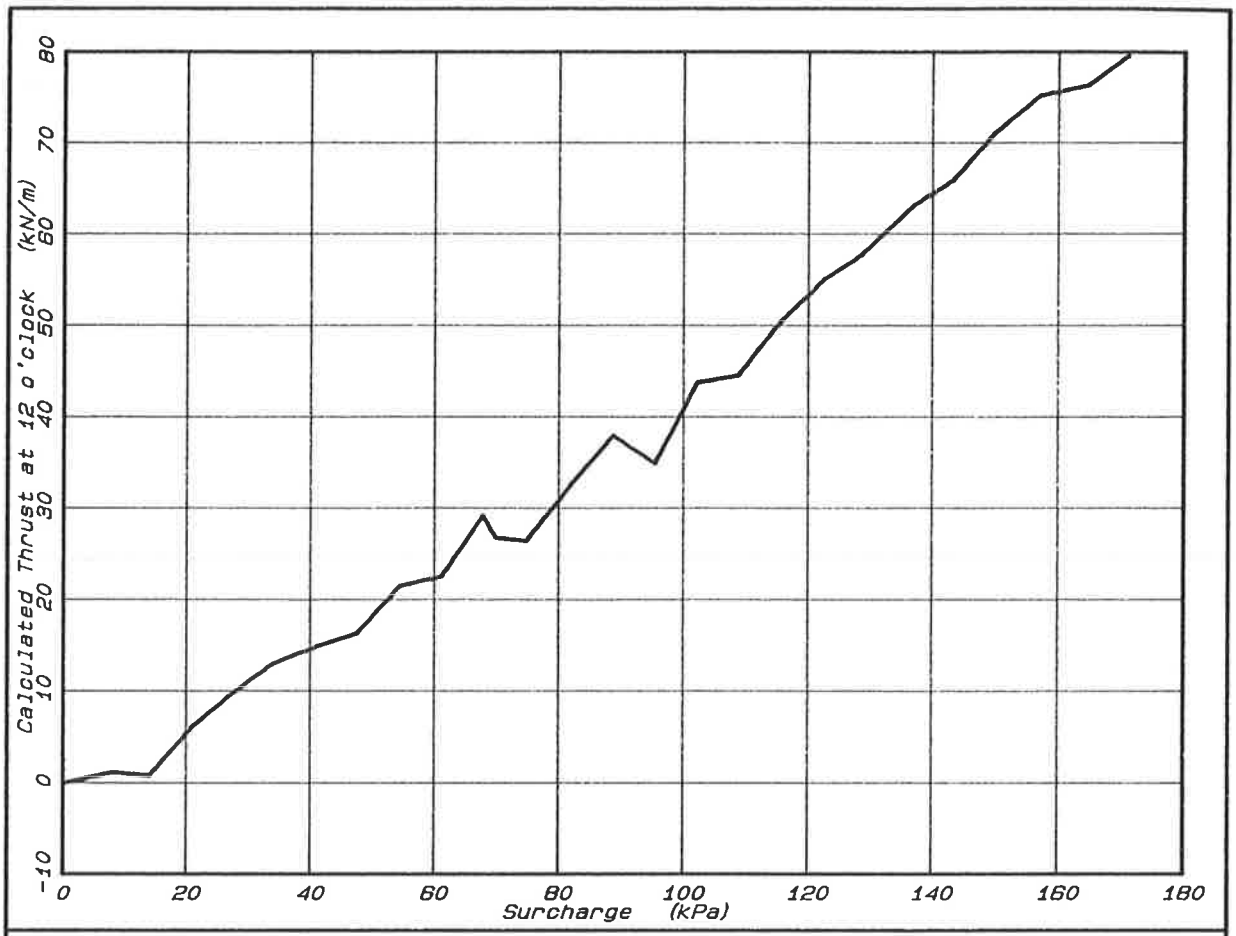

FIG.59 - MILE END TEST BIN - BEDDED PIPE TEST
THRUST AT 12 O'CLOCK VS SURCHARGE

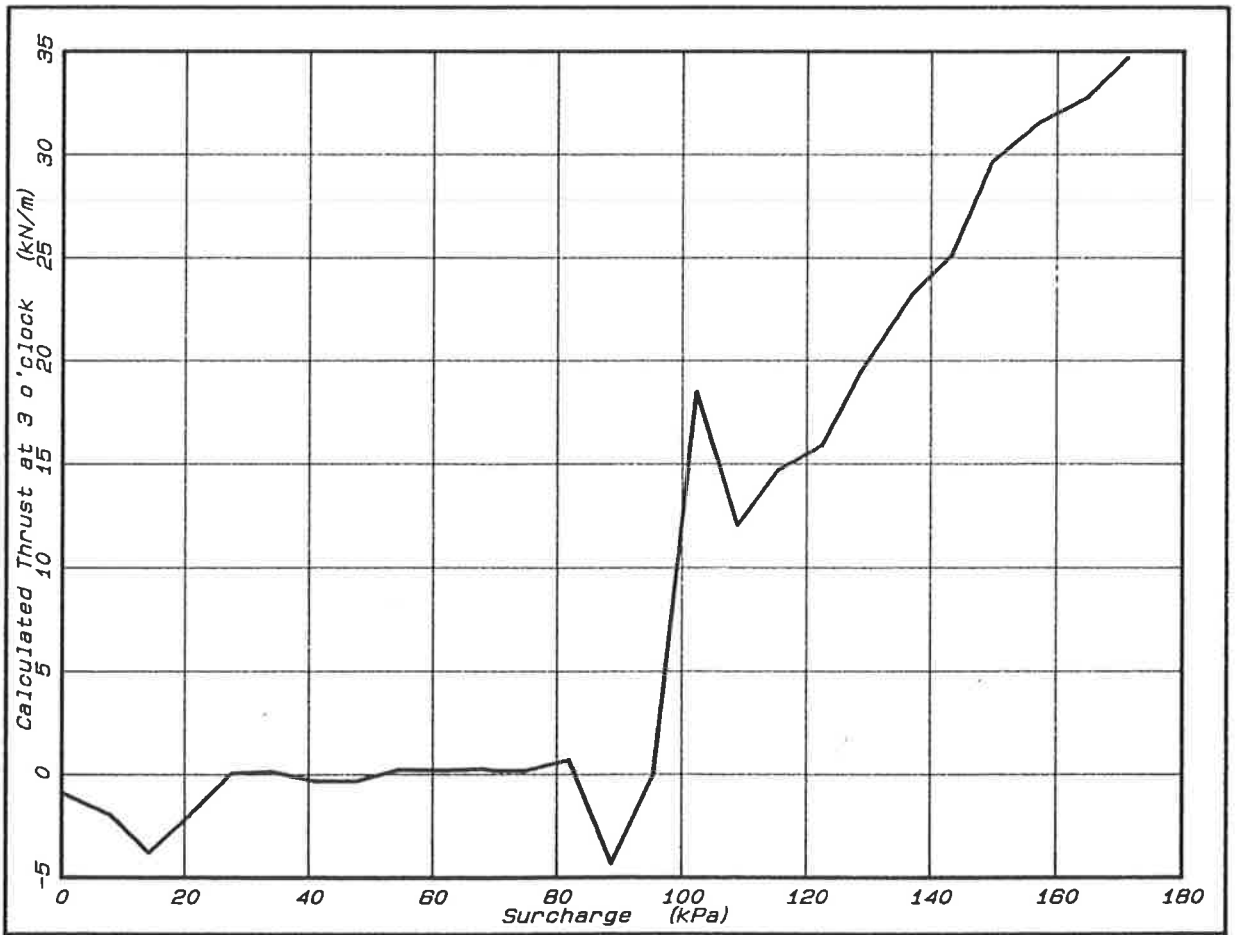

FIG.60 - MILE END TEST BIN - BEDDED PIPE TEST
THRUST AT 3 O'CLOCK VS SURCHARGE

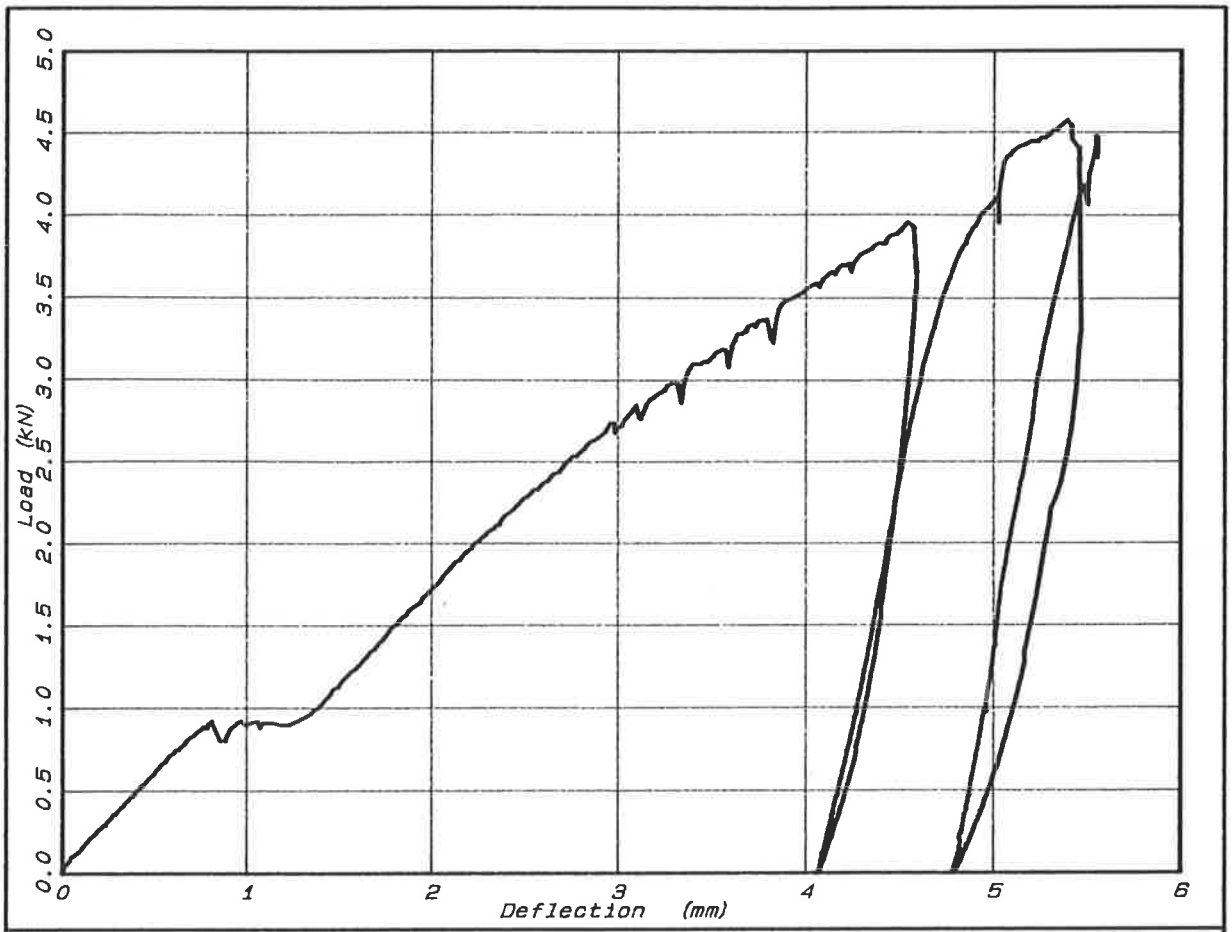

FIG. 61 - MILE END TEST BIN
PLATE LOAD TEST No.1 ON RAINED SAND

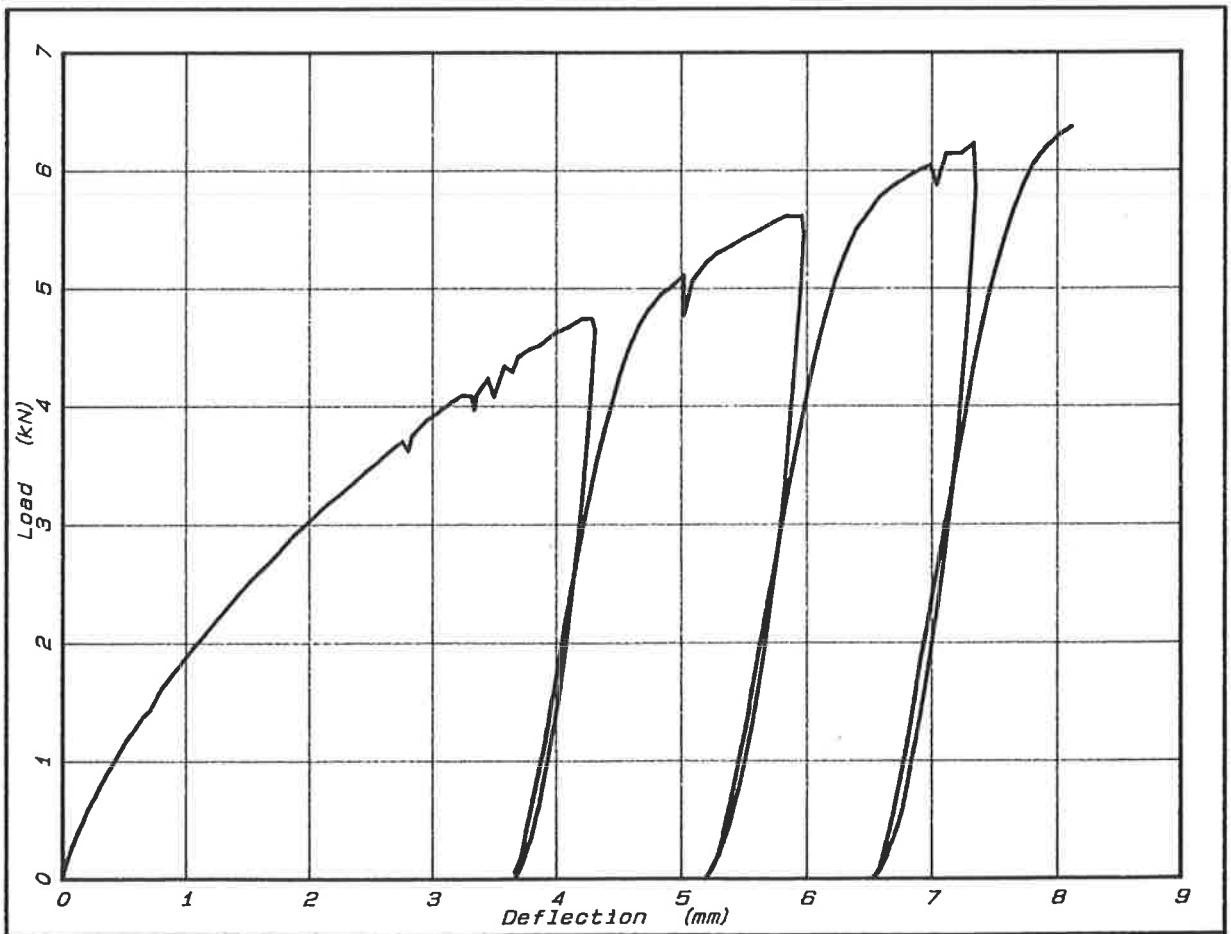

FIG. 62 - MILE END TEST BIN
PLATE LOAD TEST No.2 ON RAINED SAND

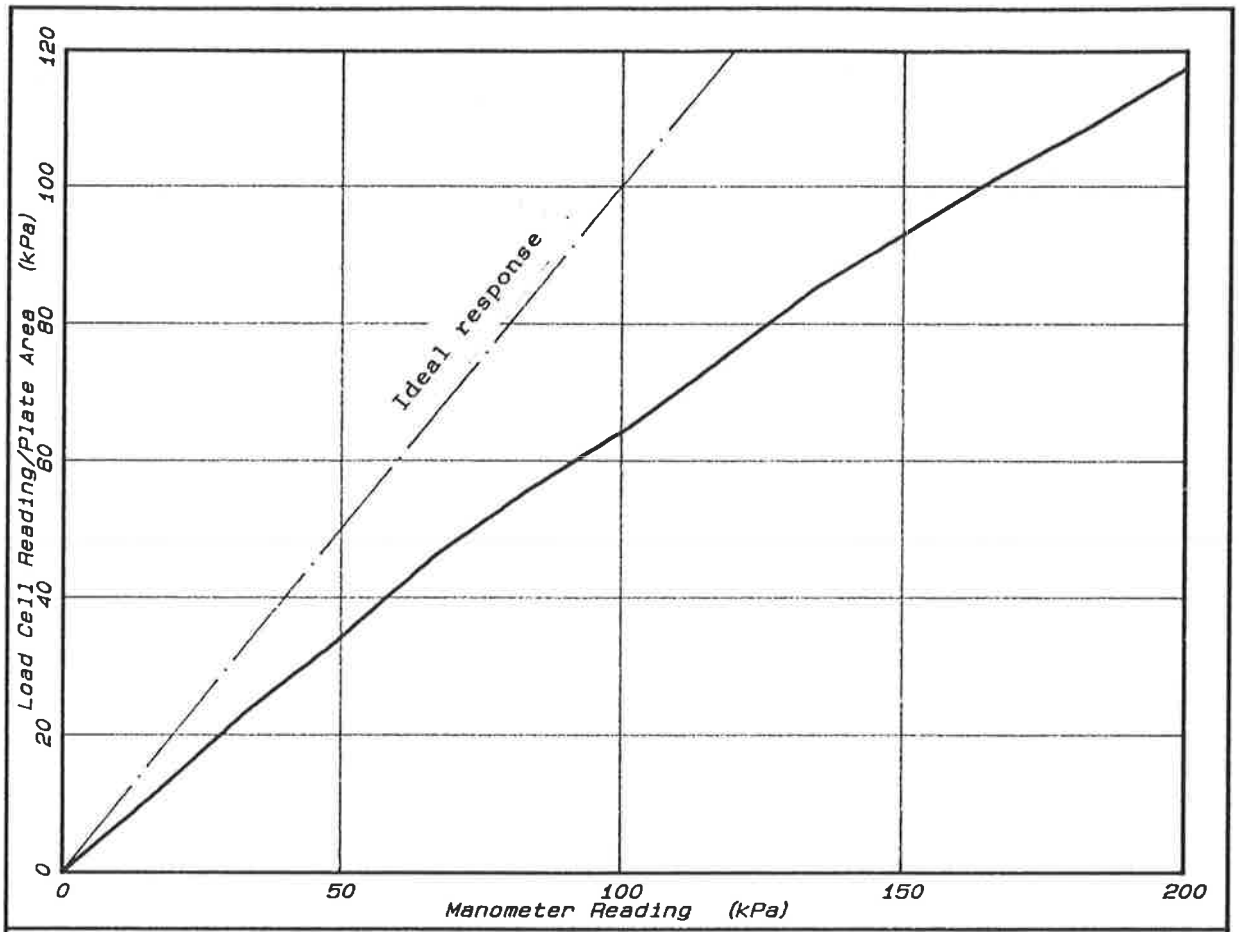

FIG. 63 - RESPONSE OF LOAD CELL TO STRESS IN SAND
PLATE PRESSURE VS AIR PRESSURE ON MEMBRANE

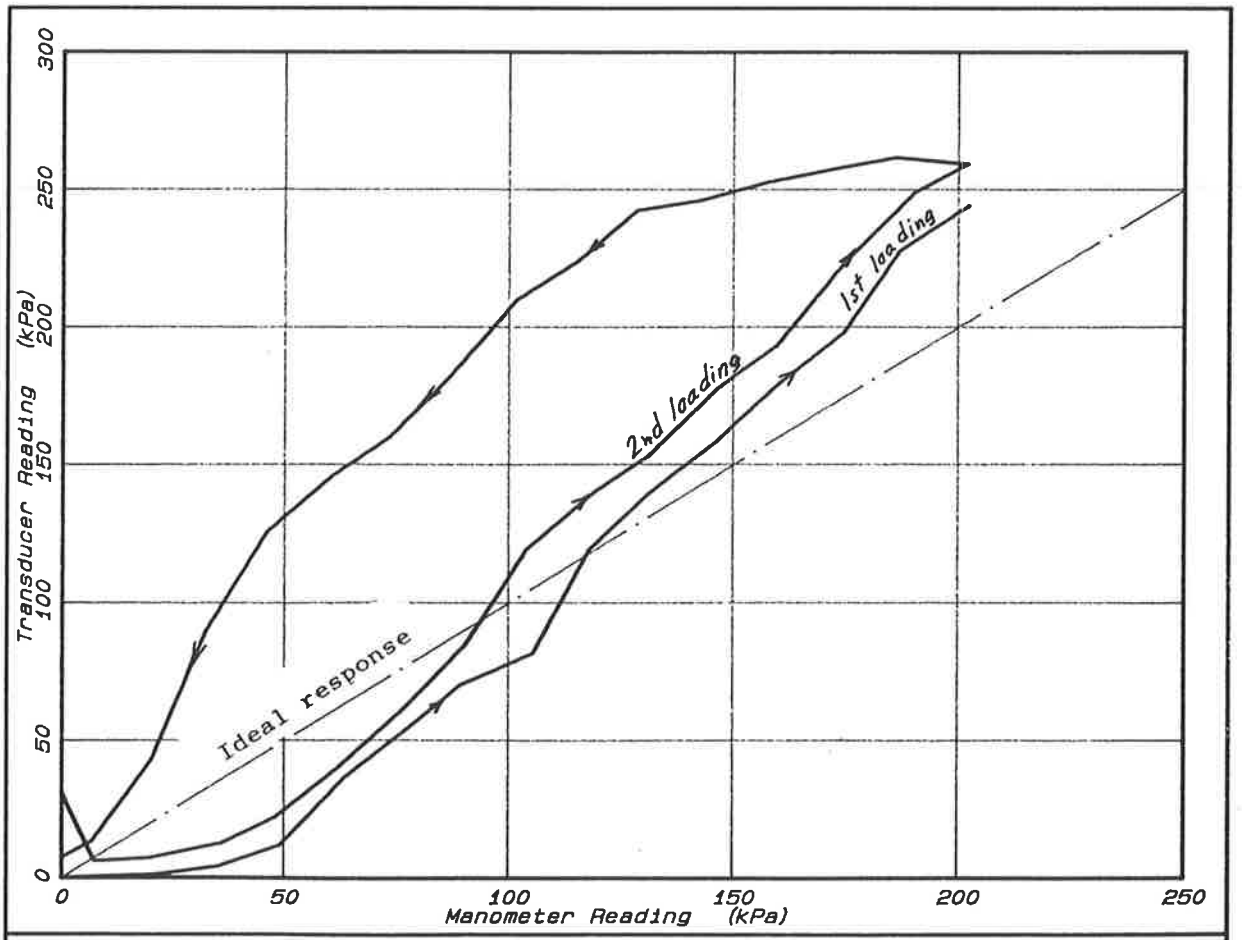

FIG. 64 - RESPONSE OF INTERFELS TRANSDUCER TO STRESS IN SAND
TRANSDUCER READING VS AIR PRESSURE ON MEMBRANE